Towards a uniform and optimal approach for safe NLFEA of reinforced concrete beams

Quantification of the accuracy of multiple solution strategies using a large number of samples

A. de Putter

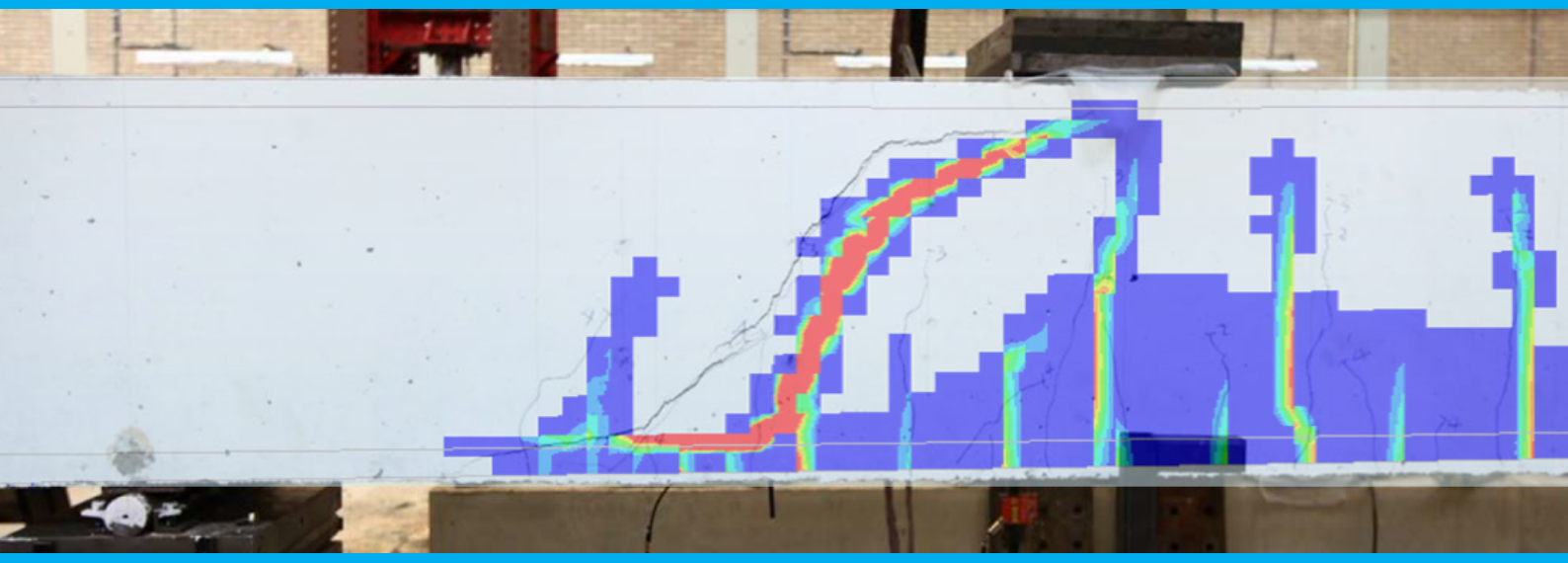

TU Delft

DIANA FEA

Towards a uniform and optimal approach for safe NLFEA of reinforced concrete beams

Quantification of the accuracy of multiple solution strategies using a large number of samples

by

A. de Putter

to obtain the degree of Master of Science
at the Delft University of Technology,
to be defended publicly on Friday April 24th, 14:00

Student number:	4207556	
Project duration:	May 6th, 2019 – April 24th, 2020	
Thesis committee:	dr. ir. M.A.N. Hendriks	TU Delft, chair
	Prof. dr. ir. J. G. Rots	TU Delft
	dr. ir. Y. Yang	TU Delft
	ing. A. A. van den Bos	DIANA FEA BV

An electronic version of this thesis is available at `http://repository.tudelft.nl/`.
Cover image: Overlay of a calculated crack pattern on a photograph of beam test B702A1 from [40]

TU Delft

DIANA FEA

Abstract

Application of Nonlinear Finite Element Analysis (NLFEA) is lagging behind the many digital advances in the structural engineering practice. This is due to the need for codes and standards. To help development of these codes and standards, 119 solution strategies were developed with different assumptions and choices for the concrete constitutive model, the finite element discretization, the way of modelling the reinforcement and the incremental-iterative procedures. The constants aspects of the constitutive model, like confinement and the reduction compressive strength due to lateral cracking, are based on the RTD1016 Dutch Guideline. All models are two-dimensional with a plane stress assumption and in all cases the analysis is force controlled with the application of an arclength method. This is done to increase the value of results for application in practice, as generally displacement loading is hard to apply in a real-life structure.

The strategies were benchmarked with 101 experiments on reinforced concrete beams selected from literature. Those beams cover a broad range of design aspects, failing both in shear and bending, reinforcement configurations with- and without shear reinforcement, both prestressed and conventional reinforcement and heights ranging from 90 to 1200 mm.

This resulted in 1919 NLFEAs which were performed with an automated approach in the DIANA multi-purpose finite element software package. It was concluded that the failure load and failure mode of the experiments can be approximated with a mean uncertainty of 1.05 with a coefficient of variation around 10 percent, provided that an appropriate solution strategy is applied. It is possible to assign an appropriate solution strategy when the structural design is known, where the main influence is the presence of shear reinforcement. Beams with stirrups are robustly modelled by a rotating crack model, while beams without stirrups were found to be better approximated by a fixed crack approach with specific choices regarding reinforcement modelling and equilibrium.

To have a more objective way of judging the ductility of a failure, a measure of the dissipated energy in the reinforcement was implemented in the DIANA code. It was found that the mean model uncertainty of a ductile failure can be as low as 1.045, with a coefficient of variation around 10 percent. Brittle failures showed a mean uncertainty of 1.131, with a coefficient of variation just below 16 percent. Therefore the ductility index was found to be a valid way to judge the reliability of an NLFEA result.

This study has demonstrated the applicability of force controlled NLFEA for reinforced concrete beams. The derived properties of the model uncertainties are a crucial input for safety formats.
Keywords: NLFEA, Concrete Beams, Model Uncertainty, DIANA, Ductility Index, ULS

Preface

This thesis concludes my Master's degree at Delft University of Technology. It is the end of an exciting period where I saw and learned lots of different things. The final year of which I spent in the DIANA FEA office to do the project resulting in this thesis. I sincerely hope and believe that this project will help the advance of NLFEA in structural engineering applications. Even though the process of graduating is individual, it is impossible to do it on your own.

Many thanks go to the wonderful people of DIANA FEA BV. Especially Ab van den Bos, Jonna Manie, Pim van der Aa and Saurabh Dahnmeher from the Engineering team. They gave me the opportunity to conduct the research required for this project in their office and supported this project by answering my numerous questions and giving me access to everything I needed. Besides that, there were the very tense table tennis matches that helped to blow off some steam.

This project would not have been possible without the academic guidance, enthusiasm and feedback of dr. ir. Max Hendriks, dr. ir. Yuguang Yang and prof. dr. ir. Jan Rots from Delft University of Technology. Their comments and input increased the relevance, quality and usability of the study a great deal.

Finally, the support of my family, friends and other loved ones can not go unmentioned. Their love, motivation and company are crucial to succeed in anything.

A. de Putter
Arnhem, April 2020

Contents

List of Tables

List of Figures

1 Introduction

This chapter will explain the motivations behind this study, the scope of the research and what questions will have to be answered. Ultimately the outline of this thesis is explained.

1.1. Non-linear analysis

The interest in computer aided engineering, automated design and optimization processes, parametric design, finite element analysis and the links between those concepts is rapidly increasing. This growth is fuelled by a concern for sustainability, efficiency and the need to design complicated structures as well as increasing computational possibilities and advances towards 'smarter' software in general.

Non-linear finite element analysis (NLFEA) generally obtains higher design resistances than 'conventional' sectional analysis, because the failure in the most unfavourable cross section of a structure does not necessarily mean that the structure fails. Plastic deformation or cracking results in redistribution of forces and this usually does not result in immediate failure. This behaviour, or 'hidden' capacity, is missed in linear calculations. Therefore, if one wishes to assess the global behaviour of a structural member or structure, non-linear finite element analysis is an important computational tool. In a report by Rijkswaterstaat[22], a comparison is made between sectional design and NLFEA of various beams, where indeed higher design loads were obtained with non-linear analysis. As the fib Model Code [12] adequately states: It appears that the effort devoted to an analysis relates to the accuracy. This is illustrated by Figure 1.1, where a 'Level of approximation' - approach is mentioned. Each level of approximation increases the accuracy, as well as the time spent on solving the problem. Advanced numerical simulation is applied in the highest levels of approximation and 'simple' partial factors are used in a level I analysis.

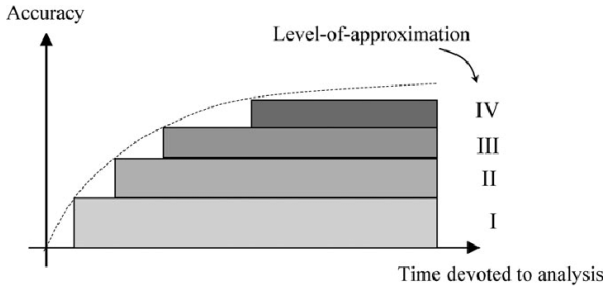

Figure 1.1: Levels of approximation, taken from MC2010 [12]

In the Netherlands, the need to re-assess old concrete bridges is increasing the interest in advanced analysis. Many bridges are at the end of their design lifetime and were designed to resist traffic loads that are lower than those of today. It is important to prove that these bridges are still safe for use. This can be done with non-linear finite element analysis (NLFEA). If advanced analysis results in higher design resistances, it can also be applied to design optimized and more sustainable structures. Yet the application of NLFEA in day to day engineering projects appears to be lagging behind. The fact that NLFEA of concrete structures has been a topic in science for many decades already makes the lack of application even more surprising. Especially

because good finite element codes and models are available. One of the answers to this has to do with norms and regulations:

1.2. Regulation of NLFEA

When an engineer does apply NLFEA, many choices have to be made in the constitutive model, kinematic and equilibrium conditions. Different constitutive models can be applied, just as different models exist for modelling the bond and behaviour of the reinforcement. The finite element discretization includes the type of element and element size applied. Solving the system is also subject to choices on convergence criteria, load step size and how many iterations are allowed. Amongst the difficulties in applying non-linear numerical analysis is those particular choices of the analyst have a large impact on the outcome of the analysis. In [15] it was stated that the uncertainty of an NLFEA solution tends to increase as the skills and knowledge of the analyst decrease. This is the case for any analysis method, as different types of models are always available, but for other types of analyses these choices are prescribed in normative documents like the Eurocodes. This means that at least the analyst is not responsible for consequences of those choices and that following a code procedure should result in a safe calculation, provided that the prescribed choices are the correct ones.

The current EC2 statement on verification with non-linear numerical analysis is that non-linear analysis techniques are allowed for verification of both ULS and SLS. This is provided that a suitable material model is used and that both equilibrium and compatibility are ensured [13], very different from analytical procedures which are described in great detail. This resuls in a situation where the analyst will have to prove to building authorities why his or her solution is correct. This is not an easy thing, because of the complex nature of an NLFEA solution and the fact that few reference projects exist.

The complexity and sensitivity to choices made by the analyst can make NLFEA results appear arbitrary, as subtle changes in the model might result in very different results. Authorities are suspicious and 'You can get any result you want out of that' is an often heard comment. Because of reasons like these, reviewing authorities are not convinced on the correctness of a solution based on NLFEA. To change this, the scatter in results and their uncertainty has to be minimised. A well-developed guideline or normative document would do this, as the NLFEA can be performed in a way that was proven to be safe. This is why both reviewing parties as well as designing parties would benefit from those documents.

A recent development in such normative documents is the publication of a Dutch guideline for the assessment of *existing* concrete structures, the RTD1016 [21], which was initiated by Rijkswaterstaat out of concern for the safety of concrete bridges. Blind prediction contests, like the workshop held in Parma, reported in [10] (specifically around an older version of the guideline from the Dutch Ministry of Infrastructure and the Environment) or the one at the university of Toronto [8], are held to prove the possibilities of non-linear finite element analysis. The scatter of results in such contests is observed to be very high. As stated in [10]: Better control of the knowledge on NLFEA is required to make it an accepted method.

The fib Model Code, a document published by the international concrete federation (fib), aims to help development and updating of codes. It is a semi-normative document that also takes into account new scientific developments. The 2010 edition [12] contains a section on NLFEA which is mainly focused on how to deal with safety formats, but does not contain guidance in choosing a solution strategy. The fib Model Code 2020 will have an extended section on verification by non-linear analysis, where the so called *model uncertainty* is used to assess the reliability of a NLFEA solution strategy. It would be even better if guidance on the choices of the analyst could be included in the guideline.

In this study, the investigation of possible solution strategies as well as quantification of their uncertainty is carried out to obtain reliable NLFEA of concrete structures. This helps the development of regulatory documents and furthers the application of NLFEA in the engineering practice.

1.3. Model uncertainty

Each non-linear analysis entails a *solution strategy* that the analyst follows. The solution strategy was described by Engen et al. as *"choices regarding force equilibrium, kinematic compatibility and constitutive relations."* [15]. Each choice in a finite element solution contributes to the model uncertainty, either explicitly or implicitly. Explicitly in a sense that different models offer different approximations to the physical reality. The implicit part is due to everything not considered explicitly. It is defined in equation 2.7 as the relation between an experimental result and the outcome of NLFEA and is an important quantity in safety and assessment of a NLFEA solution. In literature, like the JCSS Probabilistic Model Code, it is regarded a log-normally distributed random variable [27].

(a) Flexural shear failure

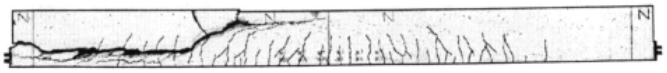

(b) Horizontal splitting due to flexural shear

(c) Crushing of the concrete compression zone (bending type failure)

Figure 1.2: Failure modes in concrete beams, adapted from figure 7 in Vecchio & Shim [37]

$$\theta = \frac{R_{exp}}{R_{FEA}} \tag{1.1}$$

If a considerable amount of benchmarks is tested, statistical properties of this random model uncertainty can be derived. This results in a mean, standard deviation or coefficient of variation for the uncertainty of a solution strategy and is a way to quantify it's accuracy. The model uncertainty is elaborated further below.

The relation between the predicted failure load and the actual failure load is however not the only important factor in the assessment of a finite element solution strategy. As mentioned above, another advantage of non-linear analysis is that an engineer gains insight in the structural behaviour. Therefore, a second requirement for the solution is that it approximates this behaviour.

1.4. Ductility and failure modes

As shown in Figure 1.2, concrete beams fail in various ways. Predicting the correct failure load of a structure is most useful if the correct failure mode is predicted as well. If a good prediction of the failure load is made, but with a different failure mechanism, questions could be asked about the correctness of such a solution.

In the analysis of failure of concrete beams, it is useful to be able to show the ductility of the failure. Ductility is an important property from a perspective of structural safety as well, because we would like a structure to 'warn' before collapse by excessive deformation, cracking or yielding. Generally, brittle failures do no exhibit this behaviour.

The determination of failure mode and ductility can be done by so called 'visual interpretation' of crack patterns and load-displacement relations. Such way of describing important properties of beams or other structures could be seen as subjective. Also, for larger structural systems, the mode of failure is not always straightforward due to redistribution of loads over the other components of the system. Engen et al. [16] proposed a more objective way to deal with ductility. A so called 'ductility index', $X_{ductility}$, was introduced. This index is defined as the ratio of energy dissipation in the steel, $W_{pl,steel}$ versus total energy dissipation, $W_{pl,total}$, as in equation 1.2. It is possible to evaluate this index in every load step, including the step at which the beam fails or is supposed to fail.

$$X_{ductility} = \frac{W_{pl,Steel}}{W_{pl,total}} \tag{1.2}$$

1.5. Project scope

The main objective of this thesis assignment is to either develop a robust solution strategy that can be applied on all reinforced concrete beams or being able to subscribe a solution strategy based on structural properties. Insights gained on the applicability of finite element models to many different cases will be important to further development of those models, solution procedures and general applicability of NLFEA.

To that extent, 101 beams are taken from various experiments in literature and the outcomes of NLFEA according to these strategies are compared to the experimental result to determine statistical properties of the model uncertainty. Here the study is limited to the load carried in the ultimate limit state of simply supported reinforced concrete beams.

The investigated solution strategies are limited to 2D plane stress models with a smeared crack approach. Strategies are varied on three components: constitutive, kinematic and equilibrium.

Assessment of the model uncertainty is done according to a Bayesian approach which is elaborated below. The ductility index will be implemented in the used finite element code and it is investigated how this index relates to observed failure modes and how it can be used to assess the reliability of the analysis.

The used finite element code is the DIANA FEA package, due to implementation of the ductility index a running development version has to be used. The consistence of results is however guaranteed by an extensive test suite that is used for every update.

1.6. Research questions

With this study, an attempt is made to further the applicability of NLFEA in the design and analysis of reinforced concrete structures by helping structural engineers, reviewing authorities and the development of normative documents with an investigation of various solution strategies and their applicability.

1. What are the important aspects of a solution strategy with respect to accuracy?

The first step towards standardization of NLFEA is to map how specific choices in a solution strategy impact the results. From there, conclusions can be drawn on how a good solution strategy can be defined.

2. Is it possible to have one robust strategy for all concrete beams ?

A robust solution strategy should successfully predict the failure any beam that is simulated using that strategy. In case a robust strategy cannot be developed, the information of as to why this is not possible is useful for further development of NLFEA. Also, if no robust strategy can be found it is important that at least a strategy can be advised based on properties of the beam like reinforcement configuration or (shear) slenderness.

3. How can a solution strategy be prescribed based on the properties of the structure?

This is useful in the case mentioned above, but even if a robust strategy exists it is expected that tweaks in a strategy result in a better approximation for beams with its specific characteristics. The intended result is an advise as to what approach one should take to model a certain structural member in the best way possible.

4. What is the relation between the ductility index and model uncertainty?

It is expected that the ductility index will be valuable in judging the reliability of an analysis, as it appears from literature and experience that brittle failures (Figures 1.2a, 1.2b) are harder to predict correctly. If beams with low ductility are found to indeed have a higher uncertainty, even with the ideal solution strategy, the ductility index could be used to judge the reliability of solutions based on the type of failure and therefore become an important analysis parameter in the future. In order to investigate this relation, the ductility index is implemented in the DIANA software package. The ductility index will be calculated for all the benchmark experiments and the relation with the model uncertainty will be studied.

1.7. Thesis outline

This thesis report consists of 8 chapters, of which the first is concluded by this outline. It is followed by an introduction of important concepts from literature in chapter 2, an elaboration of methods including solution strategies in chapter 3 and the description of the used samples on chapter 4. Chapters 5 to 7 report and discuss different aspects of the results: Model uncertainty, accuracy of failure modes and the ductility index respectively. Due to the sequential nature of the project, this report is structured with a discussion in each chapter such that conclusions from chapter 5 can be used to present results in the following chapters. Chapter 8 will recap the conclusions from the previous chapters and provide recommendations

Chapter 2 - Background and literature review

In chapter 2 the mentioned concepts are elaborated: The definitions of failure modes, how to model cracking of concrete and the probabilistic treatment of uncertainty are explained.

Chapter 3 - Methodology

First the research questions and the approach to answering them are elaborated with the information introduced from literature. The used solution strategies as well as boundary conditions and other methods surrounding the answers to the research questions are specified. After this chapter, it is clear which solution strategies were be investigated and how the results are treated.

Chapter 4 - Selection of samples

The 101 benchmark beams are generally introduced and the choice for the experiments is motivated. This chapter also offers an overview of how certain characteristics like concrete strength or reinforcement ratio are distributed over the samples.

Chapter 5 - Quantification of the model uncertainty entailed with different solution strategies

Results are presented in terms of accuracy and uncertainty for every solution strategy. In this chapter, a quantitative approach to the resulting data is taken. With all the results, comparisons are made between solution strategies with different parameters so that the impact of specific choices becomes clear. The quantitative results also offer the opportunity of investigating the probabilistic properties of model uncertainty. After this chapter the quantitative properties of model uncertainty are established and the best solution strategies for separate types of beams as well as for all beams are discussed.

Chapter 6 - Analysis of the failure modes found with different solution strategies

The accuracy of the found failure modes is investigated and wrongly described failures are discussed in a more qualitative manner. Here the inadequacies of solution strategies with respect to capturing a failure mode are discussed and conclusions from chapter 5 are revisited with an investigation of failure mode for specific results. After this chapter it is clear as to why trends observed in chapter 5 occur and how accurate failure modes are approximated by the current solution strategies.

Chapter 7 - The ductility index

Finally the ductility index is introduced in the results, such that it becomes clear as to what values it takes for the specific failure modes discussed in chapter 6. Using those thresholds, all solution strategies can be assessed based on their ductility index. At the end of this chapter, the range of values of the ductility index as well as its usability in judging NLFEA results are established. Results from chapter 5 and 6 have been revisited in order to show how the accuracy with regard failure modes can be judged based on the ductility index.

Chapter 8 - Conclusions and Recommendations

Summary of answers to research questions, recommendations for further research and recommendations for NLFEA

2

Background and literature review

This chapter explains the relevant state of the art on finite element modelling of reinforced concrete structures. Next to that, a distinction is made between relevant failure modes and the statistical assumptions around model uncertainty are presented.

2.1. Identification of failure modes in reinforced concrete beams

In the analysis of the ultimate limit state of reinforced concrete beams, some different failure modes can be identified. Making choices in a solution strategy requires to know what phenomena need to be modelled.

2.1.1. Bending failure

Bending failure is observed when the cross section is unable to resist the bending moment. First, flexural cracks will form. When the stabilized cracking stage is reached and loading is continued, the reinforcement will start yielding in one or more cracks. This causes large deformations while the load is sustained, ultimately the compression zone crushes or the bottom reinforcement fails in tension. In case the reinforcement fails, the beam is referred to as 'under-reinforced'. Failure of the compression zone, as visible in Figure 2.1a, means a beam was over-reinforced.

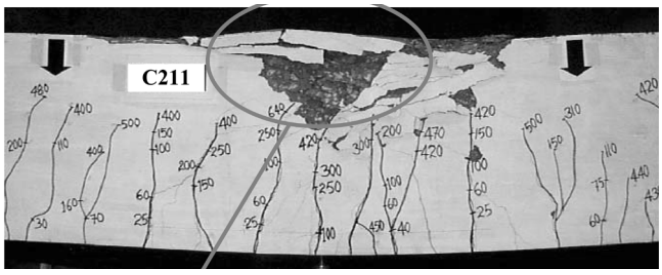

(a) Failure of the compression zone

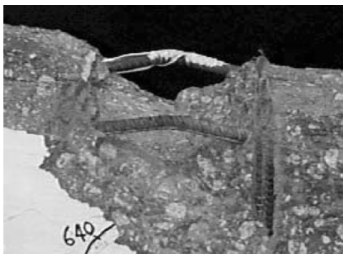

(b) Buckled top reinforcement in an overreinforced beam

Figure 2.1: Bending failure of an overreinforced beam, taken from Rashid & Mansur [29]

2.1.2. Shear failure in beams without shear reinforcement

During the formation of flexural cracks, inclination of the cracks occurs as the shear force increases and principal stresses rotate. At some point a 'critically inclined crack' opens, causing a decrease in the load bearing capacity which leads to brittle failure. Yang identified the cause of this to be the formation of secondary horizontal cracks [39], allowing a rotation which causes the inclined crack to open resulting in loss of shear retention in the crack plane. From here the horizontal branches of the crack progress in an unstable manner. The horizontal crack branches are clearly visible in Figure 2.2b.

After the loss of shear retention in the inclined crack, an arch structure emerges. Whether a beam fails in a compressive shear failure or a flexural shear failure is determined by the residual capacity of this arch as shown by Yang in [39]. If the arch is able to withstand the load at which the inclined crack forms, the beam

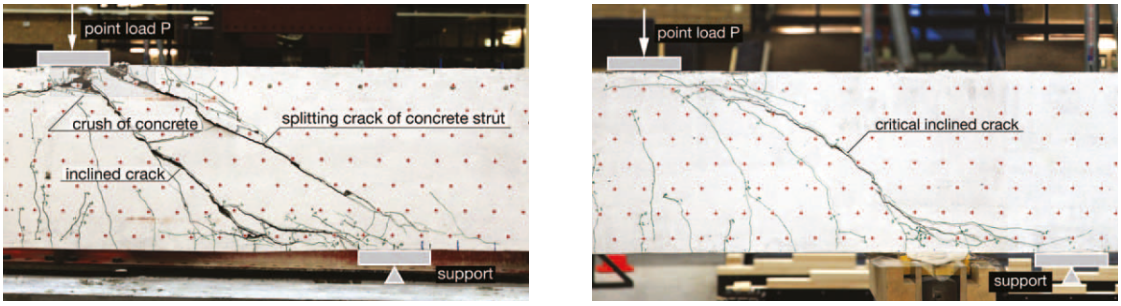

(a) Compressive shear failure

(b) Flexural shear failure

Figure 2.2: Flexural and compressive shear failure, taken from [39]

will ultimately fail with a compressive shear failure. (Figure 2.2a) If the arch is not able to withstand the load, a flexural shear failure is found (Figure 2.2b). Yang also concluded that therefore the location of the inclined crack is of importance to the failure mechanism and therefore capacity of the beam. Beams without shear reinforcement are most susceptible for this unstable and brittle failure mode. An extensive investigation and new analytical model have been presented by Yang in [39]. In this work it is stressed that the shear retention at very small crack widths is very important for buildup of shear resistance in a beam.

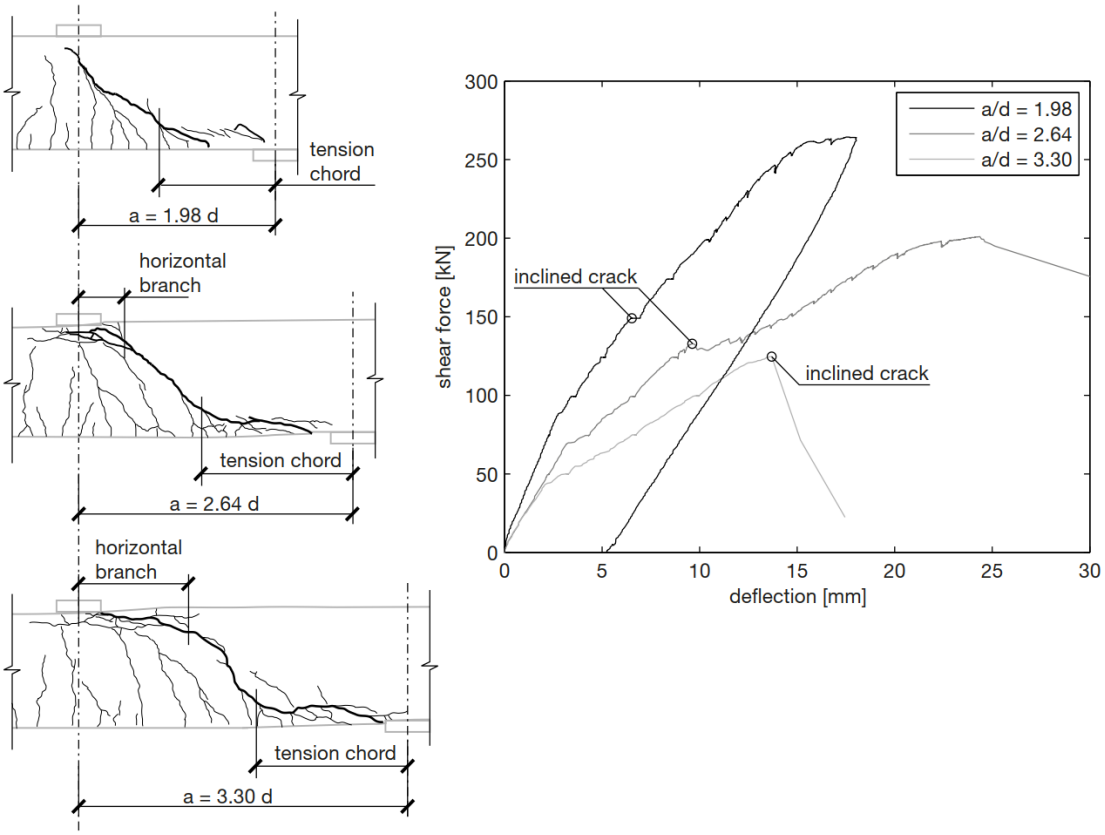

Figure 2.3: Behavior after formation of the inclined crack, image taken from Yang [39].

In Figure 2.3, which was taken from [39], this is visualized. Generally, a small shear span leads to a compressive shear failure due to the formation of a direct strut, while a large shear span will lead to brittle flexural shear failure. Inbetween those extremes, a failure mode exists where a dowel crack opens which drastically reduces stiffness while the load can still be increased with a significant amount.

2.1.3. Shear failure of beams with shear reinforcement

Beams with shear reinforcement can also fail in either a compressive shear failure. A difference is that the inclined crack is stabilized by vertical reinforcement. As described by Vecchio & Shim in [37], this failure mode is characterized by splitting and crushing of the concrete in the compression zone. Diagonal cracks can be observed, but no unstable splitting along the longitudinal reinforcement occurs. The compressive strut keeps rotating as the stirrups yield and the beam fails in the compression zone. Vecchio & Shim also noted that confinement effects in the zone below the loading plate have a significant role in the failure process [37]. A flexural shear failure is also possible; in case of inadequate shear reinforcement, stirrups will yield or even snap as the inclined crack opens.

2.1.4. Quantitative identification of failure modes in concrete beams

Determining the failure mode of a beam by inspecting crack patterns and load-displacement behavior can be an effective method. In some cases however, a failure mode might not be easily classified. It can be convenient to have a more objective way to classify failure modes. The big difference between shear failures and flexural failures is their *ductility*. Ductility is generally achieved by yielding of the reinforcement of the beam, as steel is generally a more ductile material than concrete. A way to quantify this was proposed by Engen et al. [16], by introduction of a '*ductility index*'. This is defined as the ratio between plastic dissipation in the reinforcement and plastic dissipation of the total system.

$$X_{ductility} = \frac{W_{plastic,steel}}{W_{plastic,total}} \tag{2.1}$$

In [16] a threshold value of $X_{ductility} = 0.6$ was taken into account to differentiate between brittle and ductile failures.

2.2. Two dimensional modelling of cracking and crushing in reinforced concrete beams

From the failure modes discussed above it can be concluded that modelling the cracking and crushing of concrete is a crucial aspect of correctly modelling such a failure mode. To do so, multiple approaches exist. A total strain (smeared) crack model is advised by [21]. This and the fact that a discrete crack requires some knowledge on the location of specific cracks cause that this thesis focuses on total strain crack models.

2.2.1. The smeared cracking assumption

A total strain model is a smeared approach to cracking, where the crack is modeled as a stiffness reduction in the continuum. In contrast to discrete cracks, no geometrical discontinuity is modelled. A typical quasi-brittle tensile stress-strain relation is shown in Figure 2.4a. At first, behavior is linear. After cracking the stiffness decreases drastically but the material still has some capacity. Finally the stress reduces to 0. This happens at a strain ε_{ult} [24].

$$\varepsilon_{ult} = \frac{5.136 G_f}{h f_t} \tag{2.2}$$

The strain in the cracked element is multiplied by a cracking bandwidth 'h' to obtain an absolute crack width. Note that the input parameters for the curve are the tensile strength and G_f (or G_c), the fracture energy. The area below the stress-strain relations equals G/h. This means that the ultimate strain depends on the bandwidth. From that it follows that smaller elements, generally resulting in a smaller bandwidth, show a more ductile behaviour than elements with a larger bandwidth.

The bandwidth h can either be specified for the whole model or determined per element. Two procedures are often used: The method Rots specified in his dissertation [30] or Govindjee's projection [20]. The first bases the bandwidth on the shape and other properties of the element, the latter also takes into account the direction of the crack as shown in figure 2.5. For this reason, all finite element models in this study are based on the formulation by Govindjee.

Within a total strain model, the important distinction is made between *rotating* and *fixed* crack models. A *rotating* crack keeps rotating so the crack aligns with the principal directions of the strain vector. A *fixed* crack does not rotate and contains a factor to describe shear stiffness retention of the crack. In between those

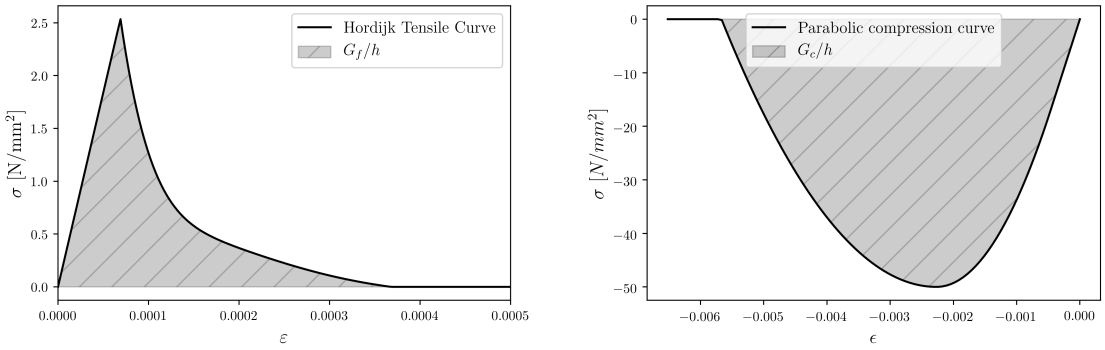

(a) Quasi-brittle tensile relation according to Hordijk [24]

(b) Parabolic compression relation for crushing of concrete. [17]

Figure 2.4: Typical stress strain relations for concrete

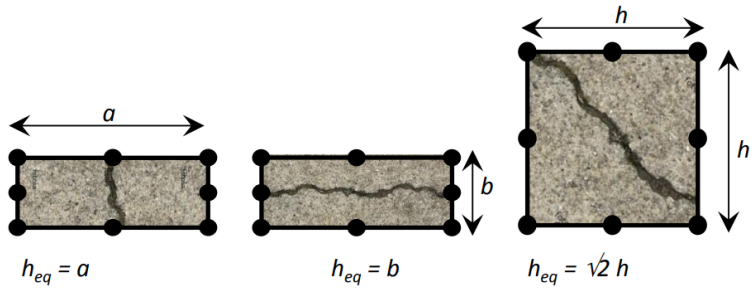

Figure 2.5: Crack band-widths with the crack orientation taken into account. Taken from [21]

models, a possibility exists to stop the crack from rotating when a certain strain is reached. It could be called 'Rotating-to-fixed' and is physically appealing, as in reality the formation of micro-cracks has some rotational capacity.

2.2.2. Shear behaviour of smeared cracks

The shear stiffness of a fixed crack can either be constant or depending on crack width. A reduction of the shear stiffness after cracking can either be based on multiplication of the shear stiffness terms by a factor β or by re-determination of the shear stiffness terms based on the reduced Young's modulus and Poisson's ratio. The reduction factor β can either be constant (2.3) or a function of the crack strain, as in (2.4)

$$G^{cr} = \beta G \tag{2.3}$$

$$G^{cr} = \frac{E^{cr}}{2(1+\nu^{cr})} \tag{2.4}$$

Physically, the shear stiffness should decrease as the crack opens. The use of constant shear relations is also discouraged in the Dutch guideline [21]. The damage based approach from (2.4) does not explicitly take aggregate interlock in to account. [39] stresses the importance of interlock at small crack widths for the development of shear force in beams without shear reinforcement. A thorough investigation of interlock behaviour was done in [38]. There relations are derived for interlock stiffness related to both crack opening as well as shear slip. An implementation of this was modelled in [3] and reported good agreement with test results. Unfortunately this model is not readily available.

The used finite element code currently takes the influence of aggregate interlock into account by a linear relation where the reduction factor of the shear modulus goes from 1 at crack opening to 0 at half the mean aggregate size. Studies like [35] have shown that this model tends to overestimate the shear stiffness in a crack and might result in an overprediction of the load bearing capacity. In [31] it was suggested to model the relation between shear modulus and crack opening as a linear relation, going to 0 where the 'ultimate crack

strain' is reached, not half the aggregate size. In that same publication, it was also suggested that a fixed crack should have little to no shear retention to avoid problems with excessive stress locking.

Stress locking is a problem occurring in smeared crack models. As no actual geometrical discontinuity occurs, reduction of the stress in a cracked integration point does not lead to relaxation of the neighbouring elements. Deformation of the cracked element results in spurious stresses that are 'locked' in around the localized crack, causing over-stiff responses as these elements do not release their energy. According to [31], it is more pronounced in models with fixed cracks with shear retention but also occurs in fixed cracks with $\beta = 0.0$ or even rotating cracks. A typical example is shown in Figure 2.6. Here the stresses around the crack are displayed for a fixed crack with constant $\beta = 0.05$.

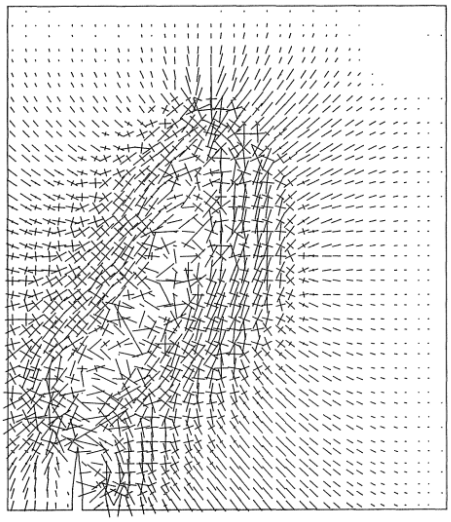

Figure 2.6: (severe) Stress-locking around a fixed crack in a notched specimen, from [31].

A smeared crack approach can also be applied to crushing of concrete. This can be important in flexural failures. Various stress-strain relations are available, those substantially more ductile than the tensile relations. A typical relation is presented in Figure 2.4b, it can be seen that after reaching the ultimate compressive strength the stress declines a more gentle manner, introducing some ductility in the behaviour.

2.3. Modelling of the bond of reinforcement in NLFEA

In Figure 2.7, the used interface models are shown for comparison. It's seen that the Shima curve, which is a function of both bar diameter and concrete strength, allows for a higher bond stress than the FIB models. For the FIB models, the most striking difference is the steep drop in strength of the unconfined concrete. In case of confined concrete, for instance because of the presence of stirrups, the degradation of bond stresses is more gradual. A gentle decline is observed because stirrups prevent splitting and finally keep confining the concrete, resulting in post-failure strength. [2]. The steep drop for unconfined models is numerically more challenging but physically attractive when compared to the brittle nature of splitting failure. Especially in beams without stirrups. The main question around the different bond-slip models is: How do they affect the global behavior of the beam? Secondly, a reinforcement bar can either be modelled fully bonded, with truss elements or with beam elements.

In recent thesis work at TU Delft it was concluded that a model with rotating cracks and fully bonded reinforcement should not be used for beams without shear reinforcement [35]. As a delamination-like behavior occurred around the reinforcement, resulting in a wrongful prediction of failure mode in all (nine) tested cases.

2.4. The influence of element size on finite element solutions of reinforced concrete beams

In a blind prediction contest about a 4000 mm deep beam without shear reinforcement at Toronto University [8], it was found in [6] that the resistance of the deep beam, solved with a fixed total strain crack model,

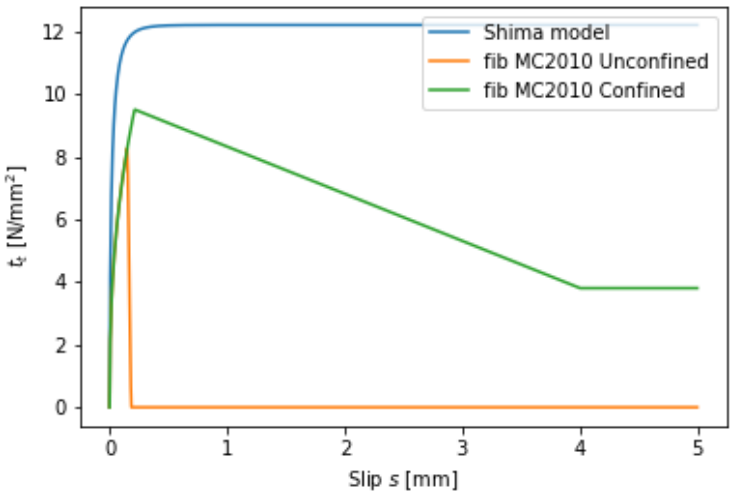

Figure 2.7: Bond-slip interfaces for a bar embedded in concrete.

exhibited strong mesh dependent behavior. Finer elements lead to an increase in both strength and stiffness while relatively large elements lead to underpredictions.

2.5. Iterative solving of the equations and the interpretation of numerical convergence

To determine whether or not an iterative solution has converged, the force and energy norms are generally used. Figure 2.8 shows how a norm is determined. The force norm indicates the unbalance force. The energy and displacement norms give an indication of the stability of the solution: when the displacements and with them the internal forces barely change between iterations, the step is converged to an equilibrium state regardless of equilibrium is found between internal and external forces.

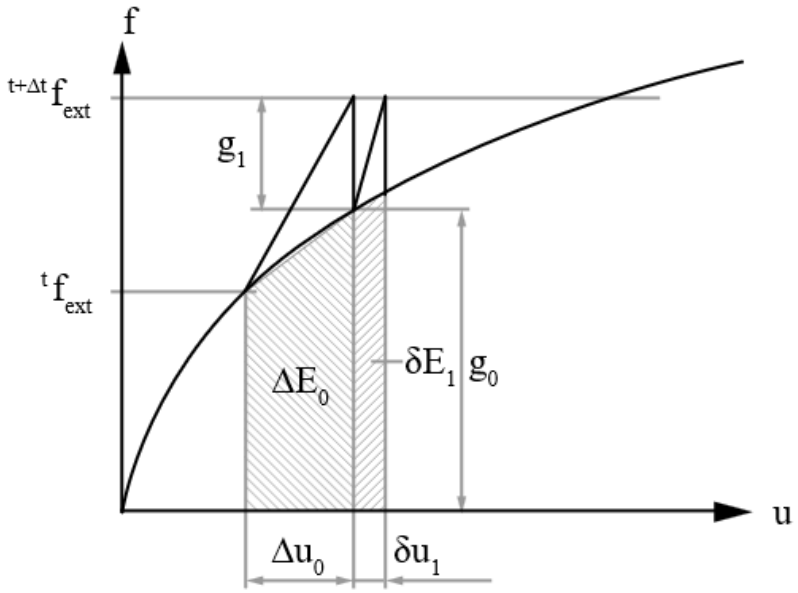

Figure 2.8: Convergence norms, taken from [5]

The relative energy variation is determined as in equation (2.5), in combination with Figure 2.8. The initial

displacement is scaled by the internal forces and compared to the additional displacement scaled by the new internal forces. When the additional energy variation is sufficiently small, convergence is accepted.

$$E = \left| \frac{\delta \mathbf{u}_i^T (f_{int,i+1} + f_{int,i})}{\Delta \mathbf{u}_0^T (f_{int,1} + f_{int,0})} \right| \tag{2.5}$$

Convergence on the force norm is judged as in equation (2.6). It checks for the euclidean norm of the out-of-balance force vector $\mathbf{g}_i$ to be a certain fraction of the euclidean norm of the initial force vector, $\mathbf{g}_0$.

$$F = \frac{\sqrt{\mathbf{g_i}^T \mathbf{g_i}}}{\sqrt{\mathbf{g_0}^T \mathbf{g_0}}} \tag{2.6}$$

A choice can be made to require either one of the norms to reach its' criterion or both of the norms (simultaneous convergence - SIMULT in Table 3.11). The standard tolerances listed in the RTD1016 are a relative variation of the energy norm of 0.001 and a relative variation of the force norm of 0.01. It is also mentioned that there is no consensus on these values [21]. Therefore the required tolerances are varied around those specified above.

It should also be noted that non-convergence is not the same as divergence. A non-converged step can be followed by converged steps and a successful analysis, while numerical divergence results in failure of the analysis and does not give information on failure of the beam.

The RTD1016 [21] advises two things on this matter: Firstly, a load step can be considered converged when either the force or energy norm is satisfied. Secondly, non-converged steps can still accepted as long as a an explanation for the temporary non-convergence can be provided and the steps are followed by converged steps. In the verification documents of this guideline [23], this translates to 'the highest applied load for which one of the convergence criteria is satisfied'.

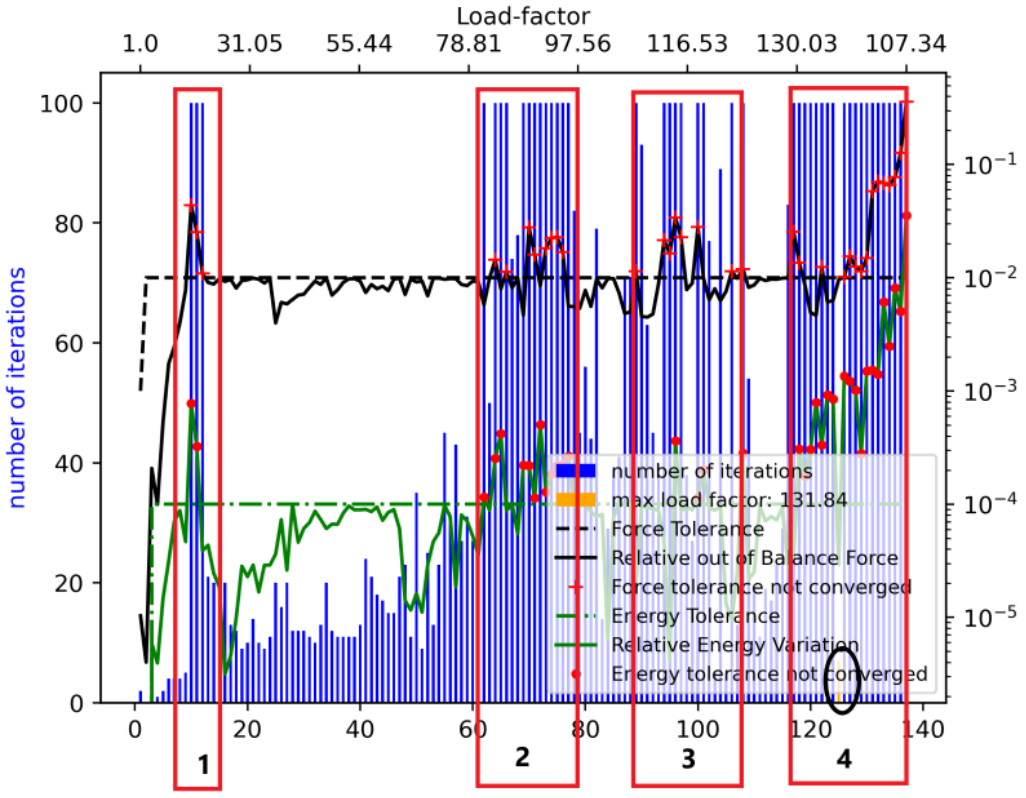

Figure 2.9: Typical convergence behavior for a reinforced concrete beam with tolerances 10^{-4} and 10^{-2} for the energy and force norms respectively.

When a total strain crack model is used for non-linear finite element analysis of reinforced concrete, convergence problems are often observed at certain stages of the analysis. Figure 2.9 displays the typical conver-

gence behaviour, in this case for beam C3 from [37]. Here the number of iterations per step is shown with a blue bar on the left-hand scale. The tolerance and relative variations are shown on the right-hand scale. At first, everything is behaving linear elastic and little to none iterations are needed. After that, cracking starts and more iterations are required. At some point, the cracks start localizing. This results in a small dip in the force displacement diagram and generally introduces convergence problems (zone (1) in Figure 2.9). The localisation is illustrated by the crack patterns in Figure 2.10.

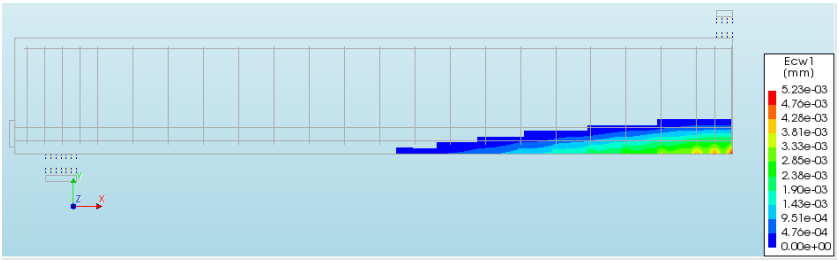

(a) Before localisation of cracking, step 8

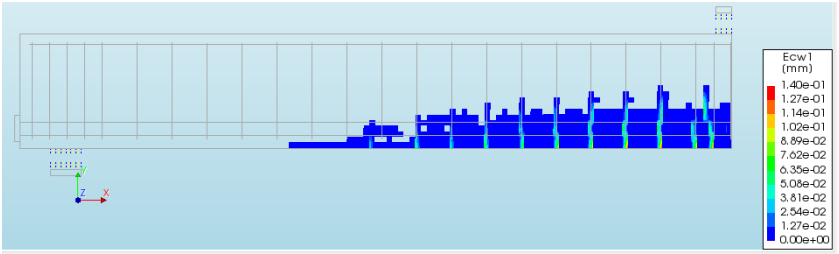

(b) After localisation of cracking, step 14

Figure 2.10: Formation of macro cracks

After some steps, the analysis starts converging again. When the cracks are opening in a stable manner, convergence is obtained easily. Then the inclination of cracks starts, as they open convergence is again more difficult (zone (2) in Figure 2.9). The opening of inclined cracks is shown in Figure 2.11.

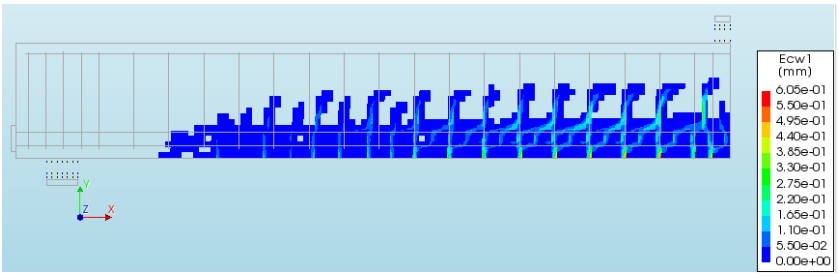

(a) Inclined cracks at step 60

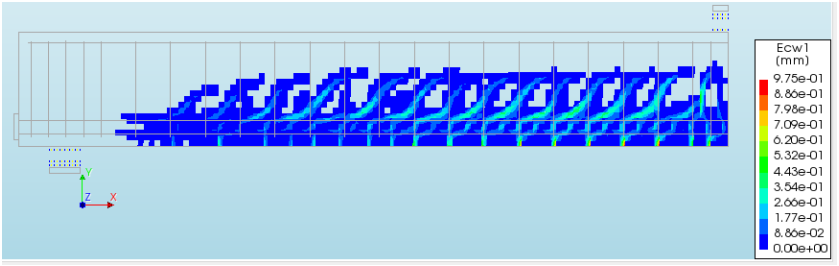

(b) Opened inclined cracks at step 80

Figure 2.11: Inclined cracking

Then, in zone (3), nonlinear effects like yielding of reinforcement and crushing of concrete start occurring, once again resulting in convergence difficulties. The plastic strain of the reinforcement is shown in Figure 2.12. Note the compressive yielding of reinforcement in the compression zone in Figure 2.12b, this indicates

substantial crushing of the concrete.

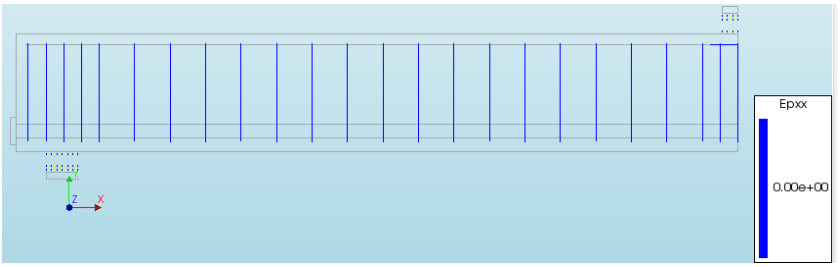

(a) Plastic strains of reinforcement at step 90

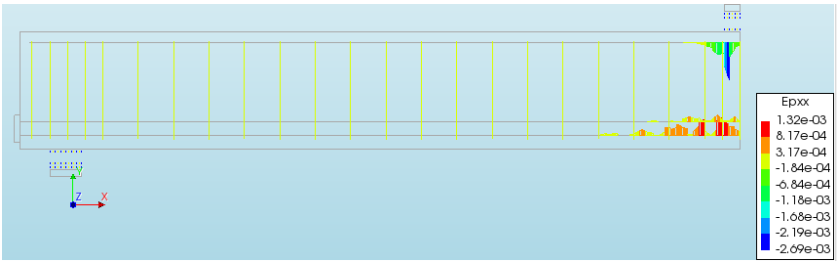

(b) Plastic strains of reinforcement at step 110

Figure 2.12: The onset of more non-linearities

When the non-linear behaviour stabilizes, the load increases again, until in zone (4) where the crushing of concrete and yielding of reinforcement come to a point where the load can no longer be increased and the beam fails. Naturally this introduces convergence problems. After the maximum load is reached (marked with the black oval in Figure 2.9), no steps converge and the load is reduced until the analysis fails.

2.6. The definition of a solution strategy for NLFEA

As mentioned above; the choices for constitutive relations, kinematic conditions and force equilibrium together make up a solution strategy. As the model uncertainty is related to the solution strategy, choices regarding physical, geometrical or other uncertainties are incorporated with different uncertainty factors. More on that will follow below.

2.6.1. Constitutive aspects of a solution strategy

In the nonlinear constitutive modelling of conrete materials, *cracking* and *crushing* play an important role. Many relations for both tensile and compressive behavior exist. For the nonlinear modelling of the reinforcement, a description of the yielding of the reinforcement is important. Other considerations concern taking into account confinement effects, reduction of compressive strength due to cracks and reduction of Poisson's' ratio of cracked concrete. Modeling confinement increases the compressive strength and ductility of the confined concrete. On the other hand, lateral cracking does the opposite for compressive strength and ductility so the compressive strength should be reduced in case of lateral cracking.

1. Concrete: Cracking(tension) and crushing(compression)model
2. (reinforcement) Steel: stress-strain behaviour and yielding behaviour
3. Elastic(linear) properties

2.6.2. Kinematic compatibility for the concrete beam and reinforcement

Within the kinematic compatibility the element discretization, boundary conditions and connectivity are specified.

In this study, finite element analysis results are compared to experimental results. It is therefore important to impose realistic boundary conditions. The kinematic assumptions also concern the *finite element discretization* and *element types* Symmetry can be used to reduce degrees of freedom and optimize the model. Boundary conditions

1. Concrete and reinforcement element type
2. Element size
3. Boundary conditions & symmetry
4. Interfaces and connectivity
5. Reinforcement bond interface

2.6.3. Equilibrium conditions

Comprises of the choices for loading, analysis control and solution of the equations. As the constitutive and kinematic conditions are specified, the load can be introduced to the model. This is done either by forcing a displacement or directly applying a force. Displacement control is often chosen because it is easier to find equilibrium. In some cases however, force controlled analysis is the only option. In those cases, an arc-length algorithm can be applied to find the equilibrium and determine the ideal load increments.

For each load increment, the equations are solved in an iterative manner, so at some point the iteration has to stop because the solution has converged towards the equilibrium state. A convergence criterion is subscribed to stop the iteration process. For these iterations, various methods can be used. When the convergence criterion is reached, the solution is accepted as converged and the load is incremented again. Often a maximum number of iterations is subscribed to prevent excessive time loss on non-converging steps.

1. Type of loading
2. Load incrementation
3. Analysis control
4. Iteration scheme and maximal amount of iterations
5. Convergence criteria

2.7. Uncertainty in NLFEA of concrete beams

2.7.1. Model uncertainty

A mechanical model is always an idealisation of a physical reality. Every choice in a solution strategy will impact the model uncertainty, just as everything that is not explicitly considered in the solution strategy. In literature like [27], the model uncertainty is described as follows in equation 2.7

$$\theta_i = \frac{P_{EXP,i}}{P_{NLFEA,i}} \tag{2.7}$$

The model uncertainty is defined as the relation between an experimental result and a result found with NLFEA, see equation 2.7. From here, a distinction between two relevant cases can be made: The modelling uncertainty can be defined as the result from various solution strategies for one experiment, as the result any solution strategy for any experiment or as the results of one solution strategy from various experiments [14]. In case one is looking to subscribe a solution strategy to a certain problem, the latter is the most relevant definition.

Engen et al reported that the model uncertainty can be represented as a log-normal variable with a mean of 1.1 and standard deviation 0.12, meaning a coefficient of variation of 11 %. [16]

2.7.2. Dutch Guidelines and Fib Model Code 2010

The Dutch guidelines offer three different ways to deal with uncertainty, these are based on the methods proposed in MC2010 [12] :
The partial factor method is a more traditional ULS verification method where design values for all the material properties are the input. The design resistance directly follows from the ultimate load in the finite element model.

$$R_{d;PF} = P_u \tag{2.8}$$

This has the downside, as also mentioned in [21], that low material parameters are input and therefore different structural behavior could be found. An alternative to the partial factor method could be the GRF (Global Resistance Factor)-method.

A global resistance factor is determined by combining the material safety factors and a modelling uncertainty factor of 1.06. The analysis is performed with slightly adapted concrete and steel properties such that the original safety factors $\gamma_c = 1.5$ and $\gamma_s = 1.15$ can be retrieved. (see [21])

$$\gamma_{GL} = \gamma_{Rd} \times 1.2 = 1.06 \times 1.2 = 1.27 \tag{2.9}$$

$$R_{d;GRF} = \frac{P_u}{\gamma_{GL}} \tag{2.10}$$

Global resistance factor The estimation of coefficient of variation, or ECOV, method requires two separate analyses to be executed. One with mean material properties and one with characteristic material properties. Assuming a log-normal distribution, a coefficient of variation is determined with the characteristic and mean result. This coefficient is used to determine γ_R. Again, the modelling uncertainty is incorporated by $\gamma_{Rd} = 1.06$

$$R_{d;ECOV} = \frac{P_{u;m}}{\gamma_{Rd}\gamma_R} \tag{2.11}$$

2.7.3. fib Model Code 2020

In the draft of MC2020 Ch27.10 : *"Design verification and assessment by non-linear finite element analyses"*, the chapter concerning NLFEA, the model uncertainty factor is important. The ECOV method is replaced by a sampling based method, allowing for Monte-Carlo like types of analysis. Factor γ_{Rd} is completely separated from any other sources of uncertainty and present in every formulation, also in the partial factor method.

By default, an analyst has to use $\gamma_{Rd} = 1.30$ as model uncertainty factor. This factor is determined by combining the uncertainty of blind predictions, so multiple strategies on one problem, with benchmarking results of various solution strategies. A Bayesian updating procedure is provided to allow an analyst to update γ_{Rd}. Benchmarking one's solution strategy will generally result in a lower factor. The details of this procedure are specified below.

2.8. Statistical and probabilistic properties of model uncertainty

2.8.1. Probabilistic distribution of model uncertainty

In literature, often a log-normal distribution is assumed for the model uncertainty. This is suggested in the JCSS model code [27]. Bayesian inference can be used to estimate the parameters of such a probability distribution. This procedure is used in [16] as well to determine a mean and coefficient of variation of the model uncertainty. When one already has information, but new information needs to be incorporated, Bayesian updating can be used for that. described in [27] and used in MC2020.

2.8.2. Bayesian inference

Bayes' theorem is used a well known part of probability theory. It is used to incorporate new information. 'What is the probability of A happening, given the fact that B is observed'. More formally put How to use this for the model uncertainty was adequately described in Engen et al. [16].
Let $\boldsymbol{\theta}$ be a sample of observed model uncertainties θ_i and $\mathbf{y}$ a set of the same size as $\boldsymbol{\theta}$ such that $y_i = \ln\theta_i$ for $\theta_i \in \boldsymbol{\theta}$. Under the assumption $\theta \sim Logn(\mu_\theta, \sigma_\theta^2)$, it holds that $y \sim N(\mu_y, \sigma_y^2)$. In case it is more likely that $\theta \sim N(\mu_\theta, \sigma_\theta^2)$, $\mathbf{y}$ should be taken as such that $y_i = \theta_i$. A statistical test can be used to determine the most likely distribution type. Often, the Shapiro-Wilk test [32] is used for this. More on this below. The sample mean and variance for $\mathbf{y}$ are than determined as in (2.1) and (2.2).

$$\overline{y} = \frac{1}{n}\sum_{i=1}^{n} y_i \tag{2.12}$$

$$s^2 = \frac{1}{n-1}\sum_{i=1}^{n} (y_i - \overline{y})^2 \tag{2.13}$$

The expected values of the posterior distribution parameters of y, given the information from sample $\mathbf{y}$, are then determined as in (2.3) and (2.4)

$$E[\mu_y|\mathbf{y}] = \overline{y} \tag{2.14}$$

$$E[\sigma_y^2|\mathbf{y}] = \frac{n-1}{n-3}s^2 \tag{2.15}$$

If necessary, recovering the expected distribution parameters μ_θ and σ_θ^2 from the distribution of y is done according to two equations specified in [16] :

$$\sigma_y = \sqrt{\ln V_\theta^2 + 1} \tag{2.16}$$

$$\mu_y = \ln \mu_\theta - \frac{\ln V_\theta^2 + 1}{2} \tag{2.17}$$

Here $V_\theta = \sigma_\theta / \mu_\theta$, means the coefficient of variation of the distribution of θ

2.8.3. Bayesian updating

When a prior distribution is known, new information can be added to prior to obtain a new posterior distribution. Let n_1, ν_1, $\overline{y}_1$ and s_1 be the prior distribution parameters. Then, with n_0 as the size of the sample, $\nu_0 = n_0 - 1$ the degrees of freedom of the sample, $\overline{y}_0$ the sample mean as in (2.12) and s_0^2 the sample variance as in (2.13).

$$n_2 = n_1 + n_0 \tag{2.18}$$

$$\nu_2 = \nu_1 + \nu_0 + 1 \tag{2.19}$$

$$\overline{y}_2 = \frac{1}{n_2}\left(n_0\overline{y}_0 + n_1\overline{y}_1\right) \tag{2.20}$$

$$s_2^2 = \frac{1}{\nu_2}\left(\nu_0 s_0^2 + \nu_1 s_1^2 + \frac{n_0 n_1}{n_0 + n_1}(\overline{y}_0 - \overline{y}_1)^2\right) \tag{2.21}$$

MC2020 has incorporated this and has given a set of prior distribution parameters that can be updated. These parameters were determined by a maximum likelihood estimate on the distribution of θ based on benchmarking solution strategies. Those values are specified in Table 2.1. With the 0-parameters coming from the sample and the prior parameters from Table 2.1, the posterior parameters are determined with (2.18)-(2.21).

Table 2.1: Prior distribution parameters in MC2020

n_1	1.4
ν_1	6.2
$\overline{y}_1$	0.02
s_1	0.1

With the posterior parameters, mean and variance of y are determined as in (2.22) and (2.23) respectively.

$$\mu_y = \overline{y}_2 \tag{2.22}$$

$$\sigma_y^2 = \frac{\nu_2(\nu_2+2)}{(\nu_2-1)(\nu_2+1)}s_2^2 \tag{2.23}$$

$$\mu_\theta \approx \exp \mu_y \tag{2.24}$$

$$V_\theta \approx \sigma_y \tag{2.25}$$

Finally, the modelling uncertainty factor can be determined as in (2.26). Here k_ν is determined in (2.27) and decreases as the number of samples increases.

$$\gamma_{Rd} = \frac{1}{\mu_\theta}\exp(\alpha_R \beta k_\nu V_\theta) \tag{2.26}$$

$$k_\nu = \frac{\nu_2}{\nu_2 - 0.25} \tag{2.27}$$

2.8.4. Normality and significance

A Shapiro-Wilkes test [32] is a statistical test which can be used to confirm whether or not it is likely that a certain set of variables was drawn from a normal distribution. Its hypothesis is that the data was indeed drawn from a normal distribution and returns a probability of this being true. If the p-value exceeds a certain value, usually 0.05, this hypothesis can not be rejected. In case the value is lower than 0.05, the normality hypothesis is rejected. This can be used to test log normality of the resulting sets of model uncertainties, as done in [16].

As the model uncertainty is regarded a random variable, a possibility exists that the uncertainty of different solution strategies is in fact the result of drawing from a distribution with the same mean. A paired t-test can be used in the same manner as the Shapiro test to verify that obtained results differ significantly. It makes use of the difference between two sets of variables and returns the probability that the set of differences has a mean of 0, meaning no significant difference exists. An important premise of this test is that the difference is normally distributed.

3

Methodology

In this chapter, the research questions are repeated and the methods towards answering them are presented. With those methods, also boundaries are set as to how the finite element results are interpreted. As specific model parameters will be varied, the choices for constant parameters are the same for all benchmarks. The standard model choices are explained and the variation of parameters in the solution strategies is presented. Finally, the judgment of the solution strategies is specified and the applied solution strategies summarized.

3.1. Approach to answering the research questions

The research questions are posed in 1.6 and are based around two important concepts. One being the accuracy and influence parameters of finite element solution strategies and the other one about usability of the ductility index.

1. What are important aspects of a solution strategy with respect to accuracy?

By simulation of many experiments from literature, solution strategies can be shown to be effective or not. The uncertainty is quantified as described in 1.3 and it is shown which strategies are the more suited ones. As the main objective is to advance the possibilities of application in the design field, all benchmark experiments are approached in exactly the same manner. The only exception is some mesh refinement for efficiency reasons, explained in 3.4. To limit the number of directions that have to be investigated, the following five aspects of the solution strategy are investigated:

1. **Total strain crack models:** The differences in performance between rotating and fixed cracks are investigated. Also the applicability of either model on different beam configurations.

2. **Convergence behavior** As, according to [21], no real consensus exists as to what norms and tolerances should be used, the impact of different configurations is investigated.

3. **Iteration process** The Dutch guideline clearly states that the maximal number of iterations is not part of the convergence criteria. It does however influence the found result, especially when incidental non-converged steps are accepted.

4. **Mesh size** The influence of element size on accuracy will be studied. A recent thesis by Teshome [35] already showed that the advise in the Dutch Guideline might be too coarse.

5. **Reinforcement models**. Many possibilities to model reinforcements exist. It will be investigated if there is a significant difference between Models to be considered will be: Embedded reinforcement, Shima bondslip curve[33] and the FIB-MC2010 [12] bondslip relation. Also, it is not clear whether beam elements or truss elements should be used for the reinforcement. This variation is investigated as well.

2. Is it possible to have one robust strategy for all concrete beams ?

The collection of beams used in the analysis is presented in chapter 4. Beams have been selected with different characteristics in mind. Some of the beams are notoriously complicated, others have been selected

because of their simplicity. Generally, attention has been paid to *four* important characteristics that are required to vary in the database:

1. **Experimental failure mode**
2. **Reinforcement configuration**, beams with shear reinforcement will behave differently from those without. For a robust approach, both need to be considered.
3. **Concrete compressive strength**, as all material parameters will be derived from this.
4. **Beam depth**

A solution strategy is judged on 3 criteria:

1. **Accuracy of failure load.** The solution strategies will be judged on the accuracy of the prediction of the actual failure load. In order to judge the accurracy, the model uncertainty is quantified for the used solution strategy. To do this, Bayesian updating is used to estimate the resulting distribution of the model uncertainty based on the benchmark analyses. The result of this is a mean model uncertainty and its coefficient of variation for the respective solution strategy.
2. **Consistency.** Consistency is regarded just as important for accuracy as the average error made. If a solution strategies produces both overpredictions and underpredictions, the standard deviation and coefficient of variation of the model uncertainty will be high. A high coefficient of variation increases the uncertainty introduced by the model choices. A consistent strategy is expected to display a relatively low coefficient of variation.
3. **The failure mechanism.** A correct prediction of the ultimate load combined with a wrong prediction of the failure mode raises questions about the credibility of the found failure load. This can be expressed as a percentage of correct failure modes.

3. How can a solution strategy be prescribed based on the properties of the beam?

Based on the results of each iteration of solution strategies, optimal strategies related to specific design parameters can be determined. When strategy 'A' yields significantly better results for beams with a certain characteristic and strategy 'B' yields better results for beams without that characteristic, it is sensible to subscribe a solution strategy based on the characteristic.

4. What is the relation between the ductility index and model uncertainty?

The ductility index is an indication of how much energy is dissipated in the reinforcement. That means it gives information on the failure mode found in the finite element model, but it does not tell anything about the correctness of the solution. To investigate the ductility index, an implementation of this factor has been made in the DIANA FEA software package. For each analysis, the ductility index at **maximum** load is reported. From here, a correlation with model uncertainty can be investigated. Next to that, the ductility index can be linked to a failure mode. The choice to look at the ductility index for the maximum load is motivated by the fact that convergence is hard after the peak load. Bad convergence often results in local spurious stresses and strains, which affect the ductility index.

The following questions can be answered for the most successful solution strategies:

1. What is the correlation between the model uncertainty and ductility for all cases?
2. What correlation can be found between model uncertainty and ductility index in case the correct failure mode is ensured?
3. What range of values does the ductility index take for respective failure modes?

3.2. Solution strategies

The boundary conditions and model parameters are, with exception from the varied parameters, the same for all models. This also holds for the way the models are set up. All the models are built with the same script where parametric input for dimensions, reinforcement, material properties, loading and support conditions is provided. In this section, the solution strategy is split into it's three components. For each component, the constant and variable parameters are presented.

3.3. The constitutive model considerations

The constant parameters of the concrete material model are based on the RTD1016 guideline [21] and the models available in the DIANA finite element package. The full selection of constitutive parameters is presented in Table 3.1 and explained below.

Table 3.1: Constant material model parameters

Density	2400 kg/m^3
Crack model	Total strain crack
Tensile curve	Hordijk (Figure 2.4a)
Compression curve	Parabolic (Figure 2.4b)
Tensile strength	f_{ctm}
Residual tensile strength	0 N/mm^2
Compressive strength reduction	Vecchio & Collins 1993 [36]
Minimal reduction factor	0.4
Confinement	Vecchio & Selby
Poisson Reduction	Damage based
Compressive strength	f_{cm}
Residual Compressive strength	0 N/mm^2
Crack bandwidth estimator	Govindjee projection

Confinement of the concrete is taken intro account using the relation proposed by Vecchio & Selby. Tension - compression interaction, better known as the reduction of compressive strength for concrete under tension is done according to the reduction factor proposed by Vecchio & Collins [36]. The minimal reduction factor is taken as 0.4, meaning that an integration point with a large enough crack retains only 40 % of its original compressive strength. The selected stress-strain relations for the concrete elements are presented in Figure 2.4. The input parameters for the curve are the tensile strength and G_f (or G_c), the fracture energy. The integral of the stress-strain relation equals G/h. This means that the ultimate strain depends on the bandwidth. From that it follows that smaller elements, generally resulting in a smaller bandwidth, show a more ductile behavior than elements with a larger bandwidth.

3.3.1. The determination of concrete material properties

All concrete material properties are derived from the mean concrete compressive strength according to the fib Model Code 2010 [12], the material properties as a function of f_{cm} are listen in Table 3.2. In Table 3.1 it is specified that f_{ctm} is used as the tensile strength in all cases. This is done because the uncertainty in the material properties is not represented in the model uncertainty, but should be accounted for with another reduction factor. For more information on this, the reader is referred to MC2010.

Table 3.2: Material properties as function of f_{cm} according to MC2010[12]

f_{ck} f_{ctm}:	$f_{cm}-8$	N/mm^2
≥ C50	$2.12 * ln(1+0.1 * f_{cm}))$	N/mm^2
< C50	$0.3 f_{ck}^{\frac{2}{3}}$	N/mm^2
E_{cm}	$21500 * (f_{cm} * 0.1)^{\frac{1}{3}}$	N/mm^2
G_F^I	$73 f_{cm}^{0.18}$	Nmm
G_C	$250 G_F^I$	Nmm

On the constitutive parameters, only the orientation of the cracks is varied, the variations can be seen in Table 3.3

Table 3.3: Variation of constitutive parameters

Set	Orientation	Shear retention
C1	Rotating	NA
C2	Fixed	Damage based

3.4. Assumptions around kinematic compatibility

Every beam is meshed with quadratic plane stress elements. The mesh for each beam is built up in the same way. A standard element size is specified as a fraction of the height of the beam. Meshes are as regular as possible and elements have an aspect ratio of 1:1 where possible. As can be seen in Figure 3.1, sometimes small inclinations are introduced by the loading plates. The thickness of the beam is taken care of in the geometry assignment. For that a 'thickness function' is used to be able to create I-profiles or other beams with a varying thickness over the length or depth. Here the thickness is defined as a function of x and y.

Table 3.4: Constant mesh parameters

Element type	Plane Stress
Element name	CQ16M - 8 Node Quadrilateral
Intgration scheme	3×3 Gaussian
Interpolation type	Quadratic
Aspect ratio	1:1 where possible

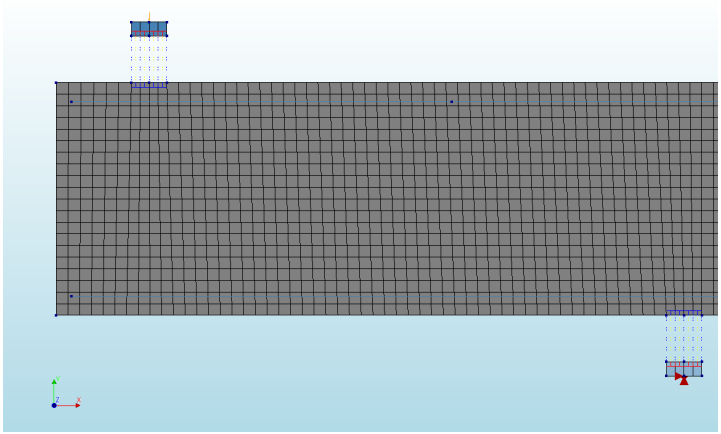

Figure 3.1: Standard mesh with 20 elements over the height of the beam

In some cases the area of interest is just a small part of the beam. In that case the beam is meshed with rough elements outside this area of interest and the finer mesh is only applied on the zone. Roughly two cases can be identified here: The first one is where the beam cantilevers out beyond the span of interest. In this case the span of interest is meshed with the actual element size and the spans outside that area are meshed with rougher elements. In the other case the beam has a large span where failure is expected in a smaller part of the span, as in the experiments by Yang & Koekkoek [40]. The refined zone then extends past the loading point over the same distance as the support to the loading point. This is shown in Figure 3.2.

Support conditions:
To accurately model support conditions, the buildup of tensile stresses near the support plates is to be avoided. Tensile stresses occur as them beam rotates over the support plate. These tensile stresses are prevented by using a no-tension interface between the plate and the beam. Other than that, the support conditions are taken from their respective papers.

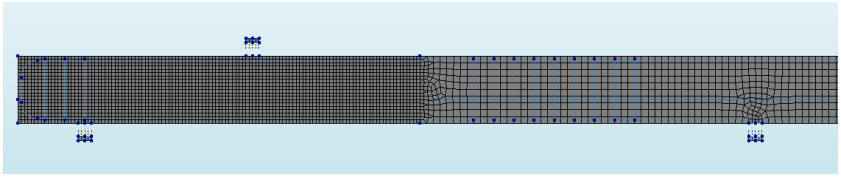

Figure 3.2: local mesh refinement

Table 3.5: Variation of kinematic parameters, with h the height of the beam is meant

Set	Mesh size
K1	h/10
K2	h/20
K3	h/30
K4	h/40

Table 3.6: Support plate properties

Element type	Plane Stress
Element name	CQ16M - 8 Node Quadrilateral
Intgration scheme	3×3 Gaussian
Interpolation type	Quadratic
Material	Linear elastic isotropic steel
Youngs Modulus	200000 N/mm^2
Poisson's ratio	0.3
Density	7800 kg/m^3

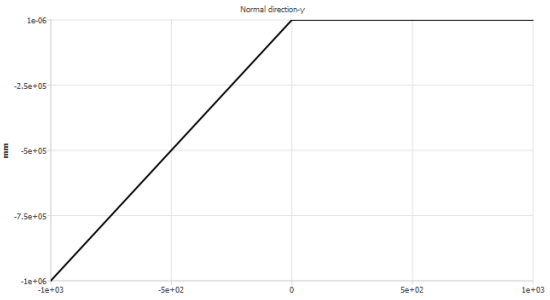

Figure 3.3: No-tension behavior of support line interface (traction - displacement)

Symmetry:
Where possible, symmetry is employed. This is done by constraining the symmetry plane for translation in x-direction. Figure 3.4 portraits these boundary conditions. It can also be seen that the reinforcement, when explicitly modeled, is constrained separately. In case of beam reinforcements, the rotation around the x-axis is constrained as well. To avoid unjustified modeling of arching effects, the leftover support is only restrained in y-direction. Symmetry is only used when the following criteria are met:

1. Reinforcement layout is entirely symmetric.

2. Beam is simply supported without unequal cantilevers.

3. Loading is symmetric, either in a four point bending fashion or one point loading in the center of the span.

Figure 3.2 is an excellent example of a beam where no symmetry was employed on grounds of both criterion 2 and 3.

Table 3.7: Support interface properties

Element name	CL12I
Element type	2D line interface
Intgration scheme	4-point Newton-Cotes
Interpolation type	Quadratic
Shear stiffness x	1 N/mm^3
Normal stiffness y	No-tension, see Figure 3.3

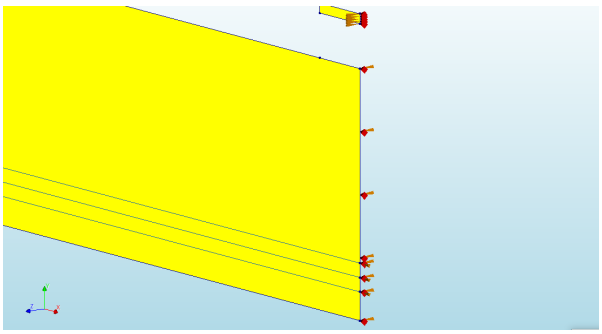

Figure 3.4: Symmetry boundary conditions

Reinforcement anchorage:
In case reinforcement anchor plates need to be modelled, as is the case in the beams from [37] and [29], this is done by applying a steel plate with the same properties as the loading plates and tying the horizontal displacement of the edge node of the reinforcement to the outer node at the anchor plate at the same height.

3.4.1. Reinforcement modeling - kinematic and constitutive choices

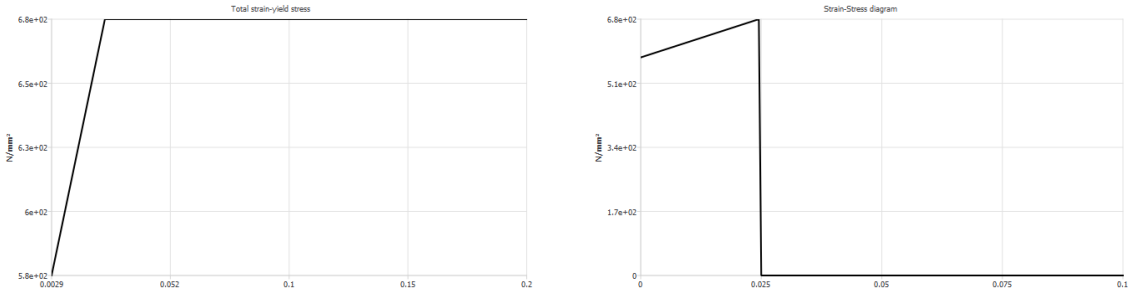

(a) Total strain - yield stress relation

(b) Plastic strain - stress relation

Figure 3.5: Stress-strain relations for reinforcement steel

The reinforcement is always modeled in as a discrete bar, so no smeared reinforcement has been applied. Table 3.8 lists the constant choices.

Table 3.8: Constant reinforcement model parameters

Plasticity model	Von Mises
Von Mises type	Isotropic linear hardening
Ultimate strain	25 ‰

Different hardening functions were used in cases of bondslip reinforcement or perfect bond. For a bond-slip bar, the 'total strain - yield stress hardening function was used as in Figure 3.5a. In case of perfect bond, an 'equivalent plastic strain - yield stress' function as displayed in Figure 3.5b was used.

Firstly, the influence of the presence of any slip is investigated, then the difference between slip models and finally the influence of the element type is investigated. Bondslip models have only been applied on the

longitudinal reinforcement. The investigated variations are listed in Table 3.9. Note that the CL9BE beam element is a class-III beam, which means shear deformation is included in the formulation.

Table 3.9: Variations of reinforcement model

Set	Element type	Element name	Interface model
R1	beam	CL9BE	Shima
R2	beam	CL9BE	FIB
R3	truss	CL6TR	FIB
R4	Embedded truss	NA	Perfect bond

3.5. Equilibrium conditions

3.5.1. Standard settings

Some standard choices have been made and listed in Table B.4. The initial step size is so that the experimental failure load would be reached in 50 steps. Because of arclength, this gets scaled back as the path becomes non-linear. All analyses are force controlled. Even though many of the benchmarks involved beams with proportional point loading that can be steered in displacement control, which is known to be more robust in numerical simulations, such displacement control was not adopted, on purpose. In practice, often distributed loads are present which means that an engineer has to resort to load control and arc-length procedures. The choice of force controlled analyses results in a requirement for arc-length control. If this would not be applied, it would be challenging to capture softening behaviour without diverging. Convergence is helped by a line search algorithm as well. The arc length needs control nodes, these are selected as the ones with maximal displacement in the linear static analysis.

Table 3.10: Analysis control parameters

Load steps	$P_{exp}/50$
Type	Force controlled
Analysis control	Arclength + Linesearch
Arclength control nodes	Max displaced in LINSTA
Iteration scheme	Regular Newton-Raphson, Tangential stiffness

3.5.2. Phases

The analysis is set up as a phased analysis. In phase 1, the self weight is applied together with pre-stressing loads (if any). In phase 2, until the analysis stops.

The analysis will stop if one of the following three criteria is met:

1. Divergence occurs
2. 350 steps have been finished
3. The crack width exceeds 15 mm

3.5.3. Convergence criteria

All iterations are done with a full Newton-Raphson, meaning the stiffness matrix is updated with each iteration. Different values for the convergence criteria explained in 2.5 will be investigated. These parameters are listed in Table 3.11

3.6. Definitions

3.6.1. Failure load and numerical stability

As this project is focusing on the *ultimate* limit state, the ultimate load has to be determined. For this the failure load of a finite element model needs to found. Here multiple definitions are possible as finite element models can fail in different ways: The best way would be to observe a decay of the capacity, paired with a drop in the force-displacement diagram and the formation of large cracks or extensive yielding of the concrete and

Table 3.11: Variation of equilibrium conditions

Set	Max iterations per step	Energy tolerance	Force tolerance	Simultaneous convergence of both norms [AND/OR]
E1	40	10^{-4}	10^{-2}	OR
E2	40	10^{-3}	10^{-2}	OR
E3	40	10^{-2}	10^{-1}	OR
E4	100	10^{-4}	10^{-2}	AND
E5	100	10^{-4}	10^{-2}	OR

steel. However, divergence could occur in the analysis before the specimen 'fails'. It should be noted that failure of the analysis is not the same as failure of the beam and that a maximum load obtained like this is not suitable for comparison with experiments. Next to that, the use of arc-length methods introduces the possibility of unloading without clear failure so just a drop in the load-deflection curve does not tell everything. It should always be accompanied by a sudden increase in crack width or plastic deformation. An example is used to explain this:

Figures 3.6a, 3.6b and 3.6c show an arbitrary beam at the maximum load step and the steps after that respectively. Figure 3.6d shows the load deflection curve of the same beam, Figure 2.9 shows the convergence behaviour, this is addressed later. Figure 3.6 shows a satisfying solution: The load-deflection curve shows a steep drop, while the maximum crack-width increases from 0.94 to 2.59 to 13.8 mm. Figure 2.9 shows that the maximal step is converged, after that equilibrium is no longer possible and the solution diverges.

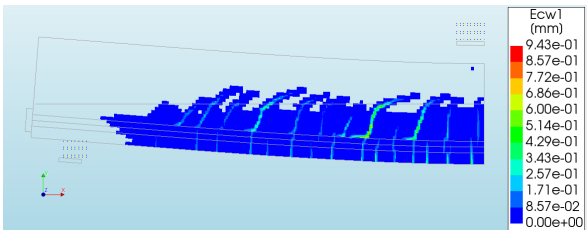

(a) Crack plot at maximum load step

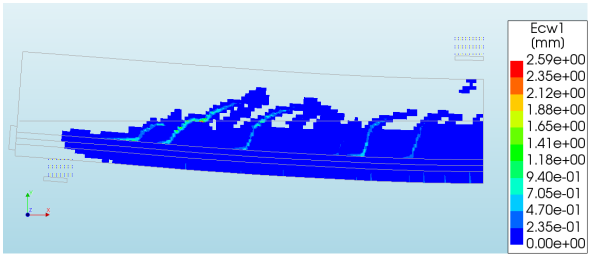

(b) One step after maximum load

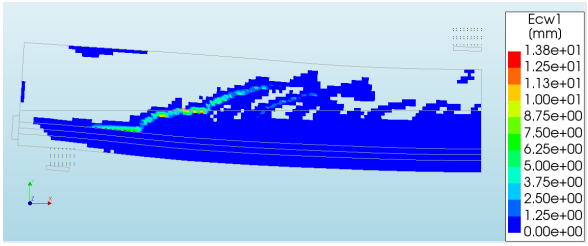

(c) Two steps after maximum load

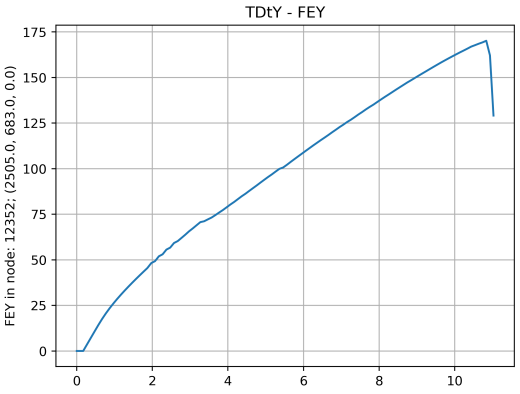

(d) Force-displacement behavior

Figure 3.6: Simulation of failure in a beam without shear reinforcement (Beam OA2 from [4])

3.6.2. Failure modes

To investigate the results for the ductility index, definitions of different failure modes are required: What is the critical event, where is the energy dissipated and what is the general shape of the force-displacement diagram.

Shear compression: Compressive shear is identified by failure of the compressive strut:

1. Splitting and crushing in the compression zone are observed

2. The energy is dissipated by the concrete, hence a low ductility index can be expected. Some stirrup yielding can result in a non-zero ductility index.

3. As the concrete is ultimately failing in compression, a more gentle drop in the force displacement relation can be expected.

The plots in Figure 3.7 show the compressive shear failure of beam VS-A1. At ultimate load, large shear cracks have opened, extending towards the compression zone (Figure 3.7a). The plastic strain in the reinforcement are shown in Figure 3.7b. It can be seen that the main plastic strain is in the vertical reinforcement and compression zone. Finally, the beam fails in the compression zone. This is illustrated in Figure 3.7c.

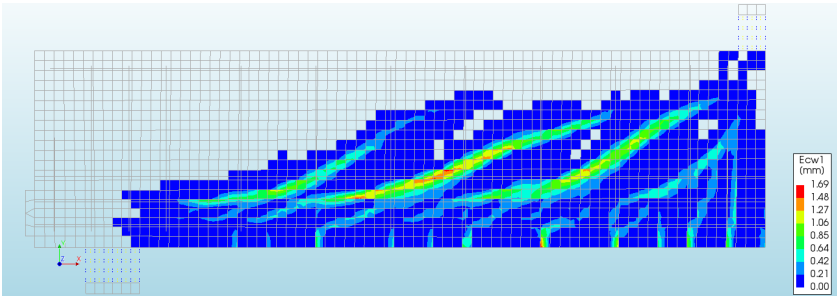

(a) Crack plot of beam A1 from [37] at ultimate load

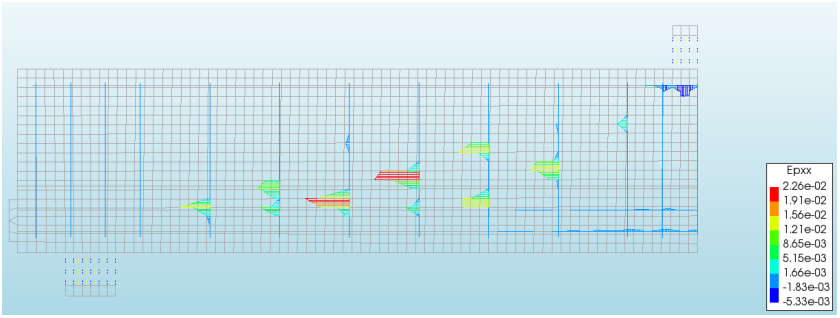

(b) Plastic strains in reinforcement of beam A1 from [37] at ultimate load

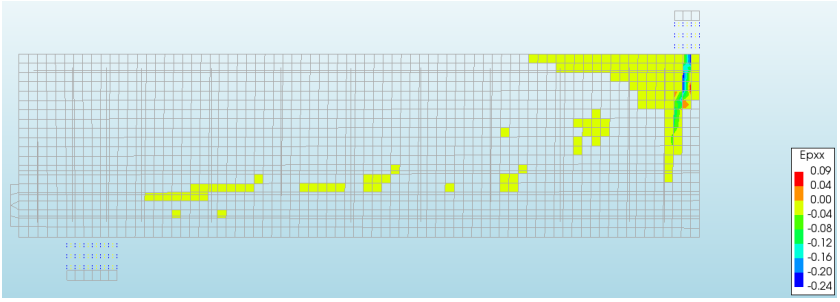

(c) Plastic strains in beam A1 from [37] post-failure

Figure 3.7: Compressive shear failure: Beam A1 from [37]

Flexural bending failure: When a beams fails in a flexural manner, yielding of the longitudinal reinforcement and ultimately crushing in the concrete compressive zone are observed:

1. The critical event is either excessive yielding of the longitudinal reinforcement, crushing of the compression zone or both. Crushing of the compression zone is identified by the observation of compressive strains in the concrete larger then 3.5 ‰. No splitting occurs in the compression zone.

2. As the beam fails in bending, not shear, most energy is dissipated by yielding of the longitudinal reinforcement, this should result in a high ductility index.

3. The force-displacement diagram should show an increase in displacement while the maximum load is sustained.

Figure 3.8 shows the class example of a flexural failure resulting from a NLFEA. The crack plot in 3.8a shows some inclined cracking, but no critical behaviour there. The main opening cracks are in no way inclined. The plot of the plastic strain of the reinforcement in 3.8b shows pronounced yielding of the longitudinal reinforcement, yet no yielding of the stirrups.

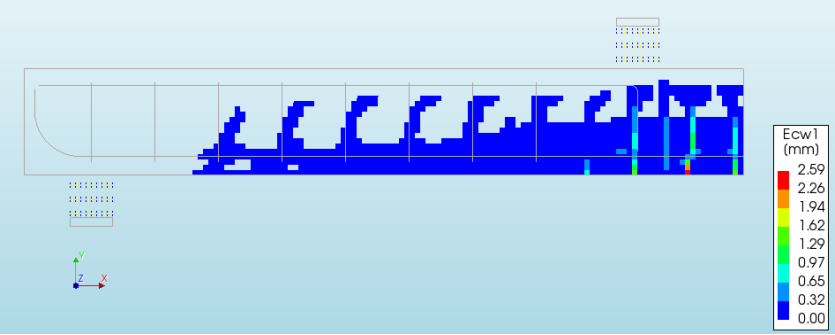

(a) Crack plot of beam M3 from [1] at ultimate load

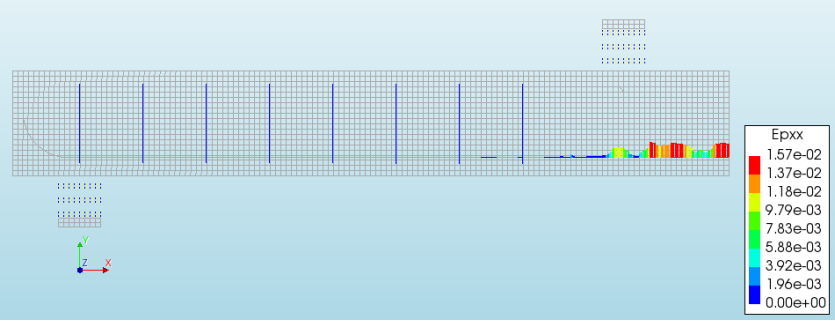

(b) Plastic strains in reinforcement of beam M3 from [1] at ultimate load

Figure 3.8: Flexural failure: Beam M3 from [1]

Flexural shear failure:

1. The critical event is loss of load carrying capacity by opening of the critically inclined crack. This can be either towards the load plate, along the longitudinal reinforcement or both.

2. It is possible that some energy is dissipated by yielding of longitudinal reinforcement before the critical crack opens.

3. A brittle failure will be indicated by immediate loss of strength.

A typical flexural shear failure can be seen in Figure 3.6.

3.6.3. Experimental failure mode

The experimental failure modes are obvious in most cases, as their respective studies either indicate the failure mode or the force-displacement characteristics and pictures of the failure are included. Experiments do not often result in dubious failure modes, as a researcher is generally interested in a specific behaviour and therefore designed his or her experiment to be able to study that behaviour.

For the study of the ductility index, this is less obvious as it is not generally reported whether an experiment fails in a brittle or ductile manner. In some cases there was some indication. For the beams tested by Vecchio & Shim it was reported that no pronounced yielding of the tension reinforcement was detected [37]. In cases where this detail was not reported, an interpretation is made with the failure mode and force-displacement behaviour. Experimental failure modes are classified ductile in case of obvious flexural failure. Semi-ductile behaviour, like crushing of the compression zone without pronounced yielding of the tensile reinforcement is regarded brittle. The same is the case for beams with stirrups that fail in shear, regardless of stirrup yielding.

3.7. Judgement of solution strategies

3.7.1. Determination of mean and coefficient of variation

For each solution strategy, the distribution parameters of the model uncertainty are determined using Bayesian inference with a non-informative prior distribution. This is the same approach as described by Engen et al. in [16]. The Bayesian updating procedure as described in the MC2020 draft and above is used to determine the actual model uncertainty factor γ_{RD} for a standard reliability index and a target reliability of 50 years. The bias of a solution strategy is something that can be corrected for, the variance is of greater importance. If a strategy were to overestimate every experiment by exactly 10 %, the variance of θ_i would be 0 and then there would be no uncertainty as the correction for the bias would result in the exact failure load. The group of beams is also split into two groups: Beams with and without shear reinforcement to show the difference in accuracy of approximation between those groups for different solution strategies.

3.7.2. Failure modes

The number of correctly found failure modes can be expressed as a percentage of the the total number benchmarks. A failure mode is correct when:

1. The force displacement behavior fits the experimental behavior qualitatively[1]
2. The critical event that leads to failure is the same as in the respective experiment.

Generally, both criteria fail when a wrong mode of failure is predicted. In the case of finding a brittle failure instead of a ductile one, the force displacement behavior will exhibit a steep drop and the critical event leading to failure will be different. The correct criteria are as described in 3.6.2.

3.7.3. Significance of results

If the premise of normality of the difference between sets θ_i was not rejected, the paired t-tests for statistical significance can be used to see if differences are significant.
All statistical tests are performed at a significance level of 0.05 in the following manner:
H_0: The mean uncertainty is the same
H_1: The mean uncertainty is not the same
Reject H_0 in favor of H_1 if $p < 0.05$
For this to be valid, the assumption that the model uncertainty is a continuous log-normally distributed variable is used.

3.8. Summary and overview of selected solution strategies

An overview has been given of all 19 choices in the solution strategy. The requirements for beams have been summed and it is specified how obtained data will be treated.

[1] This means general shape, the exact failure load may differ from the experiment

Table 3.12: Variations that have been simulated

	Constitutive	Kinematic			Equilibrium	
	Crack orientation	Mesh	Reinforcement	Interface	Max. Iterations	Convergence norms
F1	Fixed	h/20	Embedded truss	Fully bonded	40	E: 0.0001 OR F: 0.01
F2	Fixed	h/20	Beam	Shima	40	E: 0.0001 OR F: 0.01
F3	Fixed	h/20	Beam	Shima	40	E: 0.001 OR F: 0.01
F4	Fixed	h/20	Beam	fib	40	E: 0.0001 OR F: 0.01
F5	Fixed	h/30	Beam	Shima	40	E: 0.0001 OR F: 0.01
F6	Fixed	h/20	Beam	Shima	40	E: 0.01 OR F: 0.1
F7	Fixed	h/40	Beam	Shima	40	E: 0.0001 OR F: 0.01
F8	Fixed	h/20	Beam	fib	100	E: 0.0001 AND F: 0.01
F9	Fixed	h/20	Beam	fib	100	E: 0.0001 OR F: 0.01
F10	Fixed	h/20	Truss	fib	100	E: 0.0001 OR F: 0.01
R1	Rotating	h/20	Embedded truss	Fully bonded	40	E: 0.0001 OR F: 0.01
R2	Rotating	h/20	Beam	Shima	40	E: 0.0001 OR F: 0.01
R3	Rotating	h/20	Beam	Shima	40	E: 0.001 OR F: 0.01
R4	Rotating	h/20	Beam	fib	40	E: 0.0001 OR F: 0.01
R5	Rotating	h/10	Beam	Shima	40	E: 0.0001 OR F: 0.01
R6	Rotating	h/30	Beam	Shima	40	E: 0.0001 OR F: 0.01
R7	Rotating	h/20	Beam	Shima	100	E: 0.0001 AND F: 0.01
R8	Rotating	h/20	Beam	fib	100	E: 0.0001 OR F: 0.01
R9	Rotating	h/20	Truss	fib	100	E: 0.0001 OR F: 0.01

Table 3.13: Unchanged parameters

Concrete constitutive model	
Density	2400 kg/m^3
Crack model	Total strain crack
Tensile curve	Hordijk (Figure 2.4a)
Compression curve	Parabolic (Figure 2.4b)
Crack bandwidth estimator	Govindjee projection
Tensile strength	f_{ctm}
Residual tensile strength	0 N/mm^2
Compressive strength reduction	Vecchio & Collins 1993 [36]
Minimal reduction factor	0.4
Confinement	Vecchio & Selby
Poisson Reduction	Damage based
Compressive strength	f_{cm}
Residual Compressive strength	0 N/mm^2
Steel Constitutive model	
Density	7800 kg/m^3
Plasticity model	Von Mises
Von Mises type	Isotropic linear hardening
Ultimate strain	25 ‰
Kinematic assumptions	
Element type	Plane Stress
Element name	CQ16M - 8 Node Quadrilateral
Intgration scheme	3×3 Gaussian
Interpolation type	Quadratic
Aspect ratio	1:1 where possible
Support and loading interface	
Element type	2D line interface
Element name	CL12I
Intgration scheme	4-point Newton-Cotes
Interpolation type	Quadratic
Shear stiffness x	1 N/mm^3
Normal stiffness y	No-tension, see Figure 3.3
Equilibrium conditions	
(initial) load step size	P_{exp}/50
Type	Force controlled
Analysis control	Arclength + Linesearch
Arclength control nodes	10 max displaced in linear static analysis
Iteration scheme	Regular Newton-Raphson, tangential stiffness

4

Selection of experiments to benchmark the solution strategies

In this chapter, the selection of the benchmark beams will be explained and the incorporated experiments will be shortly described. For detailed descriptions of beams and experimental procedures, the reader is referred to the original publications.

4.1. Characteristics to include

In order to obtain a representative data set, the benchmark experiments need representative properties. Many beams from many experiments have been selected based on various properties. As mentioned above, attention has been paid to:

1. Experimental failure mode
2. Reinforcement configuration
3. Concrete compressive strength
4. Beam depth

The selection of benchmarks happened both by seeing what beams are often used for benchmarking as well as arbitrarily taking beams from projects that were investigating a range of different aspects of concrete beams.

Figure 4.1 shows how reinforcement ratio and concrete strength are distributed. The concrete strength is quite evenly distributed from 20 MPa to 100 MPa, this follows from both the histogram in Figure 4.1b as well as the distribution of data points in Figure 4.1a. The histogram in Figure 4.1c shows reinforcement ratio having some extremes. These can be seen in Figure 4.1a as well.

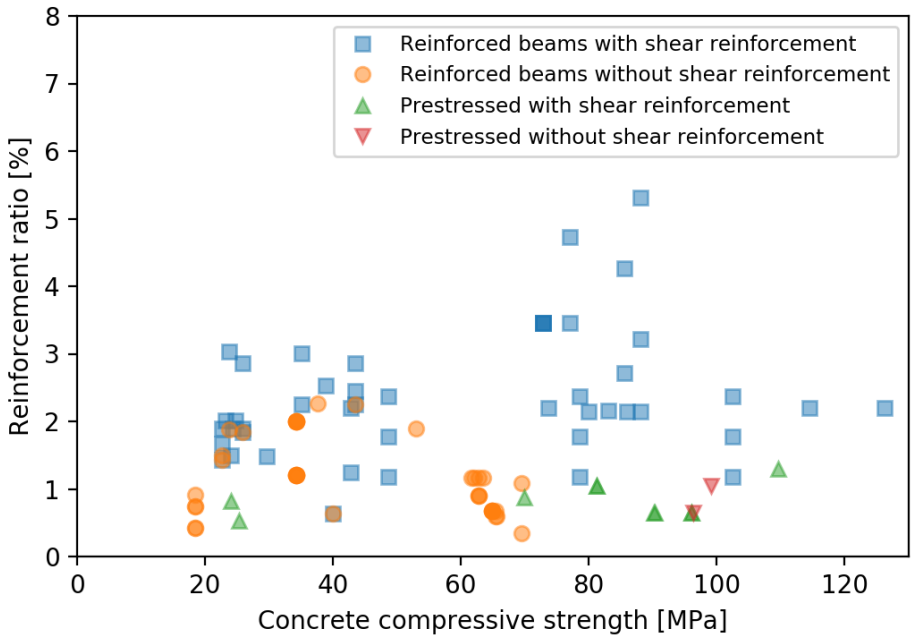

(a) Scatter of concrete strength and reinforcement ratio

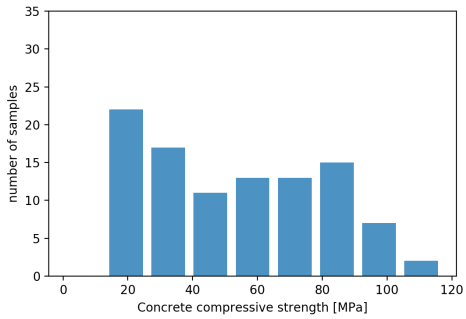

(b) Distribution of concrete strength

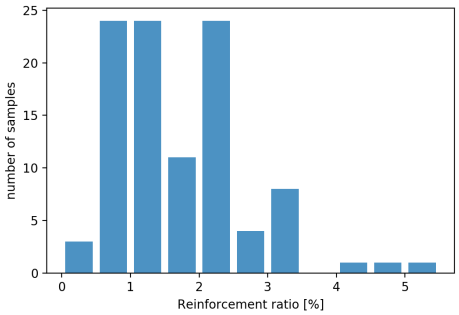

(c) Distribution reinforcement ratio

Figure 4.1: Concrete strength and reinforcement ratio of samples

4.2. List of benchmarks

4.2.1. Vecchio & Shim, 2004 [37] and Bresler & Scordelis, 1963 [4]

The beams tested in these experiments are over-reinforced and generally fail in a shear-compressive manner. Over the history, the study by Bresler & Scordelis is used often to verify finite element formulations or analytical calculation methods. In 2004, the experiments were recreated by Vecchio & Shim. As there are subtle differences in the beam compositions and results, both sets of beams were included.

These sets both contain 12 beams, of which 3 without shear reinforcement. The beams without shear reinforcement all fail in flexural shear. In other instances, the main reinforcement, shear reinforcement, beam length and concrete strength are varied. Vecchio & Shim modelled the beams as well and found that the 1963 beams were generally underestimated. They stated that this was the case because the Bresler-Scordelis beams were tested quite early. Early age and moist, concrete has favorable shear-compression behavior. [37].

4.2.2. Ashour, 2000 [1]

This study was an investigation of the flexural behavior of reinforced concrete beams made with high strength concrete. Nine beams were tested with 4-point bending tests. A distinction can be made in groups of three. Each group has a concrete strength (normal, medium and high). Over each group, the reinforcement config-

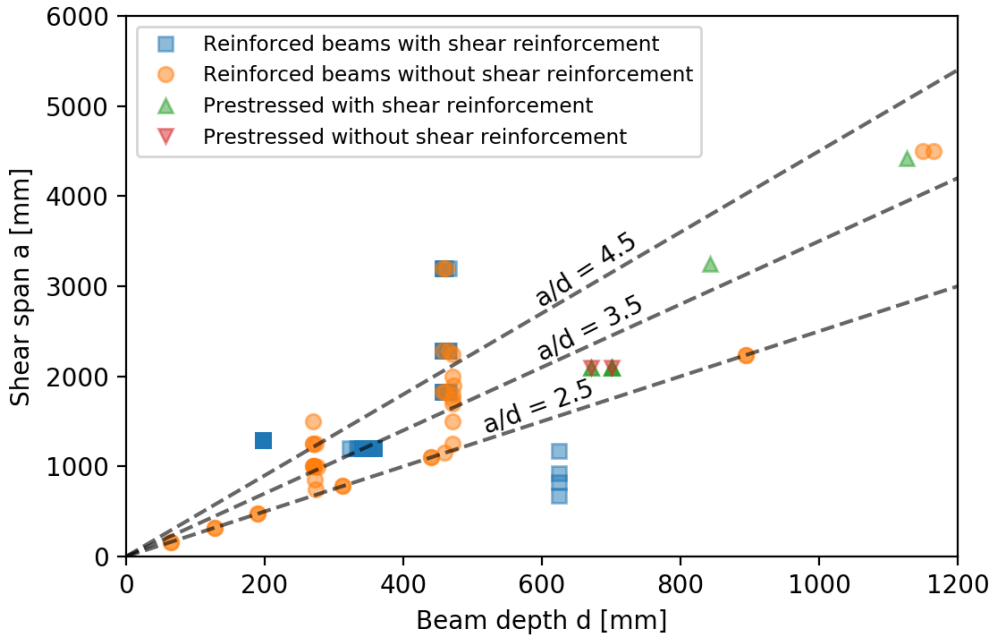

(a) Scatter of shear span and beam depth

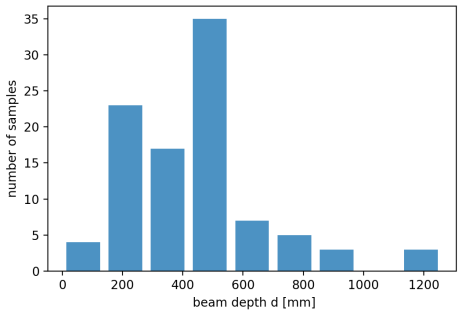

(b) Distribution of beam depth

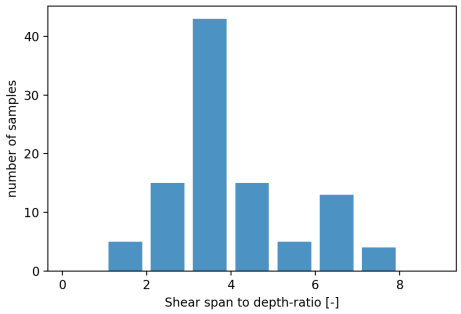

(c) Distribution of a/d ratio

Figure 4.2: Depth and shear span of selected samples

uration is varied from 2 bars to 4 bars. This results in 9 unique beams that are all included based on the idea that in many engineering situations the flexural behavior is most important.

4.2.3. Rashid & Mansur, 2004 [29]

A study similar to [1], but a more extreme variation of reinforcement ratio and concrete strength. The beams are also deeper than those tested by Ashour and since the shear reinforcement is varied, shear is as important as flexure in correctly modeling the beams from this experiment.

4.2.4. Foster & Gilbert, 1998 [18]

In 1998, Foster & Gilbert tested numerous deep beams.Some of them were included for their depth. With a beam depth of 700mm the beams are deeper then most other beams in the study. The deepest beams exhibited crushing of the loading column. As this would be the only beam with that failure mode, only 700 mm deep beams were selected.

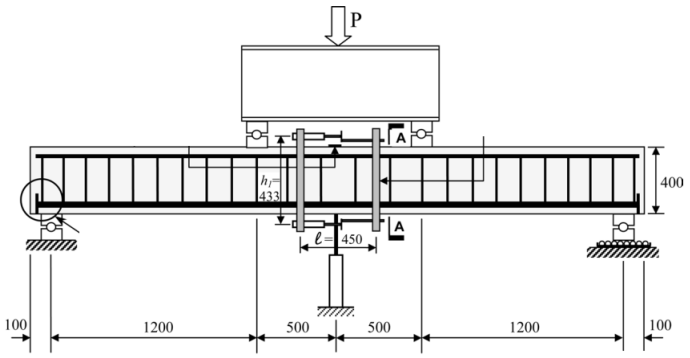

Figure 4.3: Test setup as used by Rashid & Mansur, figure taken from [29]

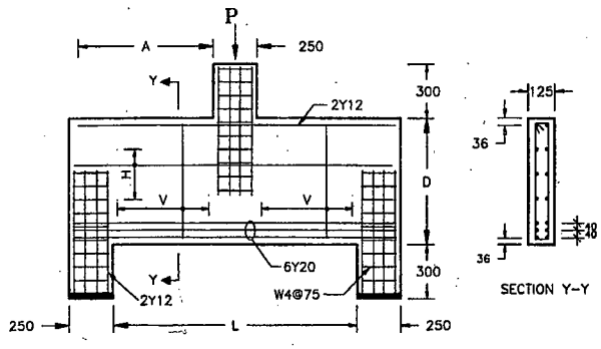

Figure 4.4: Impression of deep beam experiments by Foster & Gilbert, figure taken from [18]

4.2.5. Ghannoum, 1998 [19]

This study was done concerning the size effect in concrete beams without shear reinforcement. Beams with heights ranging from 90 to 985 mm were tested in a 4 point bending tests until one of the two shear spans failed in shear. The other shear span was more heavily reinforced and was tested after external strengthening of the first failed span. These beams were included for height variation and the fact that they do not contain shear reinforcement.

4.2.6. Collins & Kuchma, 1999 [9]

Beam SE50A-45, also known as 'Beam 8' was notoriously difficult in a prediction contest surrounding the publication and is an important beam for bench-marking finite element solutions. It was used to raise awareness of the safety concerns around unreinforced and lightly reinforced concrete structures. The beam itself has identical shear spans and the listed failure load is the average of two reported values, displaying some experimental variability as well.

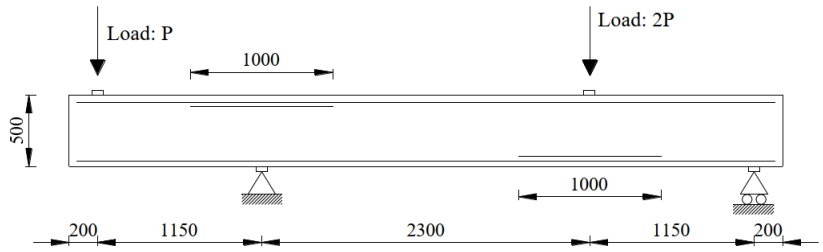

Figure 4.5: Impression of 'Beam 8' , taken from [22].

4.2.7. Yang & Koekkoek, 2016 [40]
An extensive study into the transition from flexural to shear failure in beams without shear reinforcement was done by Yang and Koekkoek. Many high strength-beams of different heights were tested, the shear span was reduced until the failure mode transitioned from flexural failure to shear failure. These beams are challenging to model, as a conservative approach about shear failure will result in not finding the flexural failures for shear spans that resulted in flexural failures in the experiment. Nevertheless, these experiments are well documented and it is accepted that sometimes the failure load is underestimated. It would however, from an engineering point of view, be unacceptable to find a numerical flexural failure while the experiment shows a shear failure.

Each beam was used for multiple tests by moving supports and load points per test to obtain multiple spans. This is not be modelled in the beams, so some stiffness differences due to previously existing flexural cracks are expected.

4.2.8. Leonhardt & Walter, 1962 [25]
Leonhardt did a lot for the development of knowledge on concrete structures. Two beams were taken from a large study on shear behaviour. One of the beams does not contain any shear reinforcement and the other one does, this is the only difference between those beams. The beams were tested in 4-point bending tests.

4.2.9. Choulli, 2005 [7]
As prestressed beams are generally deeper than reinforced beams, some were included to get more height differences. Prestressed beams do also show different failure modes as they are more likely to have non-rectangular cross sections. This particular study was part of a PhD project concerning the shear behaviour of prestressed I-girders. A large amount of beams in various reinforcement configurations were tested in a 3-point bending manner.

4.2.10. Prestressed beams from RTD1016 validation [23]
In addition to the tests by Choulli, some more prestressed beams were added:
PB1, a case from [26]. This is a post-tensioned beam with a height of 900mm which fails in flexure.
PB2, a girder with a total depth of 1600mm, from [34]. This beam failed in shear.
PB4, another beam from [26], also failing in shear.

4.2.11. Beams H123 and H352
Three beams were tested by Dr. Y. Yang at Delft University of Technology in 2019 and used in a blind prediction contest regarding the RTD-1016 guideline. Many submissions overpredicted the failure load substantially, with predicted loads going up to 200 % of the actual failure load. Both beams failed in shear. Design H352 was lightly reinforced and tested twice, in one case a dowel failure occurred and in the other case a flexural shear failure occurred, showing how experimental variability should not be forgotten. Beam H123 had double the reinforcement and was tested once, resulting in a flexural shear failure too. The design of both beams is shown in Figure 4.6. Interestingly, the failure loads of these beams were found to be significantly lower than the capacities determined with major codes as well. At the moment of writing, this is an ongoing topic of research at Delft University of Technology .

Both beams have a height of 1200mm and are meant to be representative for deep slabs without shear reinforcement, as often applied in large infrastructure. The stirrups in the right hand span are meant to enforce failure in the left hand side. Reinforcement yield strength is 580 MPa and the concrete cylinder strength 69.5 MPa.

4.3. Summary
To summarize, all specimen have been collected in Table 4.1. In this table, the used code along with the experiment, the year, concrete strength, reinforcement ratio, shear span, beam depth, failure mode, ultimate load and the presence of shear reinforcement are specified:

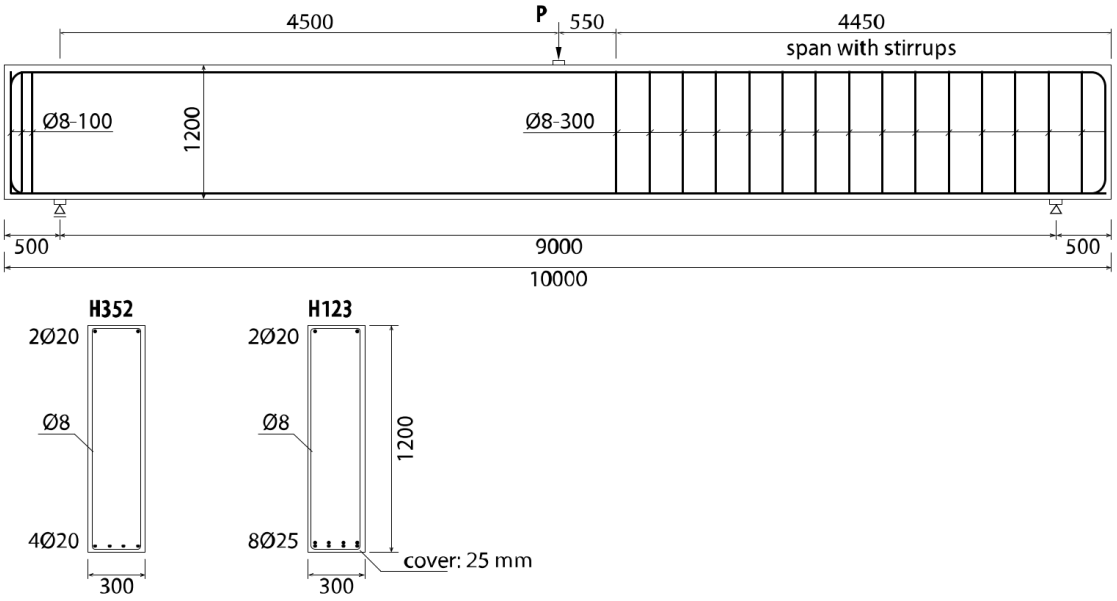

Figure 4.6: Beams H123 and H352, taken from the competition handout

Table 4.1: All selected benchmark experiments

Beam	Year	f_{cm} [N/mm^2]	ρ [%]	a [mm]	d [mm]	a/d [-]	Failure	P_{exp} [kN]	Stirrups
B-H2 [1]	1998	102.4	1.18	1290	198	6.52	F	88.06	Y
B-H3 [1]	1998	102.4	1.77	1290	198	6.52	F	128.31	Y
B-H4 [1]	1998	102.4	2.37	1290	198	6.52	F	167.60	Y
B-M2 [1]	1998	78.5	1.18	1290	198	6.52	F	89.84	Y
B-M3 [1]	1998	78.5	1.77	1290	198	6.52	F	123.89	Y
B-M4 [1]	1998	78.5	2.37	1290	198	6.52	F	160.88	Y
B-N2 [1]	1998	48.6	1.18	1290	198	6.52	F	90.19	Y
B-N3 [1]	1998	48.6	1.77	1290	198	6.52	F	124.96	Y
B-N4 [1]	1998	48.6	2.37	1290	198	6.52	F	154.34	Y
BS-OA1 [4]	1963	22.6	1.50	1830	461	3.97	FS	334	N
BS-OA2 [4]	1963	23.7	1.88	2285	466	4.90	FS	356	N
BS-OA3 [4]	1963	37.6	2.27	3200	462	6.93	FS	378	N
BS-A1 [4]	1963	24.1	1.50	1830	466	3.93	CS	468	Y
BS-C1 [4]	1963	29.6	1.49	1830	464	3.94	CS	312	Y
BS-B1 [4]	1963	24.8	2.01	1830	461	3.97	CS	446	Y
BS-B2 [4]	1963	23.2	2.01	2285	466	4.90	CS	400	Y
BS-A2 [4]	1963	24.3	1.89	2285	464	4.92	CS	490	Y
BS-C2 [4]	1963	23.8	3.04	2285	464	4.92	CS	324	Y
BS-A3 [4]	1963	35.1	2.25	3200	466	6.87	FC	468	Y
BS-B3 [4]	1963	38.8	2.53	3200	461	6.94	FC	356	Y
BS-C3 [4]	1963	35.1	3.00	3200	459	6.97	FC	270	Y
HAP2E [7]	2005	96.34	0.65	2100	700	3.00	S	435.9	N
HAP1W [7]	2005	99.15	1.04	2100	671	3.13	S	747.56	N
HAP2TE [7]	2005	95.97	0.65	2100	700	3.00	S	790.48	Y
HAP2TW [7]	2005	95.97	0.65	2100	700	3.00	S	886.92	Y
HCP2TE [7]	2005	90.24	0.65	2100	700	3.00	S	721	Y
HCP2TW [7]	2005	90.2	0.65	2100	700	3.00	S	683	Y
HCP1TE [7]	2005	81.17	1.04	2100	671	3.13	S	779	Y
HCP1TW [7]	2005	81.17	1.04	2100	671	3.13	S	741	Y
B2.0A-4 [18]	1998	86	2.15	675	624	1.08	F	1900	Y
B2.0-1 [18]	1998	83	2.15	825	624	1.32	SC	1590	Y
B3.0A-4 [18]	1998	88	2.15	925	624	1.48	F	1550	Y
B3.0-1 [18]	1998	80	2.15	1175	624	1.88	F	1020	Y
N90NORTH [19]	1998	34.2	2.00	162.5	65	2.50	FS	74.5	N
N90SOUTH [19]	1998	34.2	1.20	162.5	65	2.50	FS	41.1	N
N155NORTH [19]	1998	34.2	2.00	318.75	127.5	2.50	FS	109.8	N
N155SOUTH [19]	1998	34.2	1.20	318.75	127.5	2.50	FS	82.5	N
N220NORTH [19]	1998	34.2	2.00	475	190	2.50	FS	119.7	N
N220SOUTH [19]	1998	34.2	1.20	475	190	2.50	FS	100.6	N
N350NORTH [19]	1998	34.2	2.00	781.25	312.5	2.50	FS	173.1	N
N350SOUTH [19]	1998	34.2	1.20	781.25	312.5	2.50	FS	152.6	N
N485NORTH [19]	1998	34.2	2.00	1100	440	2.50	FS	206.7	N
N485SOUTH [19]	1998	34.2	1.20	1100	440	2.50	FS	178.9	N
N960NORTH [19]	1998	34.2	2.00	2235	894	2.50	FS	360	N
N960SOUTH [19]	1998	34.2	1.20	2235	894	2.50	FS	340.5	N
PB4 [26]	1973	24.02	0.82	3250	840	3.87	SC	1491.12	Y
PB1 [26]	1973	25.3	0.53	3250	843	3.86	F	1897.5	Y
A111 [29]	2005	42.8	1.25	1200	357.5	3.36	F	342.84	Y
A211 [29]	2005	42.8	2.20	1200	357.5	3.36	F	461.3	Y
B211a [29]	2005	73.6	2.20	1200	357.5	3.36	F	500.9	Y
B311 [29]	2005	72.8	3.46	1200	340.8	3.52	F	751.96	Y
B312 [29]	2005	72.8	3.46	1200	340.8	3.52	F	730.22	Y
B313 [29]	2005	72.8	3.46	1200	340.5	3.52	F	742.94	Y
B321 [29]	2005	77	3.46	1200	340.8	3.52	F	765.06	Y
B331 [29]	2005	72.8	3.46	1200	340.8	3.52	F	772.8	Y

B411 [29]	2005	77	4.73	1200	332.5	3.61	F	950.4	Y
C211 [29]	2005	85.6	2.71	1200	350.8	3.42	F	650.42	Y
C311 [29]	2005	88.1	3.22	1200	346.7	3.46	F	730.12	Y
C411 [29]	2005	85.6	4.26	1200	335	3.58	F	901.4	Y
C511 [29]	2005	88.1	5.31	1200	322	3.73	F	880.6	Y
D211 [29]	2005	114.5	2.20	1200	357.5	3.36	F	605	Y
E211 [29]	2005	126.2	2.20	1200	357.5	3.36	F	595.2	Y
SE50A-45 [9]	1999	53	1.90	1150	459	2.51	FS	162	N
PB2 [34]	2007	109.63	1.30	7500	1712	4.38	SC	6983	Y
VS-A1 [37]	2004	22.6	1.43	1830	457	4.00	SC	459	Y
VS-A2 [37]	2004	25.9	1.84	2285	457	5.00	SC	439	Y
VS-A3 [37]	2004	43.5	2.26	3200	457	7.00	FC	420	Y
VS-B1 [37]	2004	22.6	1.90	1830	457	4.00	SC	434	Y
VS-B2 [37]	2004	25.9	1.90	2285	457	5.00	SC	365	Y
VS-B3 [37]	2004	43.5	2.45	3200	457	7.00	FC	342	Y
VS-C1 [37]	2004	22.6	1.67	1830	457	4.00	SC	282	Y
VS-C2 [37]	2004	25.9	2.86	2285	457	5.00	SC	290	Y
VS-C3 [37]	2004	43.5	2.86	3200	457	7.00	FC	265	Y
VS-OA1 [37]	2004	22.6	1.43	1830	457	4.00	FS	331	N
VS-OA2 [37]	2004	25.9	1.84	2285	457	5.00	FS	320	N
VS-OA3 [37]	2004	43.5	2.26	3200	457	7.00	FS	385	N
A121A1 [40]	2015	62	1.17	1500	269.5	5.57	F	115.9	N
A121A3 [40]	2015	61.6	1.17	1000	269.5	3.71	FS	144.6	N
A122B1 [40]	2015	62.8	1.16	1000	270.5	3.70	FS	152.3	N
A123B1 [40]	2015	63.44	1.16	1250	270	4.63	F	138	N
A901A1 [40]	2015	62.8	0.90	1250	274	4.56	F	105.6	N
A901A3 [40]	2015	62.8	0.90	750	274	2.74	FS	145	N
A902A1 [40]	2015	62.8	0.90	995	276	3.61	FS	120.7	N
B501B1 [40]	2015	65.44	0.59	1800	471.5	3.82	FS	165.7	N
B502A1 [40]	2015	65.52	0.59	1900	472.5	4.02	F	166.9	N
B701A1 [40]	2015	64.8	0.67	2250	471.5	4.77	F	175.1	N
B701A2 [40]	2015	64.8	0.67	2000	471.5	4.24	F	179.5	N
B701A3 [40]	2015	64.8	0.67	1750	471.5	3.71	F	185.7	N
B701B1 [40]	2015	64.88	0.67	1700	471.5	3.61	F	193.6	N
B701B2 [40]	2015	64.9	0.67	1500	471.5	3.18	FS	202.4	N
B702A1 [40]	2015	65.36	0.67	1250	471.5	2.65	FS	183.2	N
C451A2 [40]	2015	18.4	0.42	1000	272.5	3.67	F	58.6	N
C451B1 [40]	2015	18.4	0.42	850	272.5	3.12	F	58.5	N
C751A1 [40]	2015	18.4	0.74	1250	270	4.63	F	76.5	N
C751B1 [40]	2015	18.4	0.74	1000	270	3.70	F+S	82.8	N
C901A3 [40]	2015	18.4	0.91	1000	271.5	3.68	FS	84.1	N
H123	2018	69.52	1.09	4500	1150	3.9	S	445	N
H352	2018	69.52	0.35	4500	1165	3.9	S	211	N
E3 [25]	1962	32.95	2.47	750	270	2.78	F+S	369.7	Y
E6 [25]	1962	34.5	2.47	750	270	2.78	FS	182.4	N
BM100 [28]	1998	46	0.76	2700	925	2.9	SC	672	Y

5

A quantification of the model uncertainty entailed with different aspects of solution strategies

Using the 19 solution strategies and 101 benchmarks, 1919 finite element models have been executed. In this chapter the results from those 1919 NLFEAs are used to establish the sensitivity of non-linear models to specific aspects of solution strategies. As the results differ substantially between beams with and without shear-reinforcement, these cases are regarded separately.

A complete overview of all obtained uncertainty parameters is listed in A and individual results were reported in [11].

5.1. The effect of the constitutive model on the variation of results

The impact of the constitutive model, which is limited to the crack orientation in this thesis, is first shown by the investigation of two solution strategies. Both solution strategies use the CEB-FIB MC2010 bondslip curve, a maximum of 100 full Newton-Raphson iterations per step with a convergence criterion of either E = 0.0001 or F = 0.01, the only difference between them is the application of a fixed crack with damage based shear retention in F9 and a rotating crack in R8. All beams have 20 elements over the height.

5.1.1. Fixed crack

The results of solution strategy F9 are displayed in Figure 5.1. Striking is that the models of beams without stirrups show good agreement with their experimental counterpart, while the failure load of beams with stirrups tends to be underestimated. Distribution parameters of the model uncertainty were calculated and listed in Table 5.1. Next to the distribution parameters of the displayed results, properties of the model uncertainty for all solution strategies are listed as well.

From Figure 5.1 it can be seen that the ultimate capacity of beams without shear reinforcement is in no case overpredicted more than 20 %. Also, only 2 cases show an underprediction of more than 20 %.

All 1010 models with a fixed crack result in an average model uncertainty μ_θ = 1.15 with a coefficient of variation of 0.20. For just the beams without stirrups μ_θ is found to be 0.99 with a coefficient of variation of 0.14. As expected from the plots in Figure 5.1, μ_θ for beams with stirrups is higher: 1.27 and it's coefficient of variation equals 0.18. The results for just solution strategy F9 are significantly better, indicating that a solution strategy with a fixed crack is quite sensitive to modelling choices.

5.1.2. Rotating crack

The rotating crack models appear to be more accurate for the beams with shear reinforcement, yet show some severe over- and under-predictions of the experimental failure load for the beams without stirrups.

Similar to strategy F9, strategy R8 does not show any overpredictions by more than 20 % for the beams with shear reinforcement. Some cases do however show an underprediction of more than 20 %.

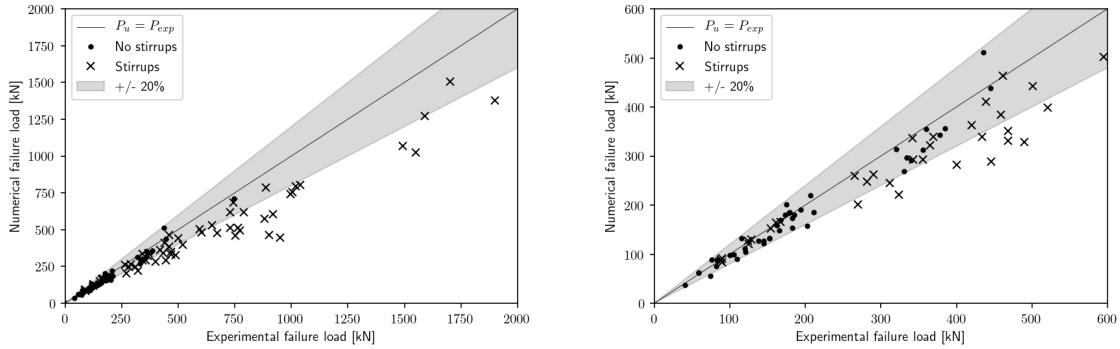

(a) All results for F9

(b) Results F9 zoomed in

Figure 5.1: NLFEA and experimental ultimate load for solution strategy F9 - Above the line is progressive, below the line is conservative

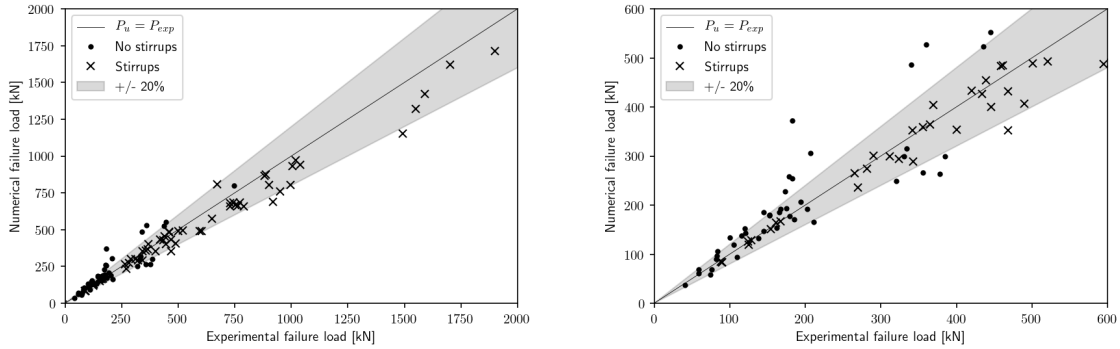

(a) All results for R8

(b) Results R8 zoomed in

Figure 5.2: NLFEA and experimental failure load for solution strategy R8

A comparison of the presented strategies is made in Table 5.1. The distribution parameters have been determined with the prior distribution adopted in the MC2020 draft. The data presented in the table confirm the appearances from Figures 5.1 and 5.2: Beams with stirrups are best approximated with a rotating crack model, with a reduction factor of $\gamma_{Rd} = 1.05$ and a mean value of model uncertainty $\mu_\theta = 1.08$. The same model results in scattered results for beams without shear reinforcement: $\gamma_{Rd} = 1.40$ and $\mu_\theta = 0.93$. The reduction factor is related to the model uncertainty as described in 2.26.
A different behaviour is observed concerning the fixed crack model. For the beams without shear reinforcement, this results in $\gamma_{Rd} = 1.08$ and $\mu_\theta = 1.05$. Beams with stirrups are systematically underestimated: $\gamma_{Rd} = 0.99$ and $\mu_\theta = 1.24$.

Table 5.1: Determined model uncertainty

	All Beams			Beams with stirrups			Beams without stirrups		
Reinforcement type	μ_θ [-]	V_θ [-]	γ_{Rd} [-]	μ_θ [-]	V_θ [-]	γ_{Rd} [-]	μ_θ [-]	V_θ [-]	γ_{Rd} [-]
R8 - Rotating (101 Beams)	1.006	0.176	1.232	1.075	0.097	1.047	0.925	0.213	1.404
F9 - Fixed (101 Beams)	1.158	0.169	1.061	1.243	0.172	0.993	1.053	0.108	1.084
All Rotating (909 Beams)	1.01	0.18	1.22	1.07	0.10	1.05	0.94	0.23	1.40
All Fixed (1010 Beams)	1.13	0.20	1.13	1.25	0.18	0.99	0.99	0.15	1.20

5.1.3. Probability density functions

The fitted log-normal probability distributions in Figure 5.3, show what is also shown with Figures 5.1, 5.2 and Table 5.1. Strategy F9 displays a high-density log-normal distribution with short tails for beams without stirrups (black line) and long tails for the beams with stirrups (red line), while R8 shows high density for beams

with stirrups and low density with a long tail for beams without stirrups. An important difference between Figures 5.3b and 5.3a is the orientation of the tails of the total distributions (blue line). For F9, the tail is at in the direction $\theta_i > 1$, meaning conservative results. The tail of R8 is oriented towards $\theta_i < 1$, meaning the opposite of that.

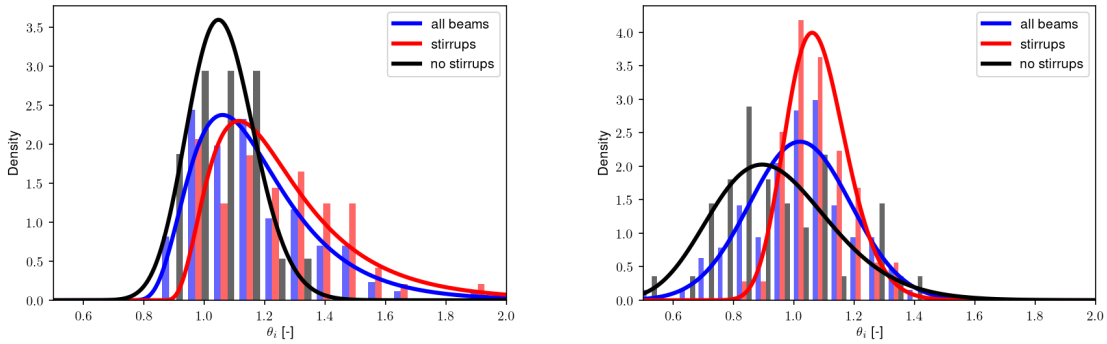

(a) Log-normal fits for all beams and with/without stirrups F9

(b) Log-normal fits for all beams and with/without stirrups R8

Figure 5.3: Distributions of model uncertainty for P8 and F9

From the results in Table 5.1, something else comes to light when comparing the found distribution parameters for R8 to the distribution parameters of all beams with a rotating crack and stirrups. Those distribution parameters are more or less equal. For the fixed crack solutions on beams without stirrups, it appears that the uncertainty is more sensitive to choices on the kinematic compatibility and equilibrium conditions. More on this behaviour of rotating and fixed cracks for beams without shear reinforcement follows below.

5.2. The effect of different kinematic conditions in solution strategies

Next to the variation of constitutive parameters, the kinematic compatibility has been varied too. Due to the substantial difference in behavior of rotating and fixed cracks, the kinematic compatibility was investigated for both types of models.

5.2.1. Mesh-dependency of models with a rotating crack

The mesh dependency of solution strategies with a rotating crack has been investigated for meshes with 10, 20 and 30 elements over the beam height. The results of this in Figure 5.4a-c show how very little variation is observed by variation of the element size in beams with stirrups. The uncertainty for beams without stirrups show a slightly increasing trend as the element size decreases , as can be seen in Figure 5.4d-f.

Resulting distribution parameters are listed in Table 5.2. The figures obtained for the beams without stirrups are included here and show a slight increase in the overprediction as the element size decreases. A coefficient of variation of 0.2 is however resulting in uncertainty factors up to 1.45. For the beams with stirrups, as also follows from Figure 5.4, no significant variation was observed.

Table 5.2: Resulting uncertainties for a variation of the element size in rotating crack models

	All Beams			Beams with stirrups			Beams without stirrups		
Relative element size	μ_θ [-]	V_θ [-]	γ_{Rd} [-]	μ_θ [-]	V_θ [-]	γ_{Rd} [-]	μ_θ [-]	V_θ [-]	γ_{Rd} [-]
R5 - 10 elements over height	1.008	0.177	1.231	1.077	0.093	1.04	0.927	0.218	1.407
R2 - 20 elements over height	0.999	0.17	1.232	1.071	0.091	1.044	0.915	0.203	1.402
R6 - 30 elements over height	0.981	0.179	1.268	1.071	0.097	1.051	0.878	0.197	1.449

A dependent T-Test on the sets $\ln(\theta_i)$ of beams with stirrups between R5 (μ_θ = 1.083, V_θ = 0.092) and R2(μ_θ = 1.076, V_θ = 0.09) shows no significant difference in the accuracy: t(56) = -0.705, p = 0.483. In a similar way, between R2 (μ_θ = 1.083, V_θ = 0.092) and R6 (μ_θ = 1.077, V_θ = 0.096) no significant difference was found: t(56) = 0.077, p = 0.939.

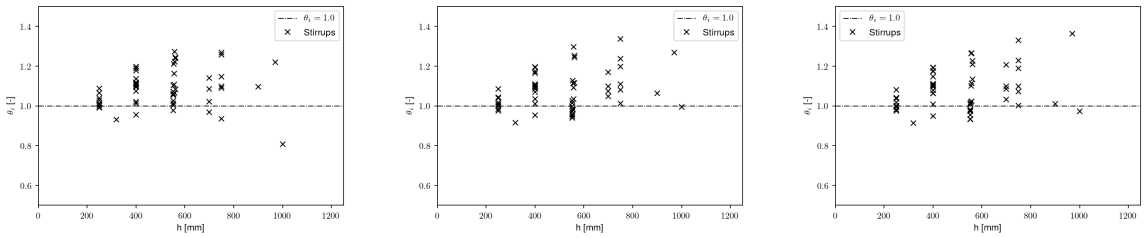

(a) 10 elements over beam height (R5) (b) 20 elements over beam height (R2) (c) 30 elements over the beam height(R6)

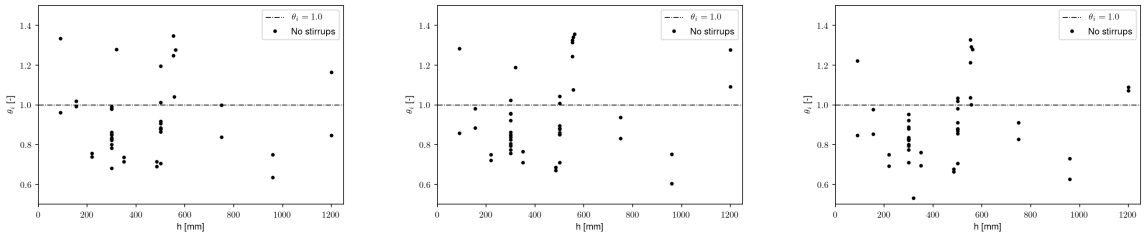

(d) 10 elements over beam height (R5) (e) 20 elements over beam height (R2) (f) 30 elements over the beam height(R6)

Figure 5.4: Distribution of model uncertainty and beam height of beams with and without stirrups - Above the line is a conservative result, below the line progressive

5.2.2. The mesh-dependency of fixed crack models with damage based shear retention

The fixed crack strategies tend to find a higher capacity as the element size decreases. This follows from Figures 5.5d, 5.5e, 5.5f and is in accordance with wat Cervenka found in [6]. It shows that beams with a large depth are affected more than smaller beams, for which the results appear reasonably mesh objective. For the beams with stirrups, the observed trend in Figures 5.5a, 5.5b and 5.5c is not so severe.

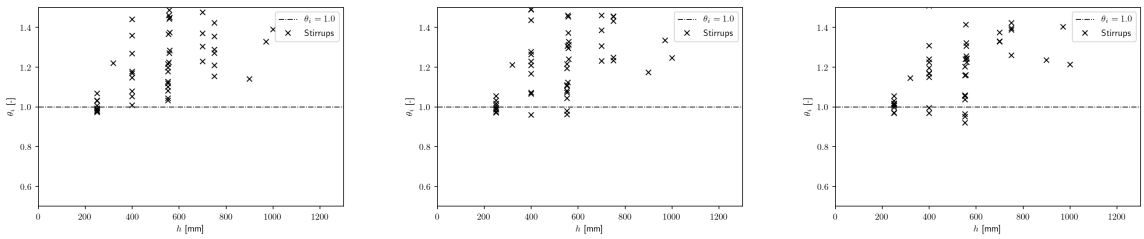

(a) 20 elements over beam height - Stirrups (b) 30 elements over beam height - Stirrups (c) 40 elements over the beam height - Stirrups

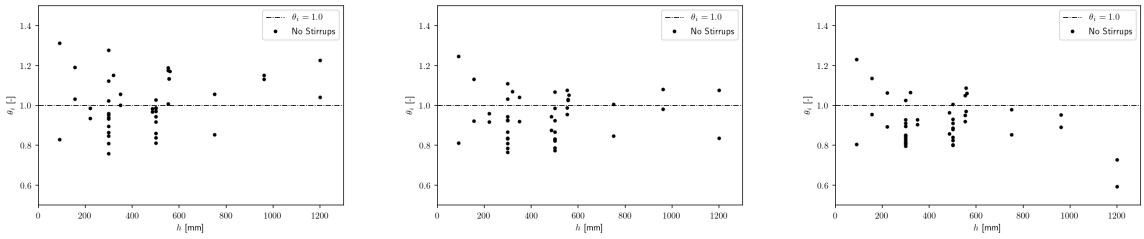

(d) 20 elements over beam height - no stirrups (e) 30 elements over beam height - no stirrups (f) 40 elements over the beam height - no stirrups

Figure 5.5: Distribution of model uncertainty and beam height of beams with and without stirrups

The distribution parameters of the model uncertainty in Table 5.3 agree with Figure 5.5. As the element size decreases, the uncertainty increases. For the beams with stirrups this is also the case, but in not as much as for beams without stirrups. The beams with stirrups are still underestimated significantly at small element sizes, indicating that their failure mode is not sensitive to the element size.

A paired t-test between beams without stirrups from F2 (μ_θ = 1.002, V_θ = 0.132) and F5(μ_θ = 0.935, V_θ = 0.120) indicates a significant difference between the sets: t(43) = -8.18, p < 0.001. F7 contains significant

Table 5.3: Resulting uncertainties for a variation of the element size in fixed crack models

	All Beams			Beams with stirrups			Beams without stirrups		
Relative element size	μ_θ [-]	V_θ [-]	γ_{Rd} [-]	μ_θ [-]	V_θ [-]	γ_{Rd} [-]	μ_θ [-]	V_θ [-]	γ_{Rd} [-]
F2 - 20 elements over height	1.132	0.188	1.111	1.242	0.171	0.991	1.002	0.132	1.173
F5 - 30 elements over height	1.088	0.196	1.168	1.223	0.16	0.994	0.935	0.12	1.238
F7 - 40 elements over height	1.07	0.211	1.208	1.216	0.168	1.01	0.907	0.129	1.29

outliers and therefore violates the assumptions of the dependent t-test. Ignoring the outliers still results in a significant difference: t(41) = -2.10, p = 0.042.

5.2.3. Reinforcement modelling

For the investigation of the impact of reinforcement modelling, the bondslip interface as well as the element type have been investigated. For beams without stirrups, the most consistent results were obtained with the fib MC2010 bondslip model. This is seen from the $V_\theta = 0.121$ in Table 5.4.

Table 5.4: Resulting uncertainties for a variation of reinforcement model in fixed crack approaches

	All Beams			Beams with stirrups			Beams without stirrups		
Bondslip interface	μ_θ [-]	V_θ [-]	γ_{Rd} [-]	μ_θ [-]	V_θ [-]	γ_{Rd} [-]	μ_θ [-]	V_θ [-]	γ_{Rd} [-]
F1 - Fully bonded	1.171	0.193	1.08	1.296	0.167	0.946	1.024	0.134	1.151
F2 - Shima	1.132	0.188	1.111	1.242	0.171	0.991	1.002	0.132	1.173
F4 - CEB-FIB MC2010	1.148	0.181	1.086	1.252	0.172	0.985	1.023	0.121	1.133

An increase in consistency of the solution is not observed for beams with stirrups and a rotating crack in case of bondslip modelling. Like the element size, variation of the reinforcement type causes little variation in the model uncertainty and its variance. This can be seen in Table 5.5.

Table 5.5: Resulting uncertainties for a variation of reinforcement model in rotating crack approaches

	All Beams			Beams with stirrups			Beams without stirrups		
Bondslip interface	μ_θ [-]	V_θ [-]	γ_{Rd} [-]	μ_θ [-]	V_θ [-]	γ_{Rd} [-]	μ_θ [-]	V_θ [-]	γ_{Rd} [-]
R1 - Fully bonded	1.079	0.207	1.193	1.072	0.092	1.044	**1.087**	**0.292**	**1.315**
R2 - Shima	0.999	0.17	1.232	1.071	0.091	1.044	0.915	0.203	1.402
R4 - CEB-FIB MC2010	1.014	0.179	1.226	1.077	0.103	1.053	0.938	0.219	1.393

The beams without stirrups show a different result for fully bonded reinforcement compared to any bondslip modelling. The average overshoot observed above does not seem to apply. Comparison of Figure 5.6 and 5.2 shows substantially more undershoots in case of fully bonded reinforcement. Other beams are overpredicted, explaining the high coefficient of variation of 30 (!) % for this case (see Table 5.5).

As the normality premise of a dependent t-test could not be satisfied, no statistical tests are performed on these results.

Finally, the reinforcement element type was varied. The results are listed in Table 5.6. It was observed that the use of truss reinforcement did not have a positive impact on the results, as can be seen from the table.

Table 5.6: Resulting uncertainties for a variation of reinforcement type

	All Beams			Beams with stirrups			Beams without stirrups		
Reinforcement type	μ_θ [-]	V_θ [-]	γ_{Rd} [-]	μ_θ [-]	V_θ [-]	γ_{Rd} [-]	μ_θ [-]	V_θ [-]	γ_{Rd} [-]
R8 - Beam	1.006	0.176	1.232	1.075	0.097	1.047	0.925	0.213	1.404
R9 - Truss	1.040	0.149	1.153	1.088	0.104	1.044	0.980	0.174	1.262
F9 - Beam	1.158	0.169	1.061	1.243	0.172	0.993	1.053	0.108	1.084
F10 - Truss	1.175	0.170	1.047	1.257	0.165	0.973	1.072	0.132	1.096

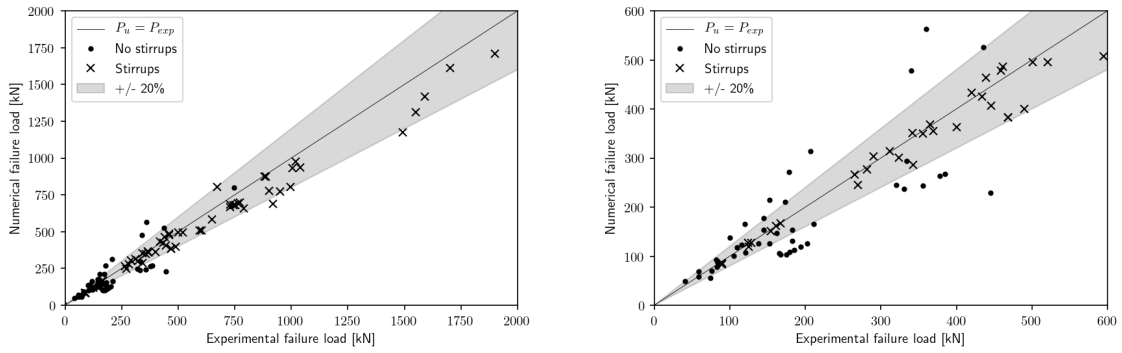

(a) All results for R1

(b) Results R1 zoomed in

Figure 5.6: NLFEA and experimental ultimate load for solution strategy R1

5.3. The impact of equilibrium requirements on solution strategies

5.3.1. Strictness of convergence criteria

The convergence criteria have been varied according to Table 3.11. Firstly, the models based on a fixed crack are assessed. The results are summarized in Table 5.7.It is clear that the model uncertainty for beams without stirrups decreases as the convergence criteria are stricter. This is not the case for the group of beams with stirrups.

Table 5.7: Observed variation of model uncertainty due to convergence criteria for fixed crack strategies

	All Beams			Beams with stirrups			Beams without stirrups		
Convergence criterion	μ_θ [-]	V_θ [-]	γ_{Rd} [-]	μ_θ [-]	V_θ [-]	γ_{Rd} [-]	μ_θ [-]	V_θ [-]	γ_{Rd} [-]
F3 - E : 10^{-2} OR F : 10^{-1}	1.087	0.226	1.212	1.239	0.191	1.019	0.917	0.137	1.289
F2 - E : 10^{-3} OR F : 10^{-2}	1.111	0.198	1.146	1.24	0.172	0.995	0.962	0.126	1.212
F6 - E : 10^{-4} OR F : 10^{-2}	1.132	0.188	1.111	1.242	0.171	0.991	1.002	0.132	1.173

Between models with a rotating crack, little variation in the results for beams with stirrups was observed. A notable difference is the increased variation in the results with loosened convergence criteria.

Table 5.8: Observed variation of model uncertainty due to convergence criteria for rotating crack strategies

	All Beams			Beams with stirrups			Beams without stirrups		
Convergence criterion	μ_θ [-]	V_θ [-]	γ_{Rd} [-]	μ_θ [-]	V_θ [-]	γ_{Rd} [-]	μ_θ [-]	V_θ [-]	γ_{Rd} [-]
R3 - E : 10^{-3} OR F : 10^{-2}	0.983	0.170	1.251	1.062	0.108	1.074	0.891	0.182	1.402
R2 - E : 10^{-4} OR F : 10^{-2}	0.999	0.170	1.232	1.071	0.091	1.044	0.915	0.203	1.402

5.3.2. The impact of the simultaneous convergence requirement

In beams without shear reinforcement, the localization of cracks is better approximated using simult. The convergence plot in Figure shows why that is. As the first integration points start cracking, the force norm is still within bounds but the energy variation increases. This can be seen in Figure 5.8a. At some point the force-norm catches up and the load level drops drastically. The solution then recovers and continues the softening path, identical to the solution without simult. This is visualized in Figure 5.7 too. The convergence behaviour with simultaneous convergence is illustrated in Figure 5.9b. The obtained model uncertainty of F9 is lower than the uncertainty obtained with simultaneous convergence.

5.3.3. The maximum amount of iterations

The results of increasing the amount of iterations are listed in Table 5.10. The variation of model uncertainty for the beams with stirrups decreases slightly, while it can be seen that increasing the amount of iterations substantially improves the results between F4 and F9 for beams without stirrups.

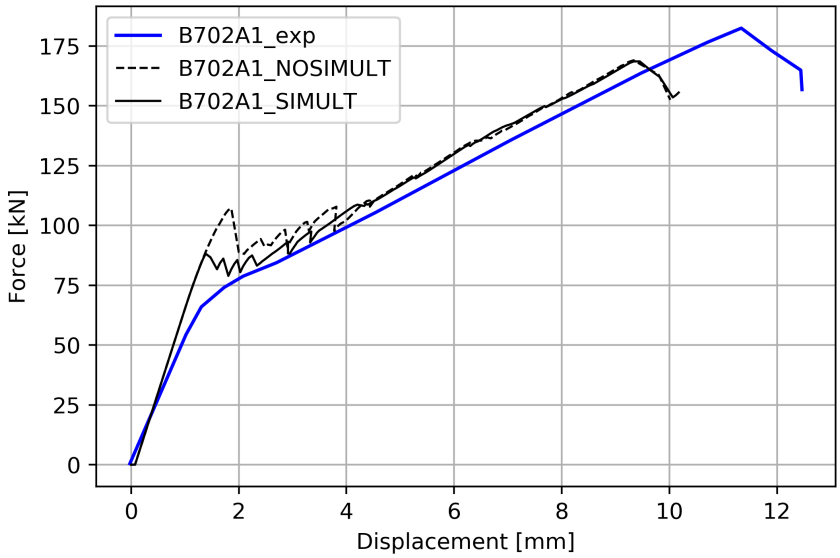

Figure 5.7: Result for B702A1 with and without simultaneous convergence

Table 5.9: Resulting model uncertainty distribution parameters for variation of simultaneous criterion

	All Beams			Beams with stirrups			Beams without stirrups		
Convergence criterion	μ_θ [-]	V_θ [-]	γ_{Rd} [-]	μ_θ [-]	V_θ [-]	γ_{Rd} [-]	μ_θ [-]	V_θ [-]	γ_{Rd} [-]
F8 - 100 iterations - SIMULT	1.175	0.179	1.059	1.262	0.180	0.987	1.067	0.128	1.095
F9 - 100 iterations - No simult	1.158	0.169	1.061	1.243	0.172	0.993	1.053	0.108	1.084

Table 5.10: Resulting model uncertainty distribution parameters for variation of the number of iterations

	All Beams			Beams with stirrups			Beams without stirrups		
Number of iterions	μ_θ [-]	V_θ [-]	γ_{Rd} [-]	μ_θ [-]	V_θ [-]	γ_{Rd} [-]	μ_θ [-]	V_θ [-]	γ_{Rd} [-]
R4 - 40 iterations	1.014	0.179	1.226	1.077	0.103	1.053	0.938	0.219	1.393
R8 - 100 iterations	1.006	0.176	1.226	1.075	0.097	1.047	0.938	0.213	1.404
F4 - 40 iterations	1.148	0.181	1.086	1.252	0.172	0.985	1.023	0.121	1.133
F9 - 100 iterations	1.158	0.169	1.061	1.243	0.172	0.993	1.053	0.108	1.084

The observed behaviour of individual cases is variable, this is illustrated by taking as example two beams. The convergence of VS-OA2 with F4 is shown in Figure 5.8a, here 3 non-converged steps were reported. The convergence with F9 is presented in 5.8b, where only one non-converged step is reported. The respective predicted failure loads are 317.64 kN and 314.38 kN, the experimental failure load 320 kN. A different behaviour is observed for beam VS-A2, the convergence behaviour in Figure 5.8c shows that 77 % of the steps converged until the maximum load level was reached at 460 kN. Figure 5.8d shows the same model with 100 iterations, resulting in only 3 out of 180 non-converged steps and a predicted failure load of 455 kN. The experimental failure load was 439 kN.

5.3.4. The convergence behaviour between bondslip models

An unexpected observation was the difference in convergence behaviour for different bondslip models. The solution strategy with the FIB bondslip model showed convergence problems on the force norm, while the Shima model did not show these problems. This behaviour is best shown by comparing the convergence behaviour in case simultaneous convergence is required. It is shown for beam B702A1 in Figure 5.9

The analysis with the FIB bondslip model, shown in Figure 5.9a, resulted in only 44 fully converged steps. That is a convergence rate of 24 %. The step with the maximum load and one of the criteria satisfied was

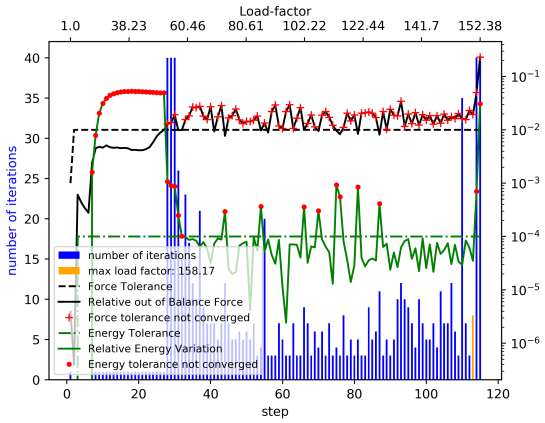

(a) Convergence behavior of VS-OA2 with a maximum of 40 iterations (F4)

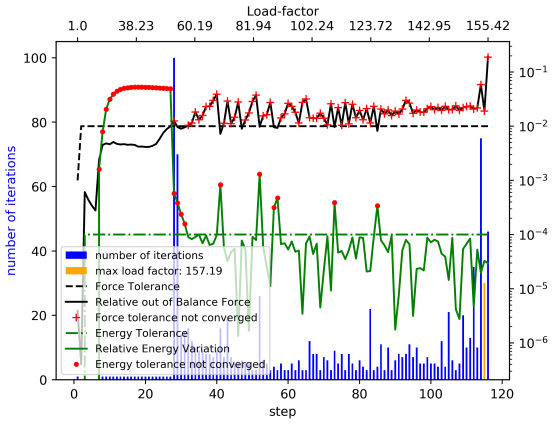

(b) Convergence behavior of VS-OA2 with a maximum of 100 iterations(F9)

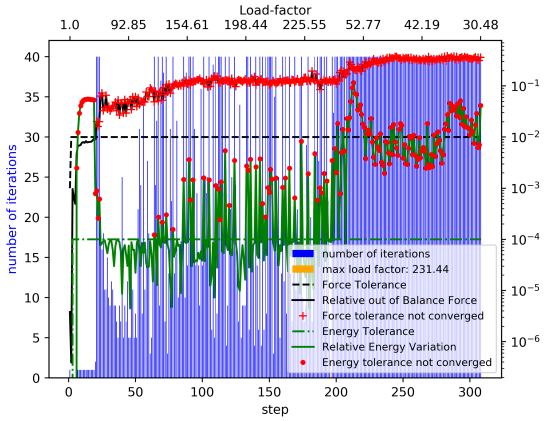

(c) Convergence behavior of A2 with a maximum of 40 iterations (R4)

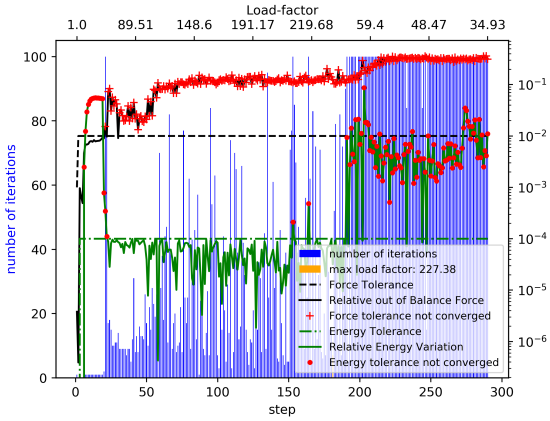

(d) Convergence behavior of A2 with a maximum of 100 iterations (R8)

Figure 5.8: Convergence behavior of beam VS-OA2 and VS-A2 from [37]

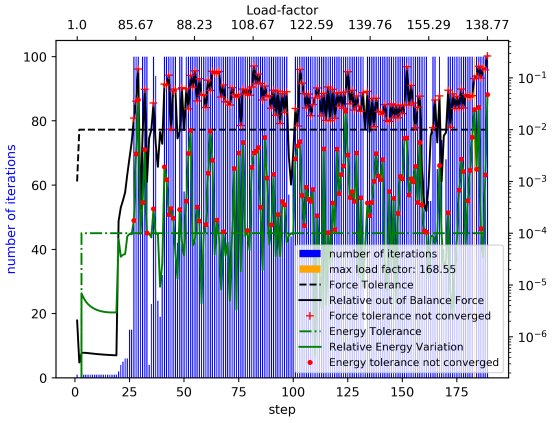

(a) Convergence behaviour of beam B702A1 with FIB bondslip (unconfined)

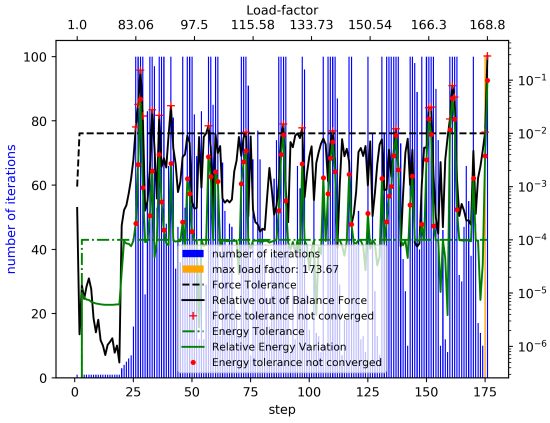

(b) Convergence behaviour of beam B702A1 with Shima bondslip

Figure 5.9: Convergence behaviour of beam B702A1 with two different bondslip models

step 178, at a load level of 167 kN. The same analysis was performed again, with the Shima curve instead of the FIB one and resulted in the convergence behaviour shown in Figure 5.9b. A convergence rate of 68% was recorded. The converged step with maximum load resulted in a load of 173 kN. As it would be impractical to present and compare 200 convergence plots this case is used as an example for the behaviour.

5.4. Summary of obtained model uncertainty

Due to the differences between the R-strategies and F-strategies, useful comparisons between other variations in the solution strategy are limited to the results obtained with the F-strategies for beams without shear reinforcement and between the results with the R-strategies for beams with shear reinforcement. A summary is offered in Tables 5.11 and 5.12 for the F - and R - strategies respectively.

Table 5.11: Summary of results with fixed crack strategies for beams without stirrups

Strategy	μ_θ	V_θ	γ_{Rd}
F1	1.024	0.134	1.151
F2	1.002	0.132	1.173
F3	0.962	0.126	1.212
F4	1.023	0.121	1.133
F5	0.935	0.120	1.238
F6	0.917	0.137	1.289
F7	0.907	0.129	1.291
F8	1.067	0.128	1.095
F9	1.053	0.108	1.084
F10	1.072	0.132	1.096

Table 5.12: Summary of results with rotating crack strategies for beams with stirrups

Strategy	μ_θ	V_θ	γ_{Rd}
R1	1.072	0.092	1.044
R2	1.071	0.091	1.044
R3	1.062	0.108	1.074
R4	1.077	0.103	1.053
R5	1.077	0.093	1.040
R6	1.071	0.097	1.051
R7	1.074	0.108	1.062
R8	1.075	0.097	1.047
R9	1.088	0.104	1.044

A full overview of the uncertainties is offered in Table A.1.

5.5. Statistical properties of model uncertainty

Different distributions have been fitted to the data of all solution strategies together. The histogram in Figure 5.10a represents the 1919 outcomes of θ_i for all the solution strategies. A maximum likelihood estimate for the parameters of the distributions is determined based on those outcomes. For those distributions, the sum of squared errors with a histogram of the data was determined. It was found that a log-normal distribution was the best fit.

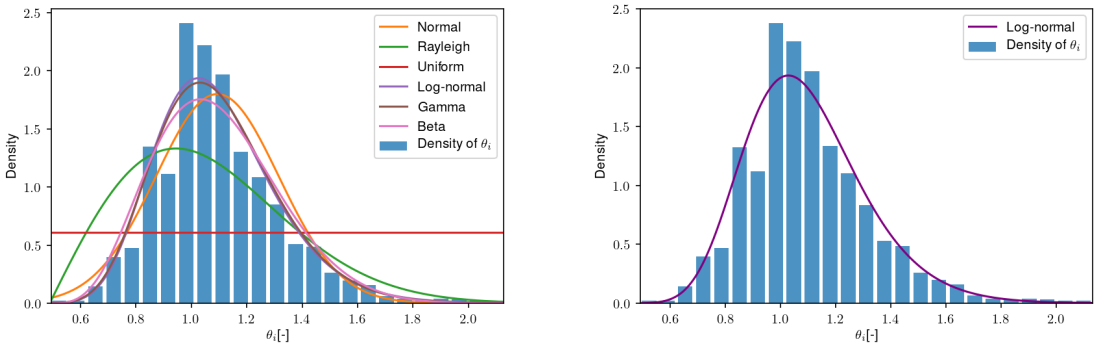

(a) Various distributions fit to all 1919 data points

(b) Lognormal distribution fitted with MC2020 procedure

Figure 5.10: Density of model uncertainty from all 1919 analyses

A log-normal distribution can be fitted to all 1919 calculated results using the MC2020 Bayesian updating procedure as well . This distributions is plotted over the data in Figure 5.10b. The resulting parameters for all data are: $\mu_\theta = 1.073$, $V_\theta = 0.197$ and from that a 'blind' model uncertainty factor $\gamma_{Rd} = 1.184$ can be determined.

Although the histogram of the model uncertainty resembles the typical shape of a log-normal distribution, a Shapiro-Wilkes test on 1919 values of $\ln(\theta_i)$ does not confirm this observation. An explanation of this are the outliers resulting from bad approximations in individual cases.

A Shapiro-Wilkes test confirms normality of $\ln(\theta)$ on the 44 beams without shear reinforcement for strategy F9: W(43) = 0.984, p = 0.82. The normality of $\ln(\theta)$ is also confirmed for the 57 beams with shear reinforcement and strategy R8: W(56) = 0.985, p = 0.71.

The QQ plots in Figures 5.11a and 5.11c show the good fits with log-normal distributions for the beams without stirrups in F9 and the beams with stirrups in R8 respectively. As expected the QQ plot of all the beams in F9, Figure 5.11b, shows a different distribution with outliers at the tails. Those outliers are the result of underpredictions in the beams with stirrups. A similar observation follows from the QQ plot in Figure 5.11d, where significant outliers are introduced by bad approximation of beams without shear reinforcement.

Finally, the probability plot of all 1919 results in Figure 5.11e shows a similar behavior. The fit is generally good, with some outliers in the tails. For comparison a probability plot with a normal distribution is presented in Figure 5.11f. This shows that the lognormal distribution is a better fit with the data.

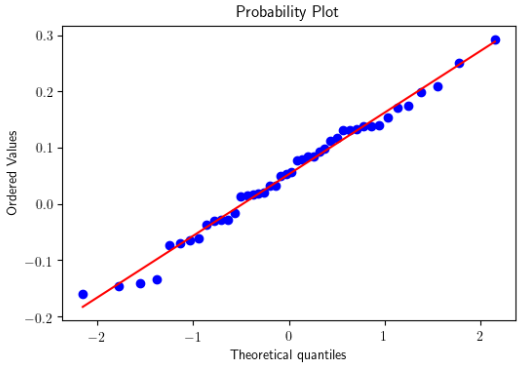

(a) F9, no shear reinforcement, lognormal QQ plot

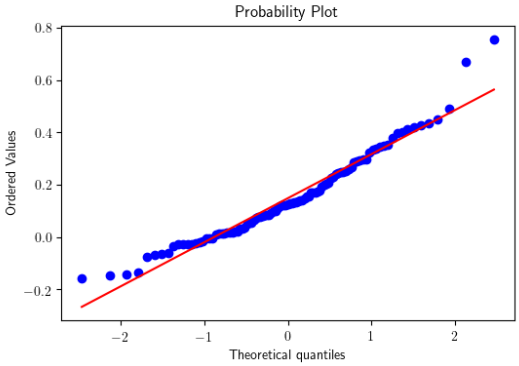

(b) F9, all beams, lognormal QQ plot

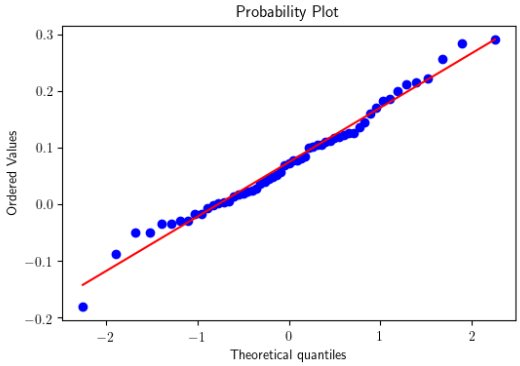

(c) R8, beams with shear reinforcement, lognormal QQ plot

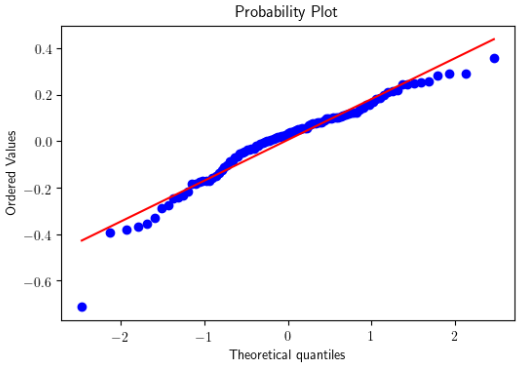

(d) R8, all beams, lognormal QQ plot

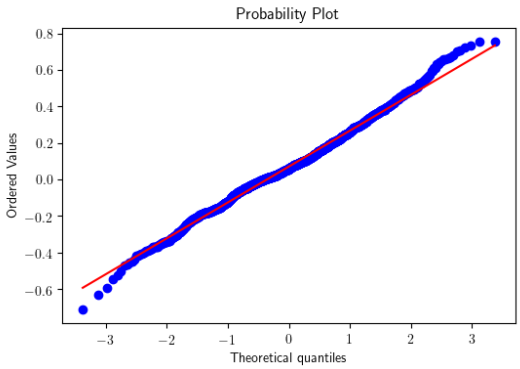

(e) Fit of all 1919 observations with a lognormal distribution

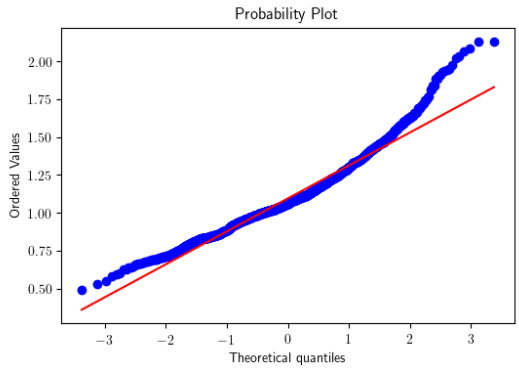

(f) Fit of all 1919 observations with a normal distribution

Figure 5.11: QQ plots the model uncertainty for different strategies and the total data set

5.6. Discussion

The presented cases do not show a solution strategy that reasonably approximates all beams. Consistent overpredictions of the rotating crack models mean that the failure load as the maximum retained load with satisfied convergence criteria can not be accepted without caution. Consistent underpredictions of the beams with stirrups by the fixed crack models are, from an engineering point of view, not necessarily bad but the high bias still makes that these strategies are not preferred. The overpredictions could be avoided by performing the analysis twice, once with a rotating crack model and once with a fixed crack model. The lowest outcome would then be conservative. This would however result in very low predictions for beams with stirrups.

The different behaviour of finite element models of beams with and without stirrups is not surprising, as the physical behaviour and failure mode are different. Therefore it is concluded that a strategy that works for any structural design can not be subscribed, at least not by accepting the highest retained load in a converged step. A different definition of failure is investigated further below.

It is however possible to 'blindly' accept the highest converged load from an analysis, provided that an appropriate strategy is used. This means that it is possible to subscribe a solution strategy when the project parameters, like the presence of shear reinforcement, are known.

5.6.1. The influence of the constitutive model

The differences in accuracy induced by the constitutive choices resulted in a separate assessment of beams with and without shear reinforcement. In the kinematic assumptions, the element size and reinforcement modelling were varied. The rotating crack strategies, as mentioned before, showed to be robust for beams with shear reinforcement.

5.6.2. The influence of bond slip modelling

An unexpected observation was the difference in convergence behaviour for the application of different bondslip models. The solution strategy with the FIB bondslip model showed convergence problems on the force norm, while the Shima model did not show those effects.

The main difference between those models is the fact that the Shima model does not reduce the bond stress as strain increases, while the fib model does. This can be seen in Figure 2.7. This means that force redistribution is required, resulting in an increase of the residual forces during a step which explains the difficult convergence of the force norm.

For the beams with stirrups where a rotating crack strategy was used, the mean uncertainty does not change between R2 (Shima) and R4 (FIB). The variance does however change, with $V_\theta = 0.09$ for R2 and $V_\theta = 0.10$ for R4. The beams without stirrups modelled with a fixed crack showed a decrease in the variance: $V_\theta = 0.13$ for F2 and $V_\theta = 0.12$ for F4. The impact of the bondslip model on the behaviour of the beam is discussed in 6.5. With the current data it is not possible to isolate the cause for this as it can be due to the change in bondslip model or the different convergence behaviour. However, both aspects are not independent from each other. Therefore a meaningful conclusion can still be obtained by looking at the solution strategies as a whole, with the failure load as defined before.

5.6.3. The influence of the element size

The element size was found to influence the results for beams without shear reinforcement, especially the results for deep beams. This is in line with what was found by Cervenka [6]. The best results were obtained with 20 elements over the beam height. This was the case for all beam heights, resulting in element sizes of 5 to 60 mm. The influence of absolute element size was not investigated. Predicted failure loads increased with a reducing element size. Only six beams without stirrups with a height over 600 mm were included in this study. The mesh-dependency is most severe for these beams. Mesh objectivity is vital to obtaining a reliable finite element solution. Further research is required to explain this as there are multiple effects that could cause this. An explanation for the overpredictions can be that there is a deficiency in the finite element model such that size effects of this complicated failure mode are not correctly included.

It was found that the fib local bondslip model should be used for beams without shear reinforcement, the mesh sensitivity tests were however done with Shima bondslip behaviour and a maximum of 40 iterations per step. To investigate the mesh sensitivity in case the fib model is used, several models were made from beam H123. A maximum of 100 iterations per step was used here. The models were meshed with 20, 30, 40 and 60 elements over the height, resulting in element sizes of 60, 40, 30 and 20 mm respectively. The results of this are displayed in Figure 5.12. It can be seen that the model with 20 elements over the height failed at a much

lower load than the other models.

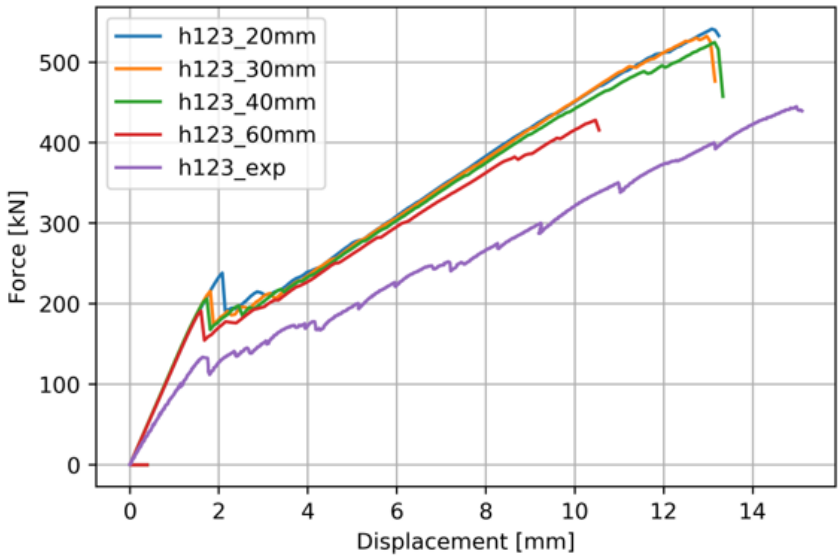

Figure 5.12: Force-displacement behaviour of beam H123 with different element sizes

The models with smaller element sizes do all result in a very similar failure load and displacement, with a model uncertainties of 0.82, 0.83 and 0.84 for the beams with element sizes 20, 30 and 40mm respectively. That is still a significant overprediction, but not as problematic as the $\theta = 0.72$ found with F7 and shows that at least the bondslip model is an important influence in the modelling of deep beams without shear reinforcement and that 40 iterations per step is not enough. Next to that, it appears that the element size of 60 mm is too large to objectively model the beam, indicating that a minimal element size might be required. As mentioned, the overprediction is still substantial. An explanation for this can be that the damage based shear retention is too progressive, that the shear behaviour of the critical crack is not correctly modelled or that the size effects of this complicated failure mode are not fully included. Based on that, a different model uncertainty factor might be required for deep beams. It is hard to conclude anything on this as only one beam was investigated. Further research on this topic is required.

5.6.4. The influence of convergence behaviour

It appears that the convergence behaviour is quite individual for a beam. One problem will converge more easily and therefore the increase of the maximum amount of iterations will not have much impact on the result. Other problems show less converged steps when the number of iterations decreases but the result of the calculation is as good as the same. Here the same principle as mentioned above applies. Because a large number of beams was tested and for every NLFEA the same definition of failure load was used, the resulting uncertainty parameters include effects due to differences in convergence behaviour.

5.6.5. Subscribing a solution strategy based on the characteristics of a beam

The main influence factor in the accuracy of the solutions was found to be the presence of shear reinforcement. Those beams should be modelled with a rotating crack model. In Table 5.1, the results for all solution strategies with a rotating crack model are listed together with the results found with one single solution strategy. The uncertainty, variance and resulting model uncertainty factor of strategy R8 are practically equal to the average over all 9 solution strategies with a rotating crack, indicating that the approximation of beams with shear reinforcement with a rotating crack is very robust. The summary in Table 5.12 confirms this. All of the combinations of μ_θ and V_θ show a lower variance and mean uncertainty than reported by Engen et al. in [16]. Any strategy listed above can be used to model a reinforced concrete beam with shear reinforcement, but the best results are obtained with beam reinforcement and a convergence requirement on the energy norm of 10^{-4}. This means that 40 iterations per step is sufficient for the beams with shear reinforcement.

The Shima bondslip model can be used for these beams, which can offer a solution when the convergence behaviour is problematic. It has not been investigated what this means for the accuracy of the crack pattern and crack widths.

The variation observed for the beams without shear reinforcement shows that these are more sensitive to subtle choices in the solution strategy. Because of that a more precise advise is required.

From the data listed above it appears that beams without shear reinforcement are best modelled using a fixed crack model with damage based shear retention. All results have been summarized in Table 5.11. Here it shows that strategy F9 has the most consistent results over all beams without shear reinforcement.

Beams higher than 600 mm show substantially different results as the element size decreases, therefore the subscribed strategy for beams without shear reinforcement is limited to beams up to 600mm. The investigation of deep beams did however show that the amount of iterations per step and the modelling of bondslip behaviour are very important for beams without shear reinforcement.

Those beams without shear reinforcement should be modelled with 20 elements over the height, use the fib unconfined bondslip model as defined in [12]. As 40 iterations per step appeared to be insufficient, 100 full Newton Raphson iterations per step are advised. If this approach is followed, the highest retained load in a converged load step can safely be assumed the ultimate load.

5.6.6. Other beam characteristics

A decline of model uncertainty was observed for the increase of the shear slenderness as shown in Figure 5.13. This is not surprising as the beam is more likely to fail in bending with an increasing shear slenderness. A comparison is made between the approximation of beams with shear reinforcement with R8 and the approximation of beams without shear reinforcement with F9. In both cases, high a/d ratios show lower uncertainty.

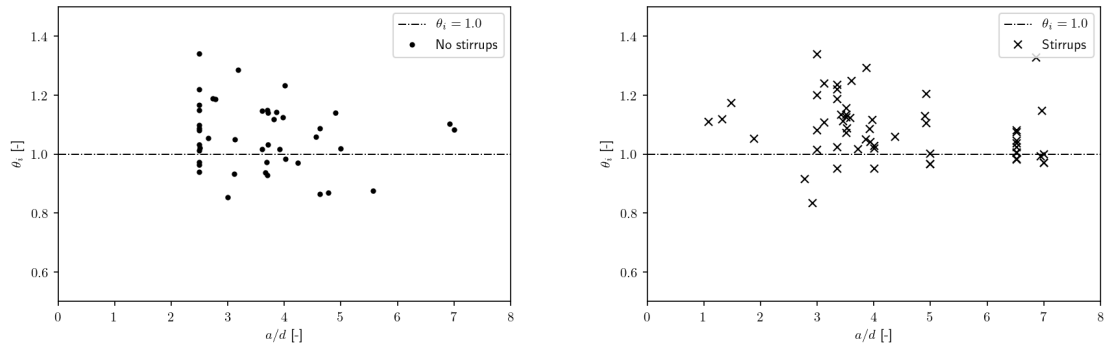

(a) F9

(b) R8

Figure 5.13: Distribution of model uncertainty over shear slenderness of strategies F9 and R8

Apart from this, no noteable differences were observed

5.6.7. The distribution of model uncertainty

The used solution strategies were 'carelessly' applied to all beams and this resulted in consistent underprediction of the beams with stirrups by one type and a consistent overprediction of the beams without stirrups by the other type of strategy. The highest load at a converged step was accepted as the failure load. This resulted in badly approximated cases. It was already argued that the highest load at a converged step can be accepted as the failure load, *provided that an appropriate solution strategy is used.* This also impacts the use of the γ_{Rd} = 1.3 proposed in the MC2020 draft as model uncertainty factors of 1.4 are determined in cases where rotating crack models are applied to the group of beams without stirrups.

It was shown in Figures 5.11a and 5.11c that log-normal distributions were applicable in case an appropriate strategy is used. This was backed up by Shapiro-Wilkes tests on the respective data. The probability plots in Figures 5.11e and 5.11f show how a lognormal distribution is a more appropriate assumption than a normal distribution of model uncertainty. The fit is generally good, except for the tails. This can be attributed to the fact that the maximum converged load step can not be regarded the failure load for a beam without stirrups modelled with a rotating crack.

Based on the results and reasoning provided above it is suggested to indeed assume the lognormally distributed model uncertainty, as is in line with literature like the JCSS model code [27] and the investigation of model uncertainty by Engen et al. [16]. This study resulted in a model uncertainty factor $\gamma_{Rd} = 1.184$, which is substantially lower than the 1.3 proposed in the MC2020 draft. It should be noted that the solution strategies in this study are not entirely random, but are made up of two main constitutive 'branches' with subtle changes between the strategies with the same constitutive model. Also, great care was taken to define correct boundary conditions and choices in the non variable part of the solution strategies. It means that with the strategies listed in this study, a 'blind' uncertainty factor of 1.184 would be appropriate. Therefore it is not recommended to reduce the γ_{Rd} of 1.3 for non-benchmarked solution strategies.

The determined model uncertainties show that an analyst is generally rewarded for benchmarking his or her solution strategy as all the solution strategies show a reduction factor below 1.3. If the correct solution strategy is selected and benchmark experiments are similar to the structural design, this reduction factor can be as low as 1.1.

5.7. Recap and Conclusions

Based on the results and their implications presented above, it was made clear that the applied solution strategies in combination with the highest retained load with convergence criteria satisfied as failure load did not result in a strategy that robustly solved every reinforced concrete beam. This is the case because a substantial difference in the behaviour and analysis of beams with and without shear reinforcement was observed. All strategies with a rotating crack show a large scatter of results for beams without shear reinforcement, sometimes predicting almost double the experimental failure load.

For beams with shear reinforcement, these strategies with rotating crack models are shown to be very robust, as presented in Table 5.12. On the other hand, some solution strategies with a fixed crack in their constitutive model reported very good agreement with test data of beams without shear reinforcement, but the beams with shear reinforcement were approximated poorly. This means that a solution strategy has to be prescribed based on what is know about the characteristics of the beam.

For the beams with shear reinforcement, any R-strategy listed above gives good results. The only advice is to apply a convergence tolerance of 0.0001 on the relative energy variation, as this results in less variance of the result than the result of a tolerance of 0.001. A maximum of 40 iterations per step is sufficient for these beams.

For the beams without shear reinforcement the most reliable results were obtained with strategy F9 and therefore this is the approach that should be taken when one is modelling a beam without shear reinforcement. It was noted that the results for beams over 600 mm showed severe mesh dependency and care should be taken with those beams. Models with 20 elements over the height resulted in safe approximations, smaller elements result in higher predictions. More research on this behaviour is required. A solution could be found in a higher model uncertainty factor, but not enough beams were tested to state anything concrete about this factor.

It was shown that convergence behaviour differs between different benchmarks and solution strategies. This does not matter because many beams were tested and the convergence behaviour is part of the model uncertainty factor of the respective solution strategy.

The study of model uncertainty parameters showed that the analyst is generally rewarded for benchmarking his or her solution strategy, as the model uncertainty factor is generally lower than the one prescribed in MC2020 for cases where no benchmarking is performed.

It was discussed why, despite of a negative Shapiro-Wilkes test on $\ln(\theta)$, the assumption of a lognormal distribution for the model uncertainty is justified. From that it was concluded that the 'blind prediction' model uncertainty following from this study resulted in $\gamma_{Rd} = 1.184$, which means the $\gamma_{Rd} = 1.3$ from MC2020 is valid.

6

Investigation of the bias towards failure modes of different solution strategies

In the previous chapter, questions on accuracy and consistency of solution strategies were answered by approaching the model uncertainty in a quantitative manner. The third criterion identified at the beginning of this thesis was the accuracy of the failure mode, as one could doubt the value of a solution with the correct failure load for the wrong failure mode. This chapter deals with the accuracy of solution strategies regarding the prediction of the failure mode. Sources of error are investigated and the results of some solution strategies are adjusted to the correct failure mode. Also, individual cases are addressed in a more qualitative manner. The model uncertainty is investigated for the cases where the correct failure mode has been assured and it is investigated whether or not high uncertainties from the previous chapter are the result of incorrect failure mode predictions.

6.1. Accuracy of the predicted failure modes

The accuracy of the failure modes was investigated for two solution strategies: One with rotating and one with fixed crack. As the most consistent strategy with a fixed crack was F9, the failure correctness of failure modes was studied for this strategy. For the strategies with a rotating crack, it was found that there's little difference between the strategies so R8 is used due to it's similarity to F9.

In Figure 6.1 a scatter of the model uncertainty over the a/d ratio is presented. NLFEA results with the correct failure mode are represented with a star, while results where the wrong failure mode was found are represented by an 'x'. 6.1a displays the results for beams without stirrups, while Figure 6.1b shows how beams without stirrups are approached with F9:

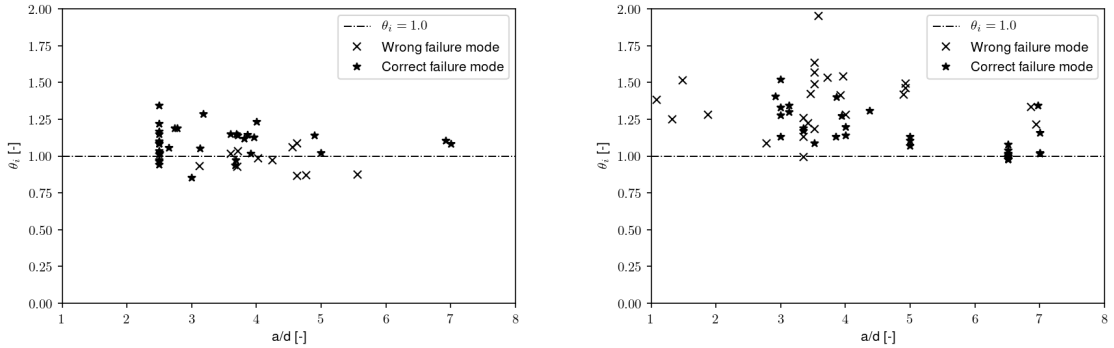

(a) Accuracy of predicted failure modes for F9, beams without stirrups

(b) Accuracy of predicted failure modes for F9, beams with stirrups

Figure 6.1: Accuracy of predicted failure modes for F9 in terms of model uncertainty and a/d ratio

From the 44 beams represented in Figure 6.1a, 12 were supposed to result in a bending failure and 32 should have failed in flexural shear. In total, 33 failures were predicted correctly. The 11 wrong failure modes were all obtained for beams from [40] and in all cases the error was finding a flexural shear failure instead of a bending failure. For beams without stirrups, F9 found the correct failure mode in 75 % cases.

For the beams with stirrups, a different behavior is observed. It already followed from chapter 5 that the failure load of many beams with stirrups is underestimated by the fixed crack strategies. For many cases, a shear failure mode was observed, at a lower load level. Localized shear cracks opened and led to premature failure of a stirrup. This failure mode is called 'Stirrup Failure' in Table 6.1. The correct failure mode was obtained in 32 of the 57 cases, which means 56 %. In totality, strategy F9 predicted the right failure mode correctly in 64 % of the cases.

A similar setup is presented in for strategy R8 in Figure 6.2: It resulted that the accuracy plots are almost the mirrored image of Figure 6.1. It appears that the failure modes of beams with shear reinforcement are approximated quite well with R8, while the prediction of the failure mode is problematic for beams without shear reinforcement.

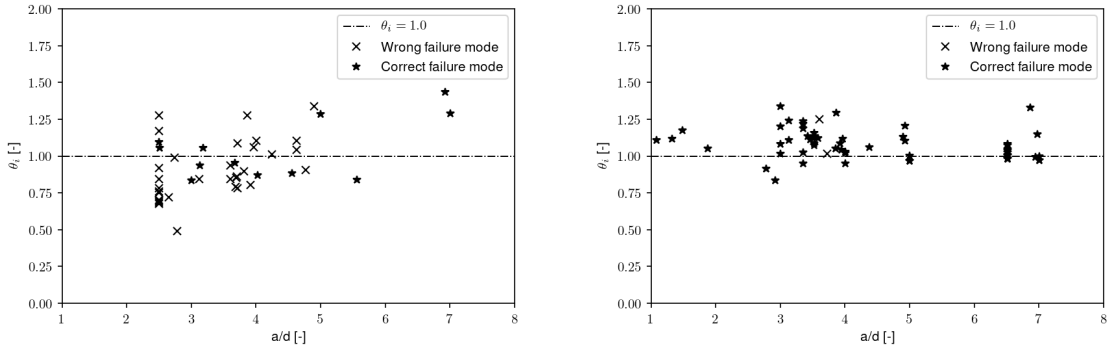

(a) Accuracy of predicted failure modes for R8, beams without stirrups

(b) Accuracy of predicted failure modes for R8, beams with stirrups

Figure 6.2: Accuracy of predicted failure modes for R8 in terms of model uncertainty and a/d ratio

In 55 of the 57 cases of beams with stirrups, the failure mode was predicted correctly. The two other cases, localized yielding of the stirrups resulted in a sudden loss of capacity like it was also found in more solutions of F9. This means the failure mode of a beam with stirrups was predicted correctly in 96 % of the cases. For the beams without stirrups, a correct failure mode was obtained in 12 of the 44 cases. Of those 44 beams, a flexural shear failure was expected in 32 cases but only found in 8 cases. In the other 24 NLFEA's, a compressive shear failure was obtained. This also results in overpredicted capacities. The right failure mode was predicted in 27 % of the cases.

Total results for both solution strategies are summarized in Table 6.1. Here it shows that strategy R8 is very well equipped to model compressive shear and bending failures, while F9 is the best on flexural shear.

Table 6.1: Summary of obtained failure modes for F9 and R8

	Experimental	NLFEA failure mode				Correct
	Failure mode	Shear Compression	Flexural Shear	Bending	Stirrup failure	%
R8	Shear Compression	27	0	0	0	100
	Flexural Shear	24	8	0	0	25
	Bending	8	0	32	2	76
F9	Shear Compression	19	0	0	8	30
	Flexural Shear	0	32	0	0	100
	Bending	4	11	14	13	33

The rest of this chapter will be a discussion of the behavior in the wrong failure modes.

6.2. The overprediction of beams without shear reinforcement with a rotating crack model

In all the solution strategies where the constitutive model contains a rotating crack assumption, severe over-predictions have been observed for beams without shear reinforcement. Figure 6.2a shows that for a/d ratios between 2.5 and 4 the failure mode is often wrongly predicted in combination with an overpredicted failure load. From Table 6.1 it is seen that 24 - so 75 % - of the 32 cases show this behavior. In the other cases the opening of the critical crack resulted in numerical divergence, preventing the analysis from continuation. The definition of the reported failure load was the highest *converged* step. So, the over-predictions were not the result of diverging matrices or other numerical problems.

6.2.1. The overprediction due to the wrong failure mode

Further investigation of those beams is done with beam B702A1 from Yang & Koekkoek [40] as example. This beam has a shear slenderness a/d of 2.65 and experimentally failed in flexural shear. In Figure 6.3, the force-displacement behavior of both the experiment and a NLFEA solution with rotating crack are presented.

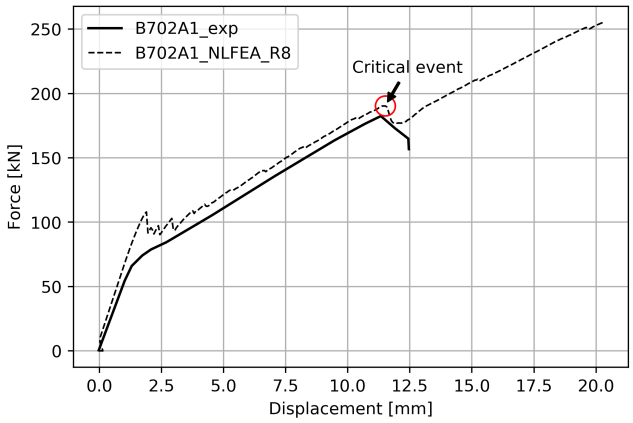

Figure 6.3: NLFEA results of beam B702A1 from [40], with strategy R8

It is seen from the drop in the force-displacement behavior that something occurs at the same load and displacement where the physical beam failed. Further investigation shows that here the critical inclined crack opens like in the experiment.

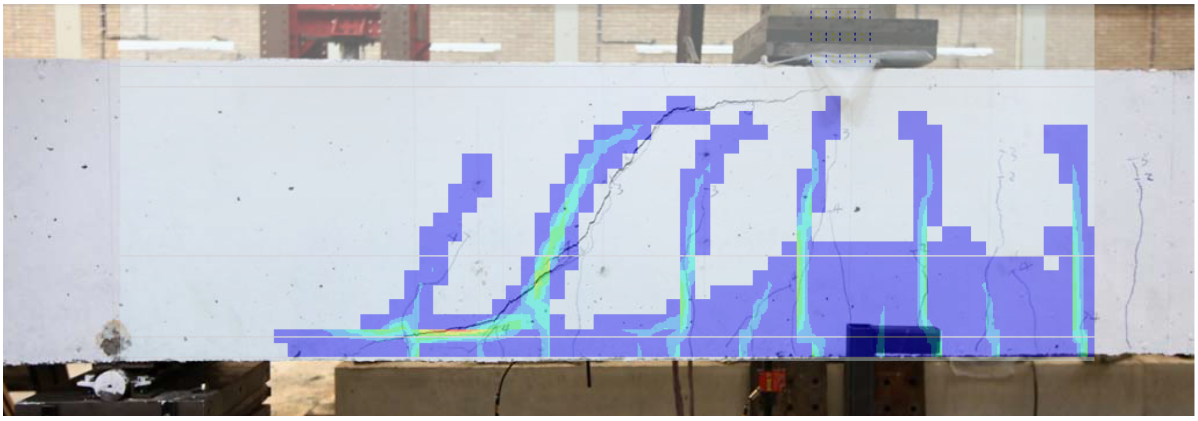

Figure 6.4: Selected correct failure event NLFEA and experimental failure load for solution strategy R8

The crack plot of the beam at the experimental failure event is shown in Figure 6.5a. Notice the location and orientation of the critical inclined crack. In Figure 6.4, a comparison is made between this crack pattern and the crack pattern at failure in the experiment. From that comparison it can be concluded that the crack plots shown in Figure 6.5a is indeed the correct prediction of the beam failure.

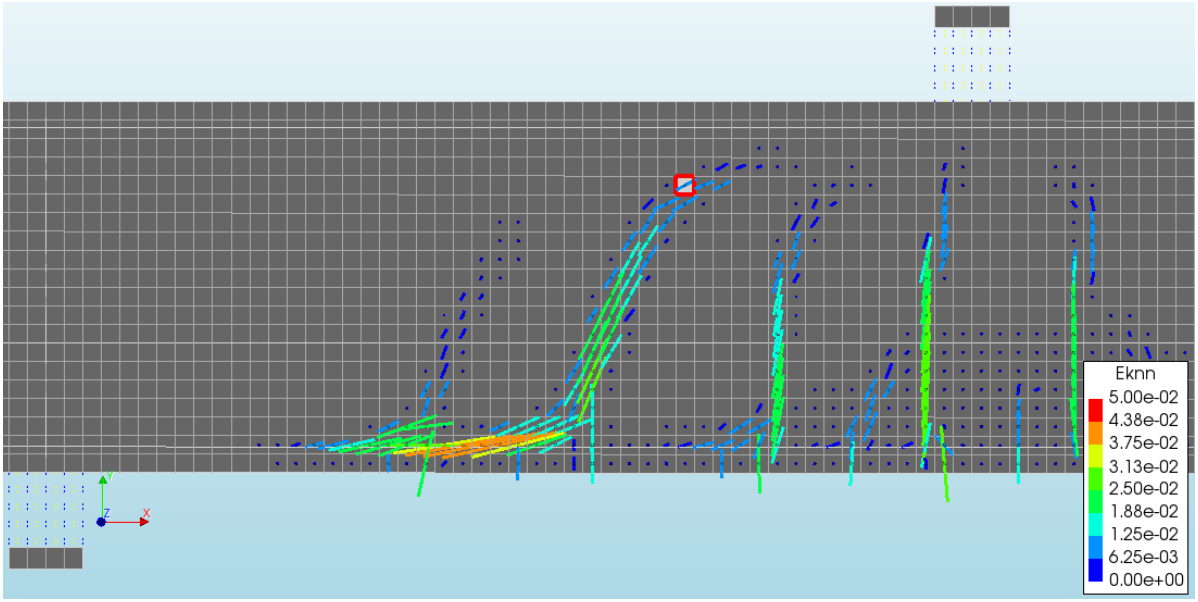

(a) NLFEA Crack plot at step marked in Figure 6.3, P = 190 kN

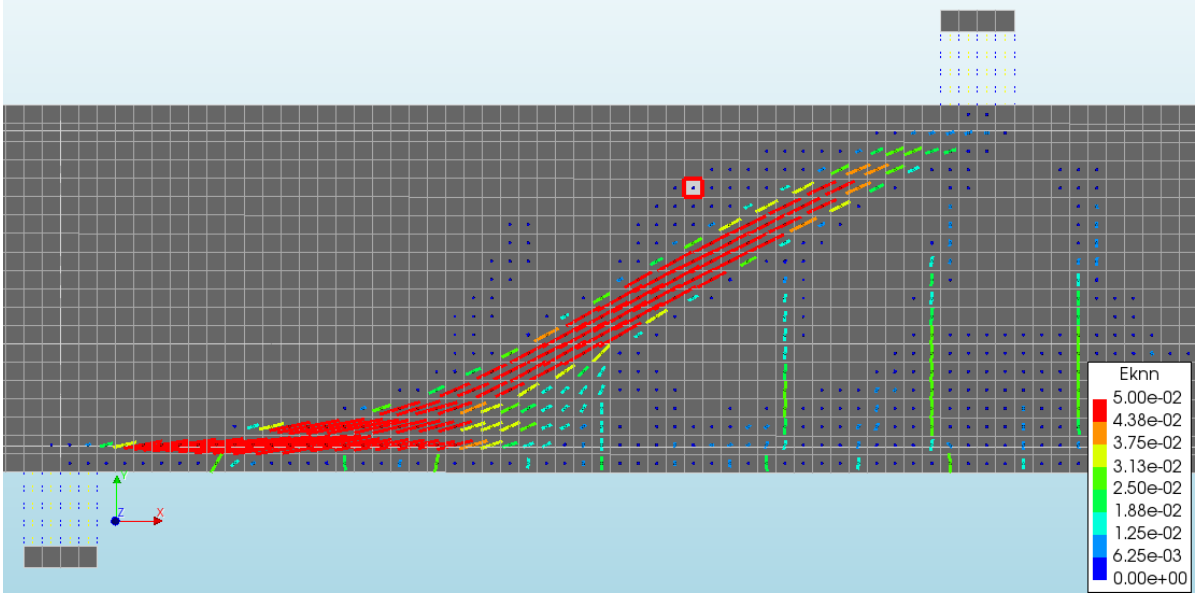

(b) NLFEA Crack plot at P = 210 kN

Figure 6.5: NLFEA crack plot of beam B702A1 before and after experimental failure. Element 1079 marked in both.

Now the attention is shifted to Figure 6.5b, where the crack plot at 210 kN is shown. Notice how the original cracks rotated or even closed to accomodate an alternative load path. Figure 6.6 shows the crack width in an element located in the critical inclined crack. It shows that it opens drastically around the failure load, but then it is closed again as the inclination of the crack decreases and the arch structure develops. As the load increases the crack is 'pushed' down until the compression zone fails.

The critical crack was predicted correctly, a drop in the load observed. However, due to rotation of the critical crack, a new equilibrium state is found. Figure 6.5 shows that the inclination of the cracks decreases and because of that the crack does not develop horizontally towards the support and load plates. Recall Figure 2.3, where it was shown that the location of the critical inclined crack directly influences the failure mode and residual beam capacity. Instead of horizontal progression, the critical crack propagates diagonally towards the load point, therefore overestimating the capacity of the remaining arch structure described by Yang in [39]. It goes for itself that overpredictions like this are dangerous and should be avoided or at least identified when occurring.

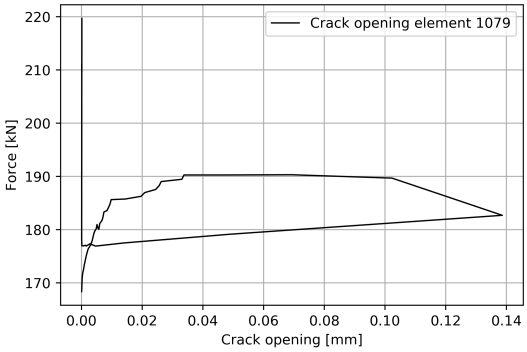

Figure 6.6: Crack opening of element 1079

6.2.2. Identification of overrotation

This change in behavior can be seen in the convergence behavior, but it is not always that clear. Figure 6.7a shows the convergence behavior of beam C751B1, which displayed a similar failure as B702A1. Between step 200 and 250, a cluster of non-converged steps can be seen. Ninety-seven percent of the steps converged up to that point. After some non-converged steps the new equilibrium path is followed and the beam continues to fail in compressive shear. Notice how the steps converge again. In this case, the moment of the change in failure mode can be easily identified by non-convergence of 9 consecutive steps. However, when the convergence behaviour of beam B702A1 in Figure 6.7b is taken into account it shows that this identification is not always simple. The transition into compressive shear failure starts at step 194 and results in 8 consecutive non-converged steps. These are harder to identify because of other, smaller clusters of non-converged steps around it. Other beams show fewer non-converged steps around the transition. What they do have in common is a local peak in the relative out of balance force, although less obvious for the model with 2000 iterations.

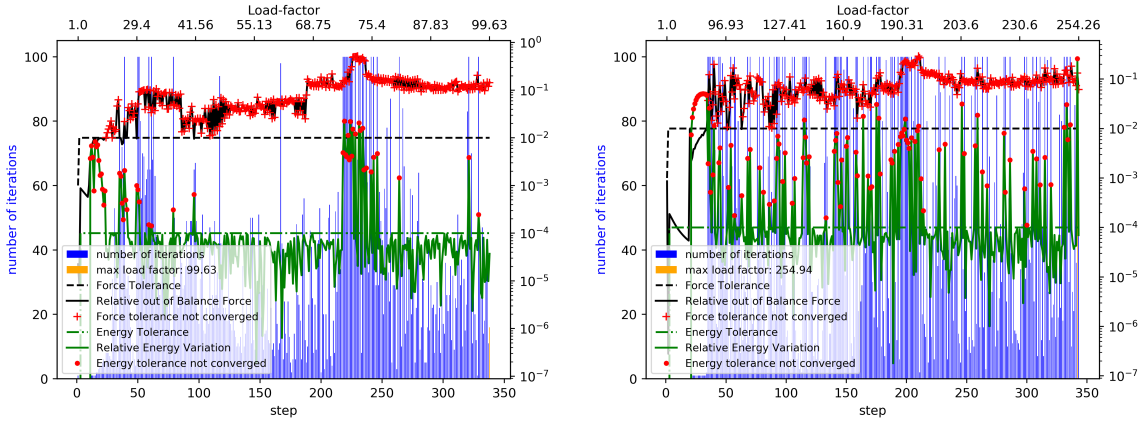

(a) Convergence behavior of beam C751B1 (97 % converged steps)

(b) Convergence behavior of beam B702A1 (75 % converged steps)

Figure 6.7: Typical convergence behavior in case of of overrotating cracks

To further strengthen this point, an analysis of beam B702A1 was performed with a maximum of 2000 iterations per step. This resulted in a 100 % convergence rate, yet this behaviour still exists. From this and the fact that the overprediction is observed consistently, it can be concluded that the problem is of a fundamental nature. This poses a problem for the current safety framework, where the prediction of ultimate load capacity is required as the only way to identify this is by interpretation of changes in the crack pattern and a drop in the force-displacement relation. The force-displacement relations for different amounts of iterations per step (= convergence rates) are drawn in Figure 6.8. For the solutions with 100 and 2000 iterations per step, a clear drop can be seen in the force displacement graph. Here the drop of the solution with 2000 iterations is more pronounced. The solution with 40 iteration per step does not show this drop, indicating a smoother transition

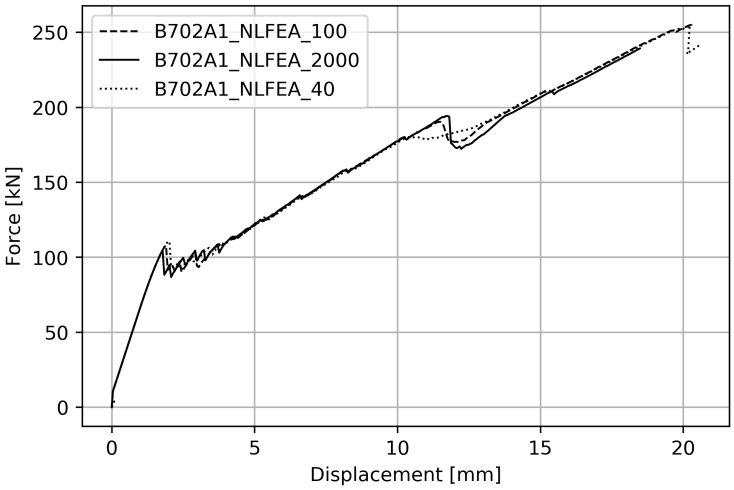

Figure 6.8: Force displacement of B702A1 for 40, 100 and 2000 iterations per step

of the failure mode. This is the case for almost any beam where this behaviour occurred.

For case R8, with 100 iterations per step, all failures were easily identifiable. Therefore beams without shear reinforcement should always be modelled with a relatively high amount of iterations per step. Based on the results of this study, a maximum of 100 iterations per step is advised. In addition to this it is recalled that from chapter 5 followed that beams without shear reinforcement modelled with a fixed crack also show a better approximation at 100 iterations per step. An investigation of values in between was not performed.

6.2.3. Rotating to fixed

Although not thoroughly investigated it is worth mentioning that a rotating to fixed cracking approach takes care of this problem, provided that the crack strain at which it is fixed is set sufficiently low. This approach did not result in results that were better than the fixed crack approach, but simply solved the problem of overrotation. It was tested for beams with stirrups as well, but the strain at which to fix the crack is different. The threshold strain required to correctly model beam VS-A3 - as a percentage of the ultimate Hordijk-strain - resulted in overrotation in B702A1. A further investigation of the rotating-to-fixed crack approach is required.

6.2.4. Manual identification of the correct failure load

Figure 6.9 shows the results for strategy R8, where all ultimate loads have been manually identified by looking at force displacement diagrams and convergence behaviour, as done for B702A1 above. It can be seen that the approximation of beams without shear reinforcement has substantially improved as the overshoots are no longer observed.

The calculated values for model uncertainty are listed in Table 6.2. It shows that beams without stirrups are now underestimated: $\mu_\theta = 1.071$, which can be preferred over an average overestimate. The coefficient of variation has decreased as well, to 0.141. This results in a model uncertainty factor of 1.11. Results for F9 have been included for comparison, showing how beams without stirrups are still better approximated by strategy F9. Performing two analyses, one with fixed crack model as in F9 and one with rotating crack model as in R8, could confirm the manual estimate of maximum load as the critical crack should be the same crack.

Table 6.2: Comparison of original strategies with a correction for the missed shear failures

	All Beams			Beams with stirrups			Beams without stirrups		
Reinforcement type	μ_θ [-]	V_θ [-]	γ_{Rd} [-]	μ_θ [-]	V_θ [-]	γ_{Rd} [-]	μ_θ [-]	V_θ [-]	γ_{Rd} [-]
R8 - Rotating (101 Beams)	1.006	0.176	1.232	1.075	0.097	1.047	0.925	0.213	1.404
R8 corrected for shear	1.075	0.118	1.074	1.075	0.097	1.047	1.071	0.141	1.110
F9 - Fixed (101 Beams)	1.158	0.169	1.061	1.243	0.172	0.993	1.053	0.108	1.084

For the newly determined distribution parameters, a histogram with the respective probability density

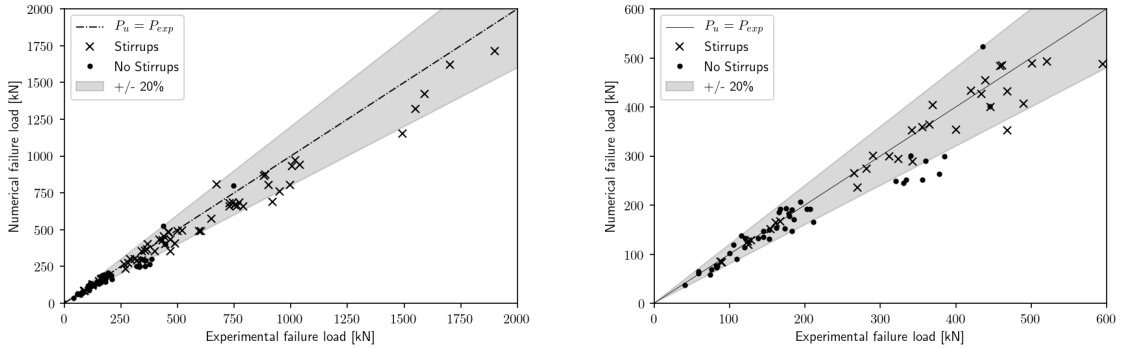

(a) Results R8, at the correct failure event

(b) Results R8, at the correct failure event, zoomed in on the lower end

Figure 6.9: Manually selected correct failure event NLFEA and experimental failure load for solution strategy R8

functions is drawn in Figure 6.10. All distributions now have a tail towards the conservative range with a higher uncertainty on beams without shear reinforcement.

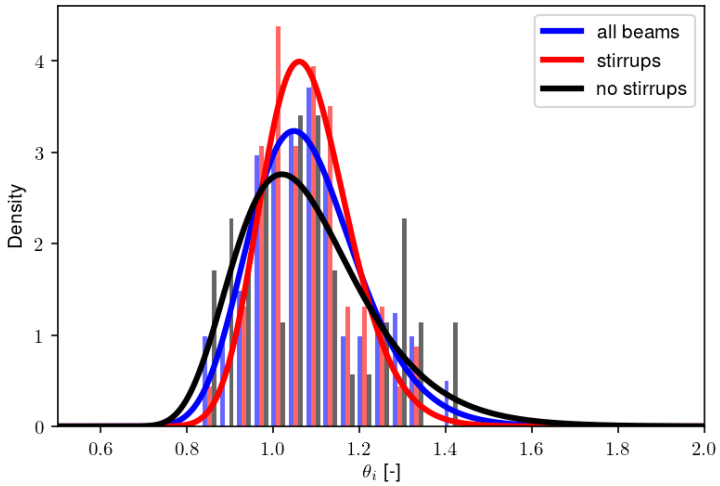

Figure 6.10: Log-normal density of model uncertainty with manual failure identification

In case one is performing a structural analysis of a beam structure this manual interpretation can be done. Often a structure does not consist of one beam, resulting in a more complex interpretation of those results. Also, the goal of this study is to be able to circumvent a manual interpretation as much as possible. Therefore beams without shear reinforcement should not be modelled with a rotating crack, unless the overrotation problem is solved.

6.3. The underprediction of beams with shear reinforcement with a fixed crack model

The overpredictions caused by the rotating crack models are contrasted by underpredictions of the capacity of beams with shear reinforcement caused by fixed crack models. From Table 6.1 it was seen that many beams that should have failed due to compressive shear or bending failed by yielding or failure of the stirrups. The wrong failure modes are shown in Figure 6.1b as well. As it can be seen from that figure, this did not result in any overpredictions.

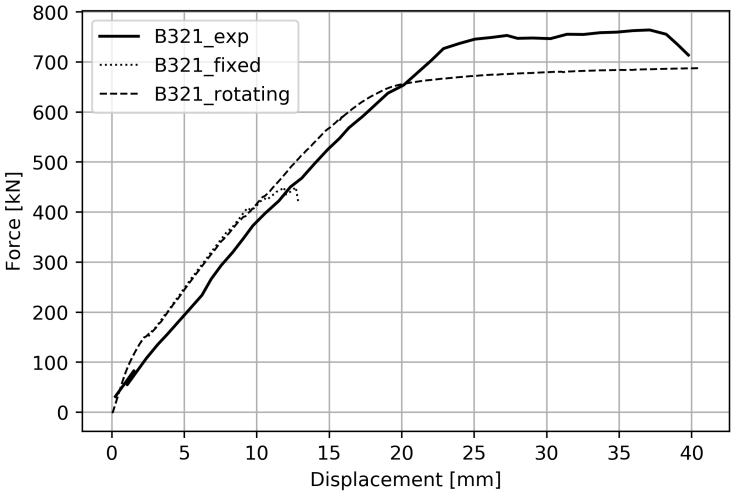

Figure 6.11: Force displacement behaviour obtained for B321

6.3.1. Example case: beam B321

As an example of this behaviour, a comparison is made between a fixed crack and rotating crack simulation of beam B321 from Rashid & Mansur. Strategy R4 resulted in a failure load of 687 kN, F9 in a failure load of 449 kN. In the experiment an ultimate load of 765 kN was measured. The force displacement characteristics are shown in Figure 6.11.

Both R4 and F9 start off very similar and at some point the fixed crack model appears to lose capacity.

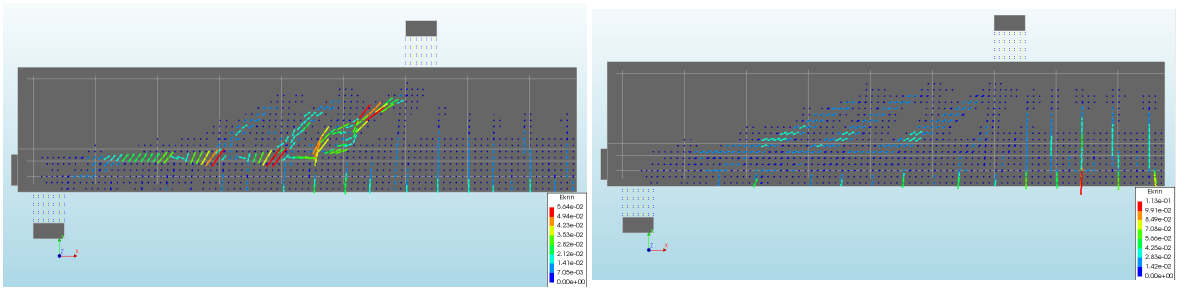

(a) crack plot for B321 with F9

(b) crack plot for B321, strategy R4

Figure 6.12: Crack plots at maximum load for B321 with R4 and F9

Figure 6.12 shows the differences in the resulting crack patterns. It is clearly seen that the inclination of the cracks is different. This means that the inclination of the struts is different as well. A steeper strut means less spreading over the stirrups for the fixed crack. Because of the conservative damage based retention function any interlock quickly decays and the stirrup at the main crack fails. The yielding of the stirrups is shown in Figure 6.13. In the model with a rotating crack, diagonals can form at a lower angle and the load is spreading over multiple stirrups. This spreading can be identified in Figure 6.13b. Secondly, it was mentioned before that the strut should be allowed to rotate due to yielding of the stirrups. The rotation of the strut is hindered when the cracks are immediately fixed and have a conservative shear model.

6.3.2. A possible solution: increase shear stiffness retention

A solution to this is to increase the shear retention factor β in the constitutive definition. This way the interlock in the shear cracks would reduce the load taken by the stirrups. It would be possible to subscribe a β value such that the beam is perfectly modeled with a fixed crack. This β would however be different for each beam and ideally be fitted to an experimental value. That has no use in an engineering situation where no experiment is available. Seeing that the beams with stirrups are very well modeled with a rotating crack, this option is not pursued because it makes more sense to model the beams with a rotating crack instead.

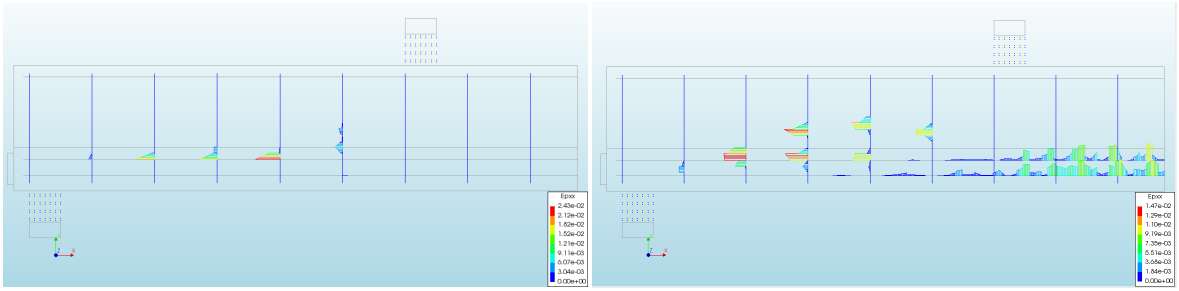

(a) Reinforcement plastic strain for B321 with F9

(b) Reinforcement plastic strain fo strategy R4

Figure 6.13: Reinforcement plastic strain at maximum load for B321 with R4 and F9

6.4. Shear failures in beams without shear reinforcement that should fail flexurally

For the beams from [40], the failure mode was often predicted wrong. Shear failures were predicted for the beams failing in bending. Solution strategy F9 resulted in a shear failure instead of a bending failure in 11 of the 12 cases. Strategy R8 was corrected for overrotation above, with this strategy the failure was predicted wrongly in 8 of the 12 cases. In case the bending failure was predicted correctly, the failure load was overestimated consistently. The beams from this experiment are the only beams that show this behaviour. The force-displacement behaviour of one of the beams is shown in Figure 6.14. It can be seen that everything about the solution is overstiff. The moment of first cracking is higher than the experiment, which is not surprising. The post-cracking stiffness and the stiffness when yielding starts are also higher.

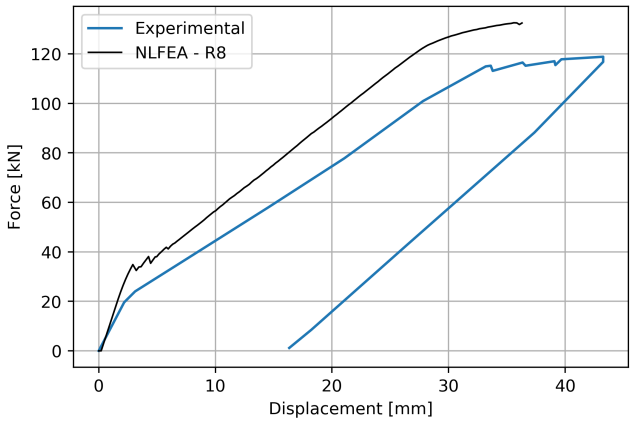

Figure 6.14: Force-displacement behaviour of beam A121A1 from [40]

The higher flexural resistance explains the high amount of shear failures instead of bending failures, especially in a study where the goal is to find the transition point between flexure and shear. Because the results predicted conservative shear failures and no flexural failures where a shear failure should have been found they are regarded acceptable.

6.5. Reinforcement modeling and failure modes

A beam without shear reinforcement can not be modelled with fully bonded reinforcement. The same behaviour as found in [35] has been observed in beams containing fully bonded reinforcement. Notice how in Figure 6.15a one large crack opens along the reinforcement for the case with fully bonded reinforcement (R1), while multiple flexural cracks form in case of bondslip reinforcement in 6.15b (strategy R4). The resulting distribution parameters of the model uncertainty for beams without shear reinforcement show this too. For R1 a mean model uncertainty of 1.14 is found for beams without stirrups. All other R-strategies overestimate the capacity (0.93 R2, 0.96 R4). R8 with corrected results, results in a mean model uncertainty of 1.08, with correct

failure modes.

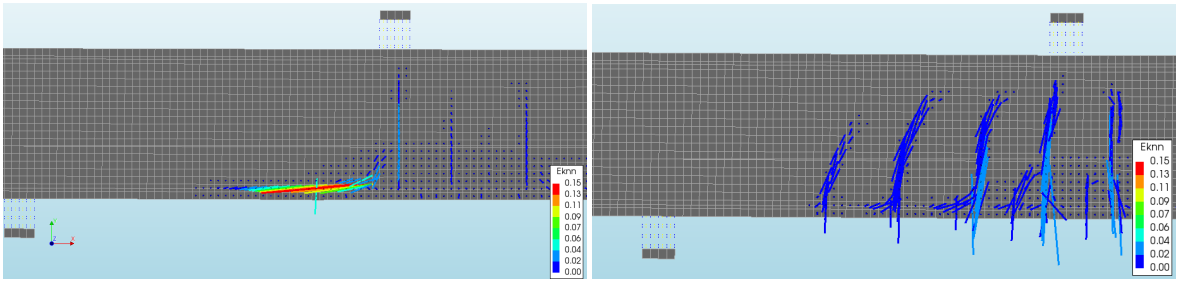

(a) crack plot for fully bonded reinforcement

(b) cack plot for

Figure 6.15: Crack plots for B702A1 with fully bonded (left) and bondslip reinforcement(right)

In chapter 5, it was concluded that the fib bondslip model should be used for beams without shear reinforcement. Further investigation showed that the slip-stress relation is important for the prediction of crack widths. The Shima model generally has a higher bond stress at which the stiffness starts decreasing significantly, this can be seen in Figure 2.7. It was found that the crack width at failure is the same for both models, while the model with Shima bondslip failed at a higher load level. The bond stress in the Shima model was higher at the same crack width, indicating it is too stiff. The failure mode of beams with shear reinforcement is generally less dependent on the crack widths, therefore the differences between bondslip models were less obvious there.

6.6. Conclusions

In this chapter, the accuracy of failure modes was presented and a qualitative context to the quantitative approach in chapter 5 was provided.

It was found that solution strategy R8, with a rotating crack, predicted the correct failure mode in 96 % of the cases. Combined with the obtained average uncertainty $\mu_\theta = 1.075$ and coefficient of variation of 0.097. It is concluded that a beam with shear reinforcement is safely modelled by applying strategy R8. That is a rotating crack model, 20 elements over the height, fib local bondslip model, convergence at E:0.0001 OR F:0.01 and a maximum of 100 iterations per step.

For the beams without stirrups, something else was found: It followed from many experiments that rotating crack models have problems detecting flexural shear failure in beams without shear reinforcement. This is due to overrotation of the critical inclined crack in a way such that a strut is able to form and the beam fails in the compression zone at a much higher load level, it was shown that this also occurs when all steps converge on an energy norm of 10^{-4}. It was discussed how this could be detected, but no concluding set of values could be established. By engineering judgement, the formation of the critical crack can be identified as long as a sufficient amount of iterations is allowed. In the study 40 iterations proved insufficient, but 100 iterations allowed for a clear detection of the formation of the critical crack followed by overrotation. It was shown that the flexural shear failures were predicted correctly with a fixed crack, provided that a damage based shear retention function was used.

Based on the beams in this study, especially a limited height, the best way to model a beam without shear reinforcement would be to use strategy F9: a fixed crack model, damage based shear retention and 20 elements over the height and fib MC2010 bond-slip behaviour. Non converged steps can be accepted, but it is advised to set a the iterations per step to at least 100.

The fixed crack with damage based retention was found to be unfit for modelling beams with stirrups, due to the fact that rotation of the compressive struts can not take place as freely as it can with a rotating crack model. The cracks are fixed immediately and the compressive struts have a high inclination. This results in limited spreading of shear force over the stirrups, because of that one or more stirrups fail before the beam fails in bending or shear compression. Therefore it is concluded that beams with stirrups should be modelled with a rotating crack.

7

The properties and application of the ductility index

The final piece of the puzzle is how the ductility index can be used in the assessment of a finite element solution. The details of implementation of the ductility index are listed in B. In this chapter, first the range of values which the ductility index takes for brittle or ductile failure modes is investigated. The relation between ductility index and model uncertainty is investigated for both between model-uncertainty and within model uncertainty. Unfortunately the ductility index displayed unexpected results for prestressed beams, so those beams were left out of the following assessments.

7.1. The definition of ductile or brittle failure

To have a more objective judgment of the way a beam fails, the ductility index was introduced. The idea is that a brittle failure is indicated by a low ductility index while a ductile failure is indicated by a relatively high value. Values obtained for the ductility index in two different strategies are visualized with the expected failure mode in Figure 7.1. It can be seen in 7.1a, that strategy F9 incidentally finds low ductility indices for beams that should fail in a ductile manner. This indicates that a failure in shear was predicted. This is caused by the behaviour described in 6.3. On the other hand, no high ductility indices are obtained for beams that should fail in a brittle manner. In 7.1b it is observed that the ductility of some beams is overestimated, such that more ductile failures are found for beams that should fail in a brittle manner.

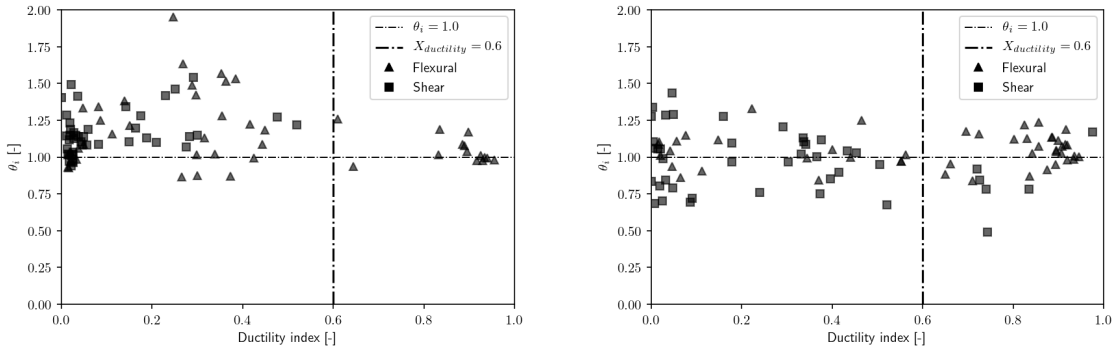

(a) Ductility index and model uncertainty for F9 (80 beams)

(b) Ductility index and model uncertainty for R8 (80 beams)

Figure 7.1: Observed ductility index with **experimental** failure mode

When the *observed* failures of R8 and F9 are combined, Figure 7.2a can be obtained. To distinguish between different models the results from F9 are plotted in blue while the results from R8 are in black.

Figure 7.2b shows the observed failure modes for R8 and F9, corrected for the overrotation of rotating cracks as done in 6.2. A comparison with figure 7.2a shows that the overshoots did not nescessarily have a

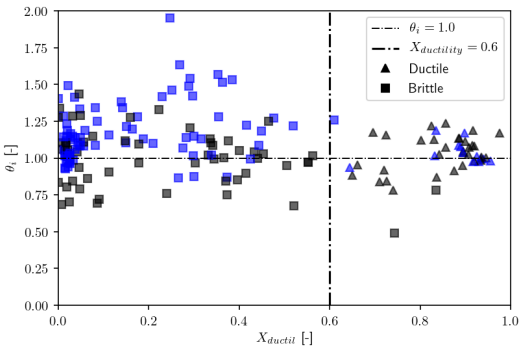

(a) Ductility index for R8 (black) and F9(blue)

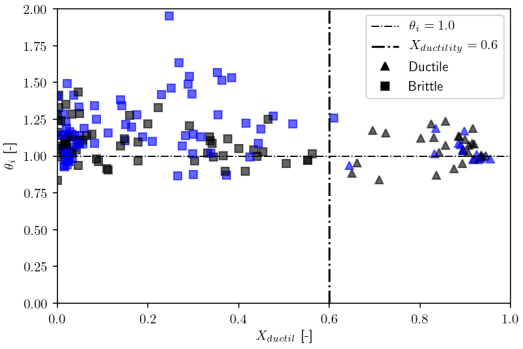

(b) Ductility index for R8 (black) and F9(blue), where the results of R8 were corrected as in 6

Figure 7.2: Observed ductility index with **NLFEA** failure mode

different ductility index. The minimum ductility index observed for a ductile failure was 0.6451, the maximum 0.9751. The mean ductility index of ductile failures equals 0.861. For brittle failures, a maximum of 0.6099 was obtained. Figures 7.2a and 7.2b show that in one case the ductility index for a brittle failure exceeded the threshold value of 0.6 set by Engen et al. in [16]. The average ductility index in case of brittle failures equalled 0.164, the minimum 0.0.
Out of 41 beams that displayed a ductile failure in their respective experiment, strategy R8 results in a ductility index over 0.6 in 28 cases. Strategy F9 resulted in 14 times a ductility index of over 0.6, indicating that a fixed crack model is more likely to predict a brittle failure.

7.2. The relationship between ductility and uncertainty

7.2.1. Within model comparison

Looking at the distributions in Figure 7.2, it appears that the model uncertainty parameters found for the beams with a ductility index lower than 0.6 are different from those found for a ductility index over 0.6.

Table 7.1: Accuracy of predicted failure for F-strategies, based on ductility index

Strategy	Failure	$X_{ductil} > 0.6$	%	$X_{ductil} \leq 0.6$	%
F1	Ductile	12	29	29	71
	Brittle	0	0	49	100
F2	Ductile	18	43	23	57
	Brittle	2	4	47	96
F3	Ductile	19	46	22	54
	Brittle	3	6	46	94
F4	Ductile	14	34	27	66
	Brittle	0	0	49	100
F5	Ductile	21	51	20	49
	Brittle	3	6	46	94
F6	Ductile	17	41	24	59
	Brittle	3	6	46	94
F7	Ductile	22	54	19	46
	Brittle	4	8	45	92
F8	Ductile	14	34	27	66
	Brittle	2	4	47	96
F9	Ductile	14	34	27	66
	Brittle	0	0	49	100
F10	Ductile	14	34	27	66
	Brittle	0	0	49	49

Table 7.2: Accuracy of predicted failure for R-strategies, based on ductility index

Strategy	Failure	$X_{ductil} > 0.6$	%	$X_{ductil} \leq 0.6$	%
R1	Ductile	22	54	19	46
	Brittle	7	14	42	86
R2	Ductile	29	71	12	29
	Brittle	9	18	40	82
R3	Ductile	30	73	11	27
	Brittle	13	6	36	73
R4	Ductile	25	61	16	39
	Brittle	8	20	41	80
R5	Ductile	29	71	12	29
	Brittle	9	18	40	82
R6	Ductile	29	71	12	29
	Brittle	10	20	39	80
R7	Ductile	26	63	15	37
	Brittle	9	18	40	82
R8	Ductile	28	68	13	32
	Brittle	6	12	43	88
R9	Ductile	24	59	17	41
	Brittle	2	4	47	96

For solution strategy F9, 14 out of 90 beams resulted in a ductility index larger than 0.6. Using the Bayesian updating procedure from MC2020 again results in: $\mu_\theta = 1.044$ with $V_\theta = 0.096$ for the beams with a ductility index > 0.6 and $\mu_\theta = 1.17$ with $V_\theta = 0.175$ for the beams with a ductility index < 0.6. Similarly, for strategy R8 it was found that 34 out of 90 beams resulted in a ductility index larger than 0.6. With this solution strategy it was found that $\mu_\theta = 0.999$ with $V_\theta = 0.171$ for ductile failures and $\mu_\theta = 0.995$, $V_\theta = 0.18$ for brittle failures. It is noted that the relatively high coefficient of variation for the model uncertainty of ductile failing beams can be attributed to some ductile failures which were in fact missed flexural shear failures.

7.2.2. Between model comparison

A next step is to look at all the results and obtain distributions of model uncertainty. Figure 7.3a shows the ductility on the horizontal axis and the model uncertainty on the vertical axis. The data points are all beams of which the *experimental* failure mode was brittle. Here, 841 of the 931 ductility indices where smaller than 0.6. This is approximately 90 % of the cases. The figure shows that most beams with a ductility index over 0.6 are beams without shear reinforcement. This is also reflected in the histogram of Figure 7.3b. In 75 % of the cases, the ductility index was smaller than 0.2. Twelve percent of the cases gave a ductility index larger than or equal to 0.6. From Figurees 7.3a and 7.3b it follows that the majority of beams with an overestimated ductility are beams without shear reinforcement.

The models which were expected to fail in a ductile manner show a different behavior. In 415 of the 779 cases, 53 %, a ductility index of over 0.6 was found. It shows from Figure 7.3d that the ductility of beams without stirrups is especially underestimated.

Summarized over all results: in 505 cases, a ductility index larger than or equal to 0.6 was found. The resulting mean model uncertainty $\mu_\theta = 0.992$ with a coefficient of variation $V_\theta = 0.137$. The other 1204 results yield a ductility index smaller than 0.6 with $\mu_\theta = 1.092$ and $V_\theta = 0.211$.

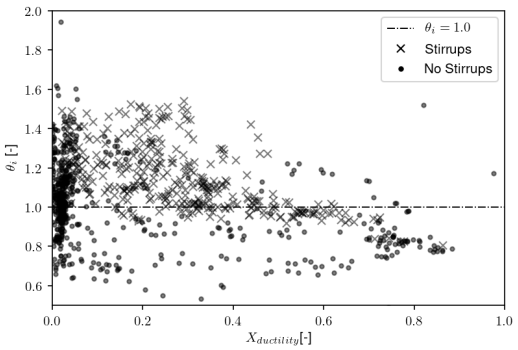

(a) Ductility index and θ_i of beams expected to fail in a brittle manner.

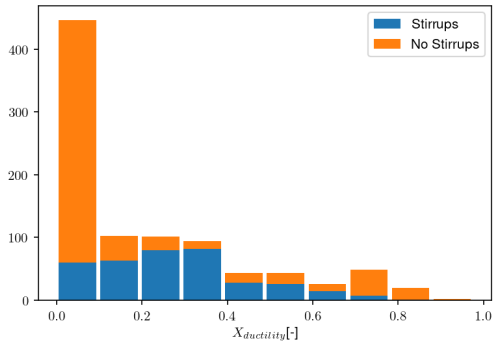

(b) Frequency distribution of ductility index of beams expected to fail in a brittle manner

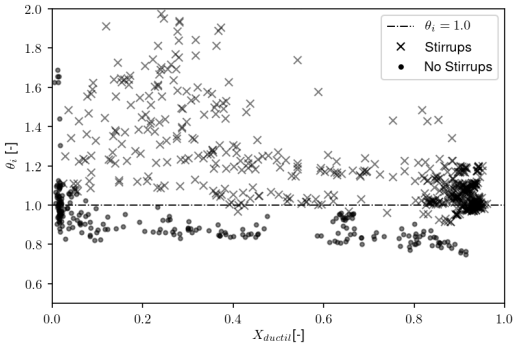

(c) Ductility index and θ_i of beams expected to fail in a ductile manner.

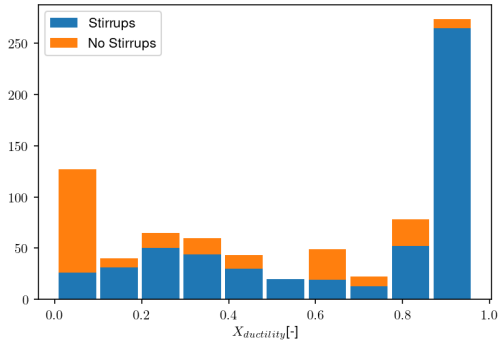

(d) Frequency distribution of ductility index of beams expected to fail in a ductile manner

Figure 7.3: Observed ductility index for all solution strategies

7.3. Discussion

7.3.1. The threshold value of 0.6

The main criterion for a ductile failure is to resist the ultimate load while deformation increases. Beams that are over-reinforced for bending and therefore fail in crushing of the concrete compressive zone before excessive yielding of the reinforcement are regarded quasi ductile. To point out the difference, the results of beams A111 and VS-C3 are investigated. Figures 7.4 and 7.5 display plastic strain in the reinforcement at maximum load and the force displacement relations of the respective beams.

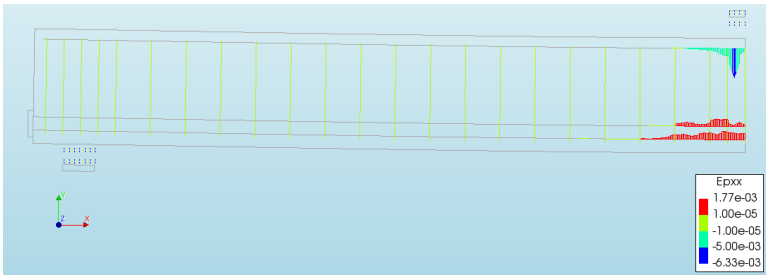

(a) Plastic strain in the reinforcement

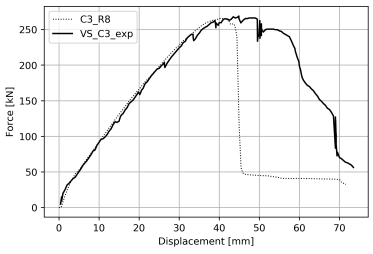

(b) Force displacement relation

Figure 7.4: Plastic strain of reinforcement and force-displacement of C3 for strategy R8

Notice the yielding in the compression zone in Figure 7.4a and the fact that the load is not retained. Limited yielding of the longitudinal reinforcement results for this case in a ductility index of 0.499. The force displacement relation (Figure 7.4b) displays a quasi-ductile failure.

A truly ductile failure is observed for beam A111. No yielding of the compression zone or stirrups was

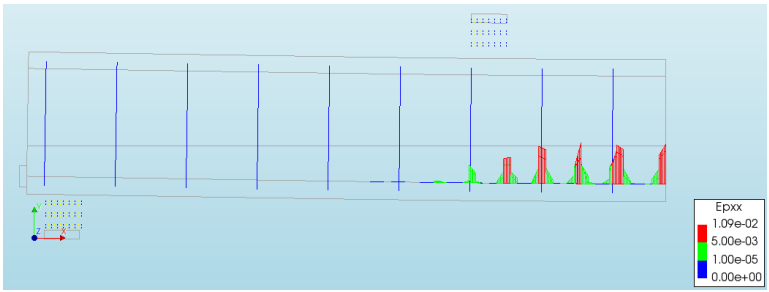

(a) Plastic strain in the reinforcement

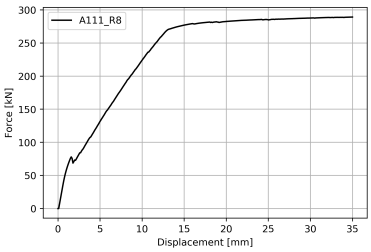

(b) Force displacement relation

Figure 7.5: Plastic strain of reinforcement and force-displacement of A111 for strategy R8

observed, as visible in Figure 7.5a and the load was retained while deformation increased substantially. This resulted in a ductility index of 0.765.

It shows from the plot in Figure 7.2 that one brittle failure occurs at a ductility index of over 0.6. This is beam D211 in F9. For this beam, failure of the stirrups occurred without yielding of the longitudinal reinforcement, the failure of the first stirrup did not cause failure of the beam right away.

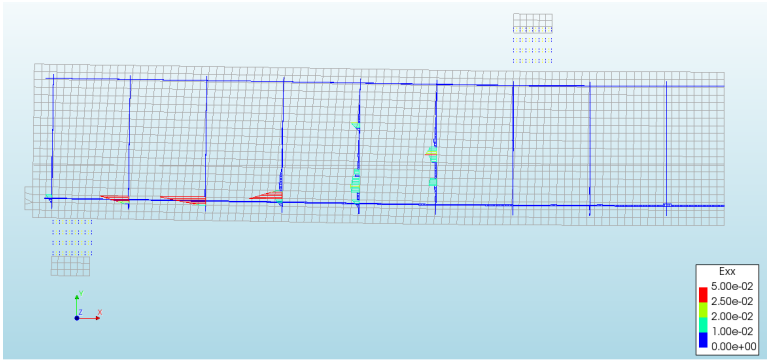

(a) Plastic strain in the reinforcement

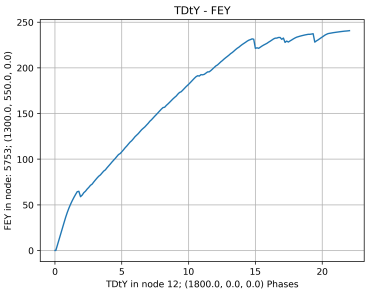

(b) Force displacement relation

Figure 7.6: Plastic strain of reinforcement and force-displacement of D211 for strategy F9

At the first drop in the load displacement diagram of Figure 7.6b, the strain in the stirrups exceeds the ultimate strain of 25 ‰at multiple locations, meaning the stirrups have failed. This is shown in Figure 7.6a. At this point the recorded ductility index equals 0.540, indicating that the failure is still brittle. After that, the analysis continues and stirrups yield even further but not at new locations, finally the analysis ended in divergence. From the load displacement diagram it is seen that the behaviour looks ductile, which would justify a high ductility index. As this beam was modelled with a fixed crack, while it was already shown that it is better to model a beam with stirrups with a rotating crack, taking the highest retained load at a converged step as the failure load can not be done without caution. If the failure load would be taken as the load that caused multiple stirrups to fail in one step, the recorded ductility index would again agree with the threshold of 0.6.

It could be argued whether or not a 'ductile' failure due to yielding of stirrups can be regarded a ductile failure. In any case, the definition of the ductility index could be improved by differentiating between yielding of stirrups and yielding of longitudinal reinforcement.

7.3.2. The ductility index as judgement for the accuracy of the failure mode

Having established that the threshold of 0.6 can be used in this case, every strategy can be judged in how accurate ductile and brittle failures are detected. The results were shown in Tables 7.1 and 7.2 and generally follow the expectations imposed by studies into the model uncertainty and failure mode, where a rotating crack is better for ductile failure modes and a fixed crack yields better results for brittle failures. It has to be noted that the ductility index does not give information on the correctness of a predicted failure mode. This is a weakness, especially when beams without stirrups are assessed. A high ductility index could in this case still mean that the shear failure was 'missed'. Also the detection of a brittle failure could mean that a compressive

shear failure instead of flexural shear failure resulted in the low ductility index. This means that the ductility index can not be used to assess the accuracy of predicted failure modes.

7.3.3. Uncertainty and ductility

The numbers listed in 7.2.2 : $\mu_\theta = 0.992$ with $V_\theta = 0.137$ for ductile failures and $\mu_\theta = 1.092$ with $V_\theta = 0.211$ for brittle failures, are still skewed by the two main problems with predicting the right failure mode, just as the results reported in 7.2.1. If the corrected set from chapter 6 is used again (see Figure 7.2), a different set of parameters is obtained. The mean uncertainty for ductile failures $\mu_\theta = 1.045$ and $V_\theta = 0.104$. A mean uncertainty of 1.083 with a coefficient of variation of 0.120 is obtained for beams with brittle failure modes. This confirms the idea that the uncertainty of brittle failures is higher than those of ductile failures and therefore the use of an appropriate solution strategy results in a value of the ductility index that can be used to estimate the uncertainty of the analysis.

7.4. Conclusions

The range of values of the ductility index was investigated for 180 cases. It was found that the threshold value of 0.6 set by Engen et al. was exceeded by a failure that could be regarded brittle in one of those cases. This resulted in the suggestion to improve the ductility index by differentiating between dissipated energy in the stirrups and longitudinal reinforcement.

Based on the threshold of 0.6, an assessment of the previously obtained 'correctness of failure mode' was done. This corresponded to the observed failure mode with one exception: In case of overrotation of the critical crack resulting in a compressive shear instead of flexural shear failure, the ductility index did not change. This means that the ductility index can not be used to assess how correct a failure mode is, but just to assess how much energy was dissipated.

The scatter of results for lower values of the ductility index was found to be different from the scatter in more ductile outcomes. Summarized over all 1709 results, a mean uncertainty of 0.992 with a coefficient of variation of 13.7 % was obtained for the beams with a ductility index larger than 0.6. For the brittle failures, with a ductility index below 0.6, the mean uncertainty was foud to be 1.092, with a substantially higher variation of 21.1 percent.

To ensure the correct failure mode, the overshoots due to overrotation of the crack were corrected. This resulted in the distribution shown in Figure 7.2b. Here, the difference in accuracy between the ductile and brittle failures became even more clear: $\mu_\theta = 1.131$ and $V_\theta = 0.157$ for $X_{ductility} \leq 0.6$ and $\mu_\theta = 1.045$ with, $V_\theta = 0.098$ for $X_{ductility} > 0.6$. Therefore it can be concluded that the ductility index can be used to estimate the model uncertainty, provided that an appropriate strategy is used.

8

Conclusions and Recommendations

8.1. Conclusions

The influence of different choices in a solution strategy to its accuracy was assessed by investigating the model uncertainty of 19 different solution strategies. Those solution strategies were developed with different assumptions and choices for the concrete constitutive model, the finite element discretization, the way of modelling the reinforcement and the incremental-iterative procedures. To investigate the influence of the concrete constitutive model, different fixed and rotating crack assumptions were selected and confinement aspects were included by reducing the compressive strength due to lateral cracking, according to the RTD1016 Dutch guideline. Regarding the finite element discretization, two dimensional models with a plane stress assumption were adopted and the effect of element size for the regular rectangular meshes was studied. For the reinforcement, either truss or beam elements were selected, the latter allowing for some dowel action, and both perfect bond and various bond-slip assumptions were evaluated. To solve the nonlinear equations, force-control in combination with an arc-length method was adopted and a line-search algorithm was applied to help convergence, because displacement control has less practical applications. Choices for step size and convergence criteria were varied. The 19 solution strategies are different combinations of choices on these four aspects.

Those 19 solution strategies were benchmarked by selecting 101 beams from experiments in literature, performing 1919 NLFEAs in the DIANA FEA multi-purpose finite element package and studying the resulting model uncertainties to assess their accuracy in different situations.

8.1.1. Important aspects of a solution strategy with respect to accuracy.

As a substantial difference in the approximation of beams with and without shear reinforcement was observed, these results were assessed separately. For beams without stirrups, the accuracy was influenced by any subtle change to the solution strategy: The constitutive model, element size, reinforcement modelling, convergence criteria and the maximum number of iterations per step. For the beams with shear reinforcement, the main factor of influence was found to be the constitutive model, as rotating and fixed crack models gave very different results. Variations of other choices in the strategy did not yield significant changes in the prediction of ultimate loads.

8.1.2. Is it possible to have one robust strategy for all concrete beams ?

It was found that application of a robust strategy, without any interpretation or engineering judgement of the result, is not possible. To be able to use one robust strategy for all concrete beams, the problems surrounding rotating crack models for beams without shear reinforcement should be taken care of. It was shown in chapter 6 that strategies with a rotating crack model are able to very well predict failure loads of both beams with and without shear reinforcement. The problem with this is that the moment of failure needs to be determined by visual inspection of the rotation of cracks and force-displacement behaviour. In some cases, the mentioned 'dip' in the force-displacement characteristic and change in mode of failure is justified, in other cases it is not. On the other hand, a fixed crack model with damage based shear retention results in very conservative predictions and wrong failure modes for beams with stirrups.

The spurious results of the rotating crack model were corrected for one solution strategy where the point of overrotation of the crack could be identified. It was found that this was possible when 100 or more iterations per step were applied, but impossible when this was limited to 40 iterations. This resulted in a mean model uncertainty of 1.075 with a coefficient of variation of 0.12 for all the beams, this would be the most robust approximation. Beams without stirrups were modelled with a mean uncertainty of 1.07 and a coefficient of variation of 0.14. Other strategies resulted in better results for beams without stirrups and therefore it is not advised to model every beam with the same solution strategy, but to use different solution strategies based on characteristics of the beam.

8.1.3. How can a solution strategy be prescribed based on the beam characteristics?

It was found that for beams without shear reinforcement, that are not higher than 600 mm, reliable results can be obtained by application of solution strategy F9. For the beams with shear reinforcement, any strategy with a rotating crack model as described in this study can be applied. This solution strategy should have convergence criteria of E:0.0001 OR F:0.01.

Strategy F9 models the beams in the following manner: The constitutive model consists of a fixed crack model with a damage based shear retention function. The mesh is built up with 20 elements over the height of the beam and the reinforcement is modelled with beam elements and the unconfined FIB bondslip model. The convergence criteria should be 0.0001 on the relative energy variation and 0.01 for the relative out of balance force. Steps can be regarded converged if one of the criteria is satisfied. Non converged steps can be accepted, as long as 100 full Newton-Raphson iterations are allowed in a step. The ultimate load is the maximum retained load in a converged step.

This solution strategy resulted in a mean uncertainty of 1.05, with a coefficient of variation of 0.108 for a total of 44 beams without shear reinforcement. All these results were within plus or minus 20 % of the experimental failure load. The failure mode of a beam without stirrups was predicted correctly in 75 % of the cases, all wrongly predicted failure modes concerned conservative shear failures where the experiment recorded a bending failure.

The beams higher than 600 mm showed severe mesh dependency and great care should be taken with modelling those beams, the best results were obtained for meshes with 20 elements over the height. Smaller elements resulted in higher predictions.

If a beam contains adequate shear reinforcement, any of the used strategies with a rotating crack model in the constitutive model is applicable. All 9 strategies combined resulted 513 NLFEA results for 57 beams. With this a mean model uncertainty of 1.07 with a coefficient of variation of 0.10 was obtained. It was shown that the failure mode of a beam with stirrups was predicted correctly in 96 % of the cases when strategy R8 was applied. This is the same strategy as described above, but with a rotating crack model instead of fixed crack model.

8.1.4. 4. What is the relation between the ductility index and model uncertainty?

A relation between the ductility index and model uncertainty has been established.

To do so, a more objective indication of failure modes was obtained by implementation of the ductility index. It was found that the threshold value of 0.6 can be used to distinguish between brittle and ductile failures, with the note that results can be improved by differentiating between dissipated energy in vertical and horizontal reinforcement. For all results with a ductility index below 0.6 , a mean uncertainty of 1.131 with a coefficient of variation of 0.211 was obtained. The results with a ductility index higher than the threshold resulted in a mean uncertainty of 0.992, with a coefficient of variation of 0.137 .

In case the appropriate strategy is used, a ductility index larger than 0.6 significantly reduces this uncertainty. A mean model uncertainty of 1.045, with a coefficient of variation of 0.098 was obtained in this case. This means that the ductility index could be used to estimate the model uncertainty, provided that the subscription of solution strategies above is followed.

8.1.5. Rules and regulations

It was shown that the assumption of model uncertainty as a lognormal distributed random variable occurring in literature is justified by fitting different distributions to the total set of 1919 obtained model uncertainties. With these results, the uncertainty factor for non-validated solution strategies of 1.3 was found to be valid as the results of 1919 analyses resulted in a reduction factor of 1.184.

The benchmarking of solution strategies was used to determine the model uncertainty factor as described in the MC2020 draft. This showed that an analyst is rewarded for benchmarking his or her solution strategy,

provided that an appropriate solution strategy is benchmarked with beams that are similar to the investigated beam. Except for the application of rotating crack models to beams without shear reinforcement, substantially lower uncertainty factors were obtained by benchmarking the solution strategies.

This study has shown that it is very well possible to reliably model the ultimate limit state of reinforced concrete beams with NLFEA. Reliable solution strategies were prescribed for beams with and without stirrups, showing that a standardized approach to NLFEA of reinforced concrete beams is possible. The uncertainty approach in the MC2020 draft was verified and it was suggested to include the ductility index to estimate the uncertainty based on a failure mode.

8.2. Limitations of the study

The reader should be aware of two limitations of this study:

1. The employed strategies are all based on the **total strain crack model**, as implemented in the **DIANA FEA package**. It should be noted that other cracking formulations exist.

2. Very few deep beams (h>600mm) were included in the benchmarks. As results indicate that a different approach or uncertainty factor might be required, therefore some care should be taken when the described strategies are applied to deep beams.

8.3. Recommendations for further research

It was identified that the uncertainty decreased as the shear slenderness increased. This makes sense as the beams with a higher shear slenderness are more likely to fail in bending. The amount of beams with a high slenderness in this study is however not high enough to justify a different reduction factor. It is recommended that the library of benchmark beams is expanded with many more 'ordinary' beams. That different model uncertainty factors can be used, as it does not make sense to include the uncertainty of beams failing in shear in the analysis of beams failing in bending.

The investigated influence of the amount of iterations per step was limited to 40 and 100 iterations. To have a more optimal solution strategy, values between 40 and 100 iterations should be investigated as 100 iterations take a lot of time.

This study focussed on the ultimate limit state of reinforced concrete beams. NLFEA can also be used to predict crack widths and deformations, which are important to SLS calculations. This behaviour was not investigated and therefore further research on this part is required.

The matter of overrotating cracks in beams without shear reinforcement was identified as the main cause of overpredictions of the failure load of these beams. A rotating-to-fixed approach showed promising results for beams without shear reinforcement, but did not solve the problems with beams containing shear reinforcement. A more systematic approach to this is required, either describing the rotating-to-fixed cracking approach or the fundamentals of the rotating crack model.

It was shown that the robustness of incremental-iterative procedures could be better. The bad numerical stability at the onset of cracking and at snap-backs and snap-troughs in brittle failure might result in bifurcations. If this is solved, convergence is no longer an issue and the uncertainties could be even lower than reported here.

The quantification of failure modes can be expanded further. The definition of the ductility index resulted in a total energy dissipation of the steel in the model, this included stirrups. The results might be better if a yielding of stirrups and longitudinal reinforcement are regarded separately.

Reliable modelling of deep beams without shear reinforcement remains an important challenge. This study did not contain enough of those beams to state anything but anecdotal proof of what might work. A thorough investigation of mesh sensitivity and size effects is required. It is recommended to further investigate this in terms of stress fields and crack plots. This was not reported in this report, but the possible impact of stress locking might be of interest. Next to that the influence and behaviour of reinforcement bond stresses appears to play a role in this matter. Also, the effects of different aggregate interlock models were not fully investigated.

Bibliography

[1] S.A. Ashour. Effect of compressive strength and tensile reinforcement ratio on flexural behavior of high-strength concrete beams. *ENGINEERING STRUCTURES*, 22(5):413–423, MAY 2000. ISSN 0141-0296. doi:10.1016/S0141-0296(98)00135-7.

[2] György Balázs, John Cairns, Rolf Eligehausen, Steffen Lettow, Giovanni Metelli, Stavroula Pantazopoulou, and Giovanni Plizzari. *Bond and anchorage of embedded reinforcement: Background to the fib Model Code for Concrete Structures 2010*. 01 2014.

[3] B Belletti, R Esposito, and J Walraven. Shear capacity of normal, lightweight, and high-strength concrete beams according to model code 2010. ii: Experimental results versus nonlinear finite element program results. *Journal of Structural Engineering*, 139(9):1600–1607, 2013. doi:10.1061/(ASCE)ST.1943-541X.0000743.

[4] B Bresler and A. C. Scordelis. Shear strength of reinforced concrete beams. *ACI Journal Proceedings*, 60, 1 1963. doi:10.14359/7842.

[5] DIANA FEA BV. *DIANA User's Manual – Release 10.4*. DIANA FEA BV, 2020. Retrieved from `https://dianafea.com`.

[6] Vladimir Cervenka, Jan Cervenka, Radomír Pukl, and Tereza Sajdlová. Prediction of shear failure of large beams based on fracture mechanics. 05 2016. doi:10.21012/FC9.029.

[7] Y. Choulli. *Shear Behavior of Prestressed I-Beams made with High-Strength Self Compacting Concrete*. PhD thesis, UNIVERSITAT POLITÈCNICA DE CATALUNYA, 09 2005.

[8] M. Collins, E. Bentz, P. Quach, and G. Proestos. The challenge of predicting the shear strength of very thick slabs. *Concrete International*, 37:29–37, 11 2015.

[9] M.P. Collins and D. Kuchma. How safe are our large, lightly reinforced concrete beams, slabs, and footings? *ACI STRUCTURAL JOURNAL*, 96(4):482–490, JUL-AUG 1999. ISSN 0889-3241.

[10] A. de Boer, M. A. N. Hendriks, C. van der Veen, and B. Belletti. Organizing an international blind prediction contest for improving a guideline for the nonlinear finite elements analysis of concrete structures. In Meschke, G and Pichler, B and Rots, JG, editor, *COMPUTATIONAL MODELLING OF CONCRETE STRUCTURES. EURO-C 2018*, pages 545–552, 2018. ISBN 978-1-315-18296-4; 978-1-138-74117-1. Conference on Computational Modelling of Concrete and Concrete Structures (EURO-C), Bad Hofgastein, AUSTRIA, FEB 26-MAR 01, 2018.

[11] A. de Putter, M.A.N. Hendriks, J.G. Rots, Y. Yang, and A.A. van den Bos. Supplement to master thesis 'towards a uniform and optimal approach for safe nlfea of reinforced concrete beams'. April 2020. doi:10.4121/uuid:fa79ca89-04cc-4caa-a09e-b73160f15f54.

[12] Federation Internationale du Beton. *fib Model Code for Concrete Structures 2010*. FIB/International Federation for Structural Concrete, 2013.

[13] *EN 1992-1-1 Eurocode 2: Design of concrete structures - Part 1-1: General rules and rules for buildings*, Brussels, 2005. EN, CEN.

[14] M. Engen, M.A.N. Hendriks, G. Monti, and D.L. Allaix. Treatment of modelling uncertainty of nlfea in fib model code 2020. unpublished manuscript, 2020.

[15] M. Engen, M. A. N. Hendriks, J. A. Overli, and E. Alstedt. Solution strategy for non-linear finite element analyses of large reinforced concrete structures. *STRUCTURAL CONCRETE*, 16(3):389–397, SEP 2015. ISSN 1464-4177. doi:10.1002/suco.201400088. JCSS Workshop, Ghent Univ Dept Structural Engn, BELGIUM, OCT 01-02, 2014.

[16] M. Engen, M. A. N. Hendriks, J. A. Overli, and E. Alstedt. A quantification of the modelling uncertainty of non-linear finite element analyses of large concrete structures. *STRUCTURAL SAFETY*, 64:1–8, 2017. ISSN 0167-4730. doi:10.1016/j.strusafe.2016.08.003.

[17] P. H. Feenstra. *Computational Aspects of Biaxial Stress in Plain and Reinforced Concrete*. PhD thesis, Delft University of Technology, 1993.

[18] S. J. Foster and R. I. Gilbert. Experimental studies on high-strength concrete deep beams. *ACI Structural Journal*, 95(4), 1998. doi:10.14359/554.

[19] W. M. Ghannoum. Size effect on shear strength of reinforced concrete beams. Master's thesis, McGill University, 1998.

[20] Sanjay Govindjee, Gregory J. Kay, and Juan C. Simo. Anisotropic modelling and numerical simulation of brittle damage in concrete. *International Journal for Numerical Methods in Engineering*, 38(21):3611–3633, 1995. doi:10.1002/nme.1620382105. URL `https://onlinelibrary.wiley.com/doi/abs/10.1002/nme.1620382105`.

[21] M.A.N. Hendriks, A. de Boer, and B. Belletti. *Guidelines for Nonlinear Finite Element Analysis of Concrete Structures*. Rijkswaterstaat Centre for Infrastructure, 2017. Report RTD 1016-1:2017.

[22] M.A.N. Hendriks, A. de Boer, and B. Belletti. *Validation of the guidelines for Nonlinear Finite Element Analysis of Concrete Structures - Part : Prestressed Beams*. Rijkswaterstaat Centre for Infrastructure, 2017. Report RTD 1016-3B:2017.

[23] M.A.N. Hendriks, A. de Boer, and B. Belletti. *Validation of the guidelines for Nonlinear Finite Element Analysis of Concrete Structures - Part : Reinforced Beams*. Rijkswaterstaat Centre for Infrastructure, 2017. Report RTD 1016-3A:2017.

[24] D. A. Hordijk. *Local approach to fatigue of concrete*. PhD thesis, Delft University of Technology, 1991.

[25] F. Leonhardt and R. Walther. *Schubversuche an einfeldrigen Stahlbetonbalken mit und ohne Schubbewehrung*, volume 151. Deutscher Ausschuß für Stahlbeton, 1962.

[26] F. Leonhardt, R. Koch, and F.S. Rostacy. *Schubversuche an Spannbetonträgern*, volume 227. Deutscher Ausschuß für Stahlbeton, 1973.

[27] Joint Committee on Stuctural Safety. *Probabilistic Model Code*. 2001. 12th draft.

[28] Bogdan Podgorniak-Stanik. The influence of concrete strength, distribution of longitudinal reinforcement, amount of transverse reinforcement and member size on shear strenth of of reinforced concrete members. Master's thesis, University of Toronto, department of Civil Engineering, 1998.

[29] M.A. Rashid and M.A. Mansur. Reinforced high-strength concrete beams in flexure. *ACI Structural Journal*, 102:462–471, 05 2005.

[30] J. G. Rots. *Computational Modeling of Concrete Fracture*. PhD thesis, Delft University of Technology, 1988.

[31] J. G. Rots and J. Blaauwendraad. Crack models for concrete, discrete or smeared? fixed, multi-directional or rotating? *Heron*, 34(1):1–33, 1989.

[32] S. S. SHAPIRO and M. B. WILK. An analysis of variance test for normality (complete samples)†. *Biometrika*, 52(3-4):591–611, 12 1965. ISSN 0006-3444. doi:10.1093/biomet/52.3-4.591.

[33] H. SHIMA. Micro and macro models for bond behavior in reinforced concrete. *Journal of the Faculty of Engineering, Univ. of Tokyo*, 39(2):133–194, 1987. URL `https://ci.nii.ac.jp/naid/80003653180/en/`.

[34] S. Sun and D. Kuchma. Shear behavior and capacity of large-scale prestressed high-strength concrete bulb-tee girders. Technical Report NSEL-002, Department of Civil and Environment Engineering University of Illinois at Urbana- Champaign, 2007.

[35] T. T. Teshome. Model uncertainty of non- linear finite element analysis of reinforced concrete beams without shear reinforcement. Master's thesis, Delft University of Technology, 2019.

[36] F. J. Vecchio and M. P. Collins. Compression response of cracked reinforced concrete. *Journal of Structural Engineering*, 119(12):3590–3610, 1993. doi:10.1061/(ASCE)0733-9445(1993)119:12(3590).

[37] F.J. Vecchio and W. Shim. Experimental and analytical reexamination of classic concrete beam tests. *JOURNAL OF STRUCTURAL ENGINEERING-ASCE*, 130(3):460–469, MAR 2004. ISSN 0733-9445. doi:10.1061/(ASCE)0733-9445(2004)130:3(460).

[38] J. C. Walraven. *Aggregate interlock: A theoretical and experimental analysis.* PhD thesis, Delft University of Technology, 1980.

[39] Y. Yang. *Shear Behaviour of Reinforced Concrete Members without Shear Reinforcement.* PhD thesis, Delft University of Technology, 04 2014.

[40] Y. Yang and R.T. Koekkoek. Measurement report on the transition between flexural and shear failure of rc beams without shear reinforcement. Technical report, Delft University of Technology, 2016. draft.

A

Model uncertainty per solution strategy

A.1. Distribution parameters of model uncertainty for all solutiion strategies

A complete overview of the results is given in Table A.1. Here the mean and coefficient of variation of the observed distribution are presented together with the updated MC2020 distribution and resulting model uncertainty factor.

A.2. Resulting parameters of solution strategies based on a rotating crack

A.2.1. R1

- Rotating crack
- 20 elements over height
- Fully bonded reinforcement
- convergence E: 0.0001 OR F: 0.01
- max 40 regular Newton-Raphson iterations

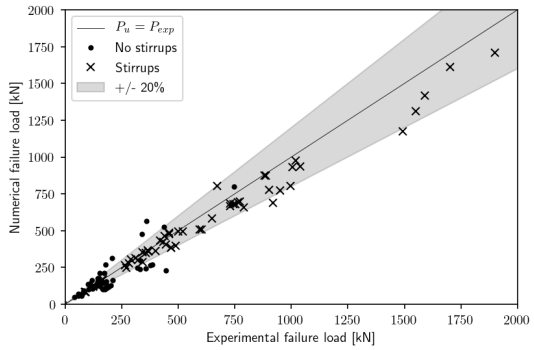

(a) All results for R1

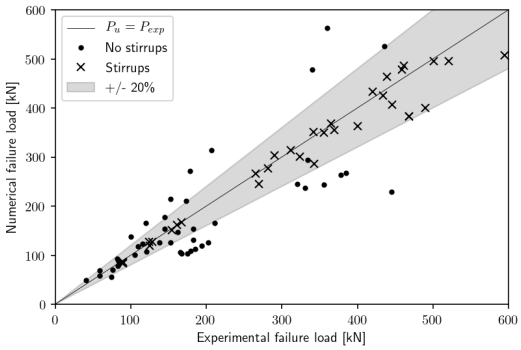

(b) Results R1 zoomed in

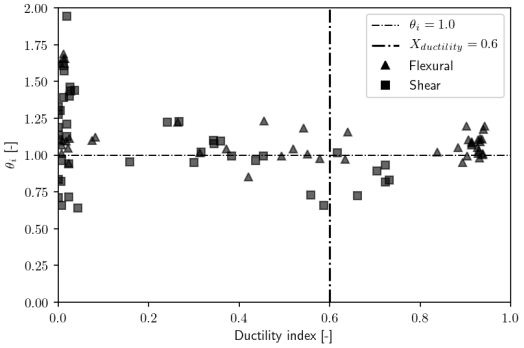

(c) Ductility index and model uncertainty for **experimental** failure mode

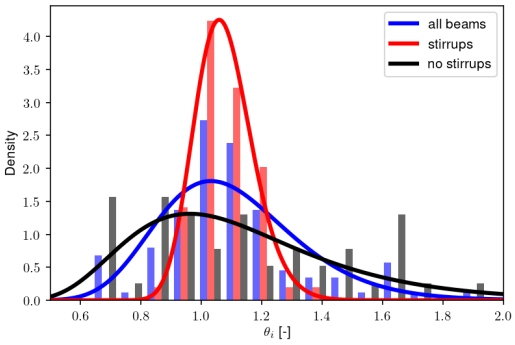

(d) Log-normal distributions fit to data

Figure A.1: NLFEA results for R1

A.2.2. R2

- Rotating crack
- 20 elements over height
- Shima beam bondslip reinforcement
- convergence E: 0.0001 OR F: 0.01
- max 40 regular Newton-Raphson iterations

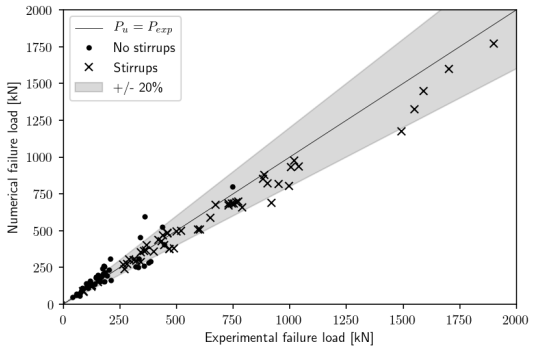

(a) All results for R2

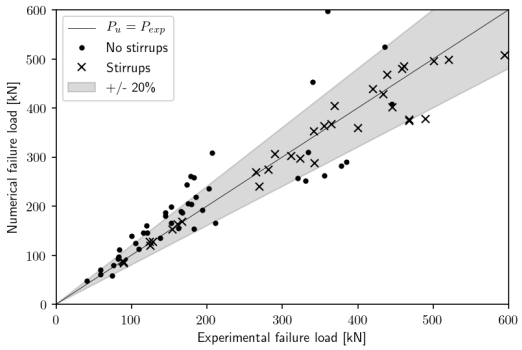

(b) Results R2 zoomed in

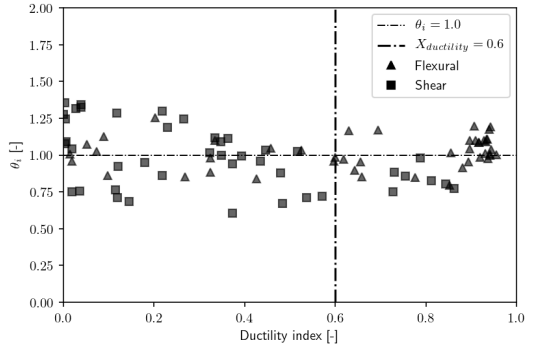

(c) Ductility index and model uncertainty for **experimental** failure mode

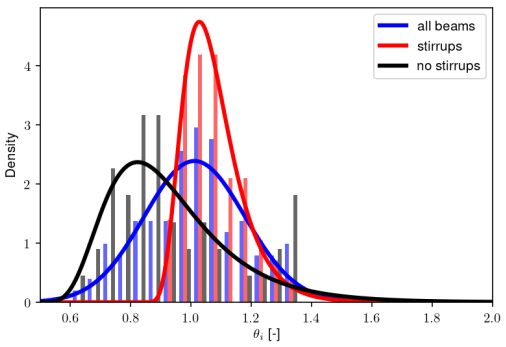

(d) Log-normal distributions fit to data

Figure A.2: NLFEA results for R2

A.2.3. R3

- Rotating crack
- 20 elements over height
- Shima beam bondslip reinforcement
- convergence E: 0.001 OR F: 0.01
- max 40 regular Newton-Raphson iterations

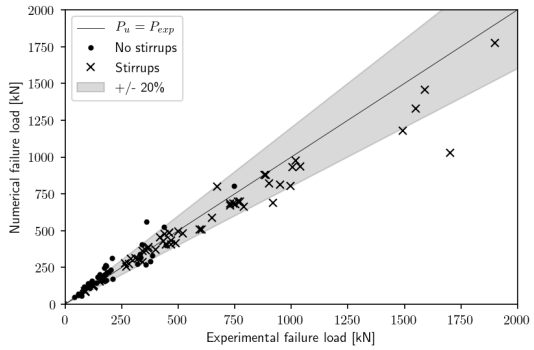

(a) All results for R3

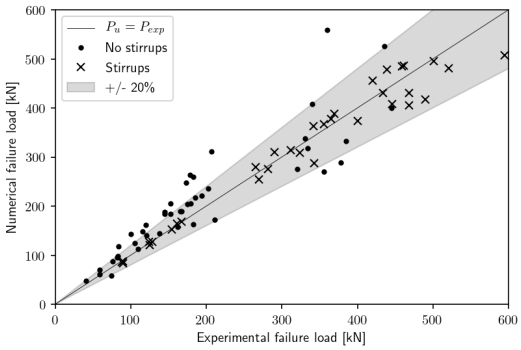

(b) Results R3 zoomed in

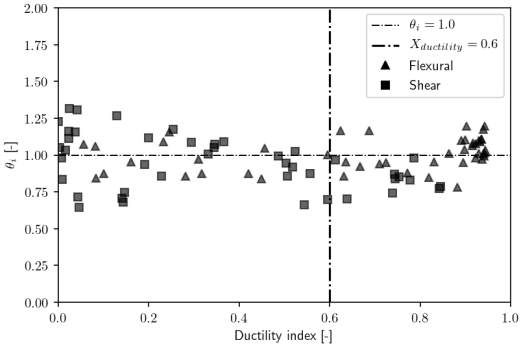

(c) Ductility index and model uncertainty for **experimental** failure mode

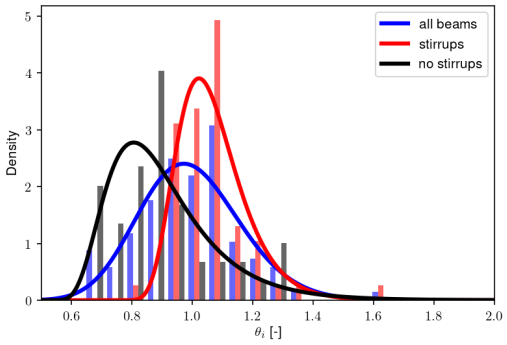

(d) Log-normal distributions fit to data

Figure A.3: NLFEA results for R3

A.2.4. R4

- Rotating crack
- 20 elements over height
- FIB MC2010 beam bondslip reinforcement
- convergence E: 0.0001 OR F: 0.01
- max 40 regular Newton-Raphson iterations

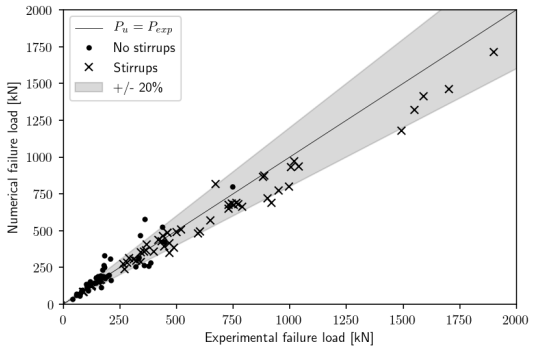

(a) All results for R4

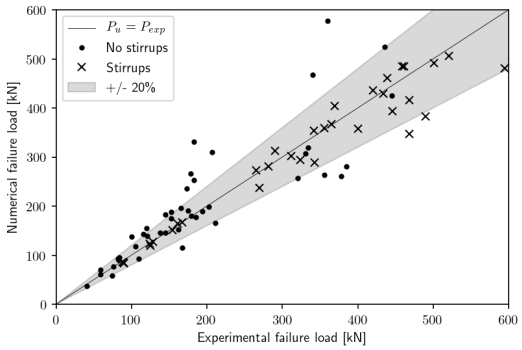

(b) Results R4 zoomed in

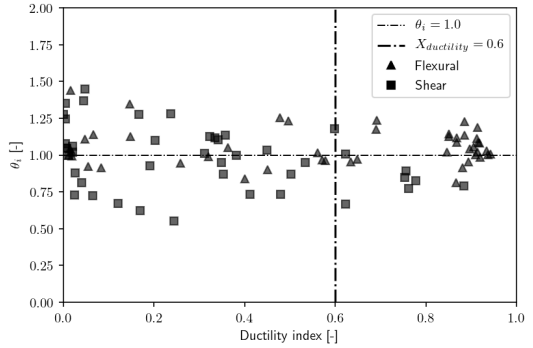

(c) Ductility index and model uncertainty for **experimental** failure mode

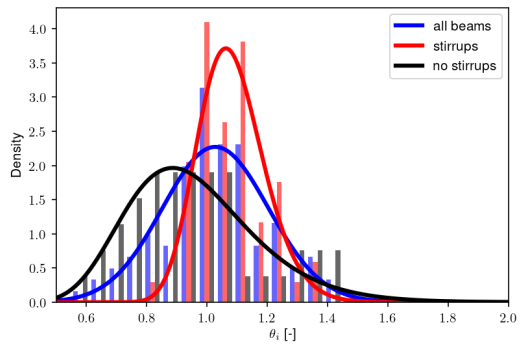

(d) Log-normal distributions fit to data

Figure A.4: NLFEA results for R4

A.2.5. R5

- Rotating crack
- 10 elements over height
- Shima beam bondslip reinforcement
- convergence E: 0.0001 OR F: 0.01
- max 40 regular Newton-Raphson iterations

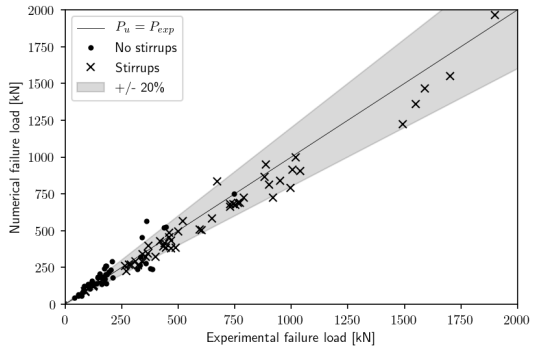

(a) All results for R5

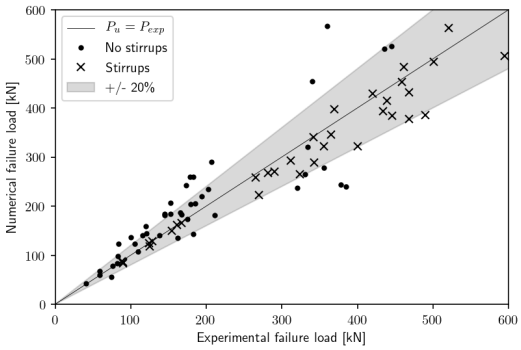

(b) Results R5 zoomed in

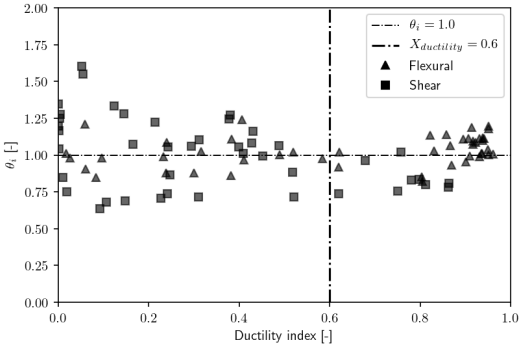

(c) Ductility index and model uncertainty for **experimental** failure mode

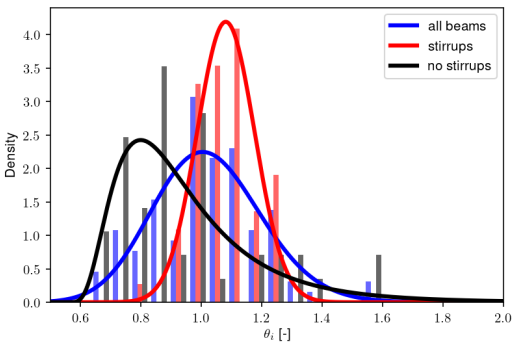

(d) Log-normal distributions fit to data

Figure A.5: NLFEA results for R5

A.2.6. R6

- Rotating crack
- 30 elements over height
- Shima beam bondslip reinforcement
- convergence E: 0.0001 OR F: 0.01
- max 40 regular Newton-Raphson iterations

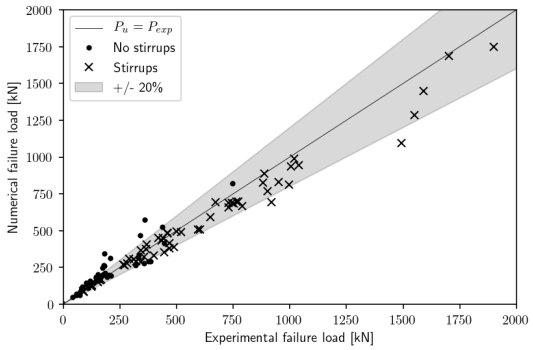

(a) All results for R6

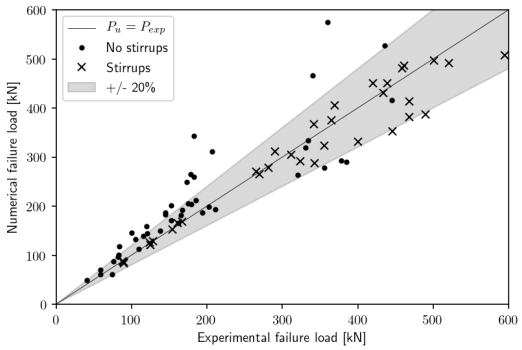

(b) Results R6 zoomed in

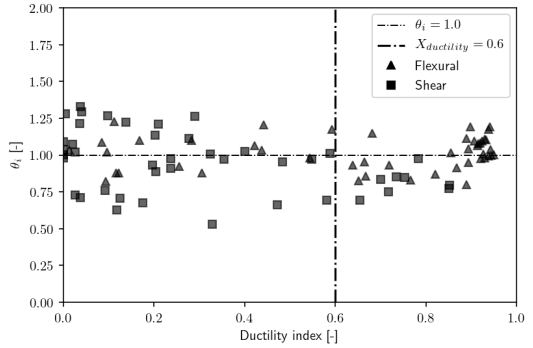

(c) Ductility index and model uncertainty for **experimental** failure mode

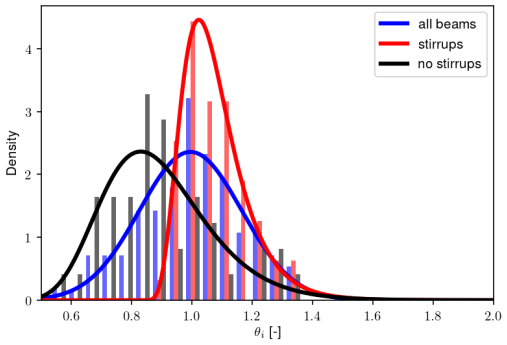

(d) Log-normal distributions fit to data

Figure A.6: NLFEA results for R6

A.2.7. R7

- Rotating crack
- 20 elements over height
- Shima beam bondslip reinforcement
- convergence E: 0.0001 AND F: 0.01
- max 100 regular Newton-Raphson iterations

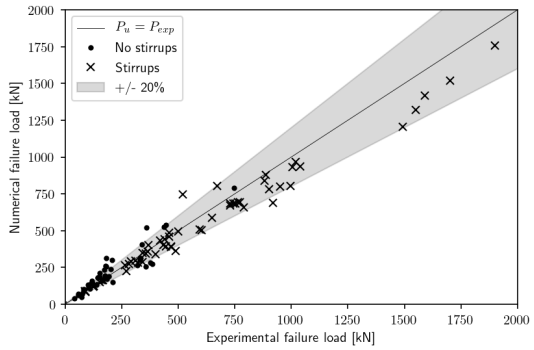

(a) All results for R7

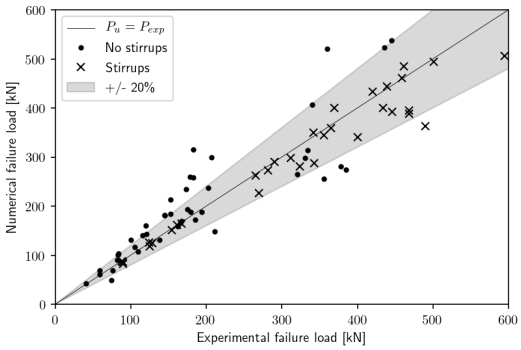

(b) Results R7 zoomed in

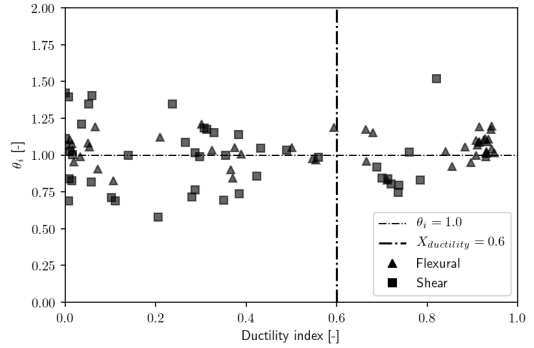

(c) Ductility index and model uncertainty for **experimental** failure mode

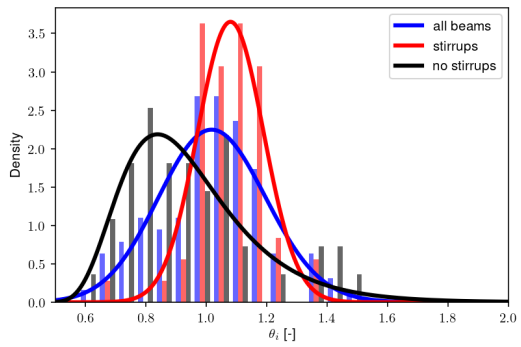

(d) Log-normal distributions fit to data

Figure A.7: NLFEA results for R7

A.2.8. R8

- Rotating crack
- 20 elements over height
- FIB MC2010 beam bondslip reinforcement
- convergence E: 0.0001 OR F: 0.01
- max 100 regular Newton-Raphson iterations

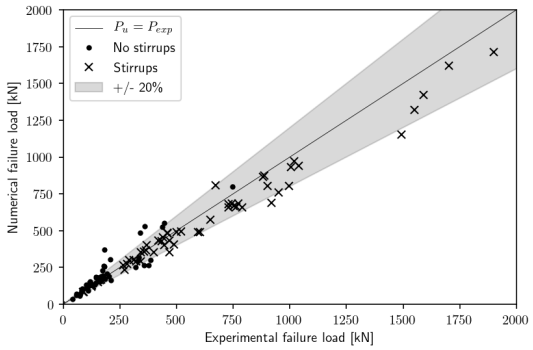

(a) All results for R8

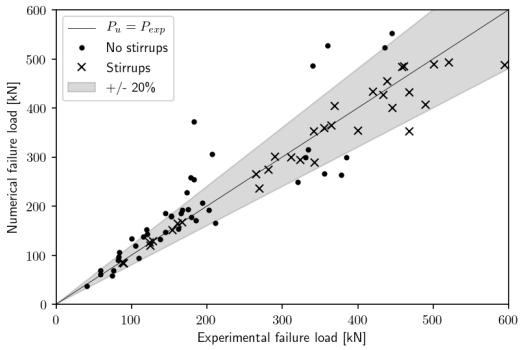

(b) Results R8 zoomed in

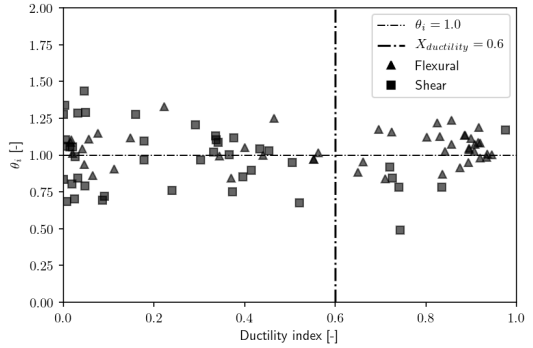

(c) Ductility index and model uncertainty for **experimental** failure mode

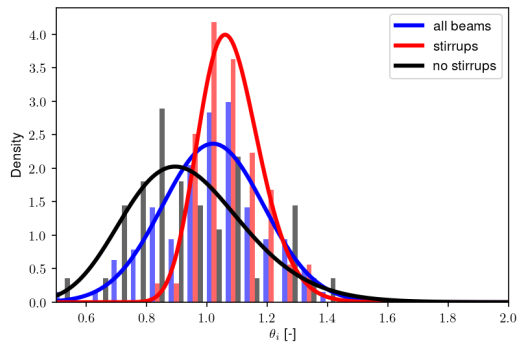

(d) Log-normal distributions fit to data

Figure A.8: NLFEA results for R8

A.2.9. R9

- Rotating crack
- 20 elements over height
- FIB MC2010 Truss bondslip reinforcement
- convergence E: 0.0001 OR F: 0.01
- max 100 regular Newton-Raphson iterations

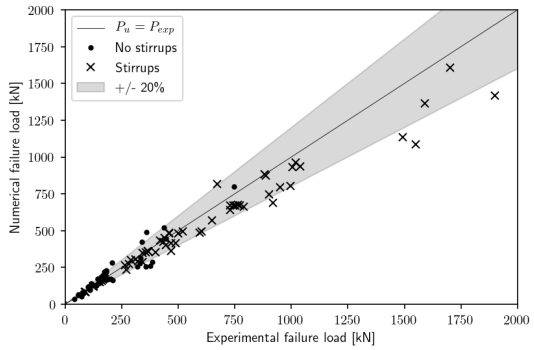

(a) All results for R9

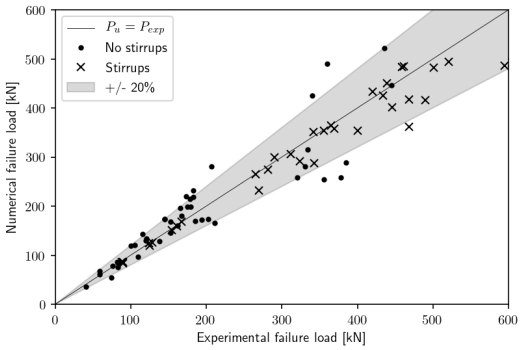

(b) Results R9 zoomed in

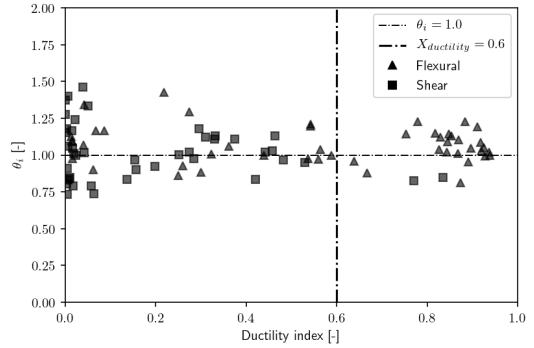

(c) Ductility index and model uncertainty for **experimental** failure mode

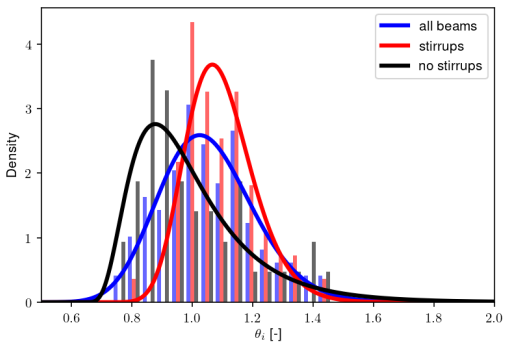

(d) Log-normal distributions fit to data

Figure A.9: NLFEA results for R9

A.3. Resulting parameters of solution strategies based on a fixed crack

A.3.1. F1

- Fixed crack, damage based retention
- 20 elements over height
- Fully bonded reinforcement
- convergence E: 0.0001 OR F: 0.01
- max 40 regular Newton-Raphson iterations

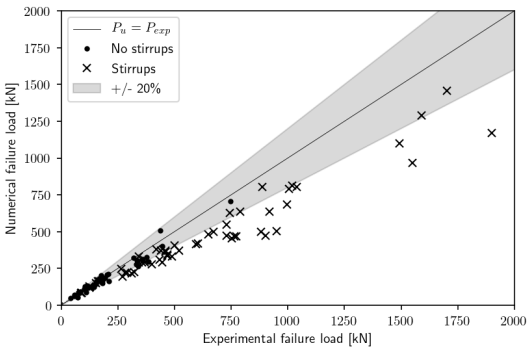

(a) All results for F1

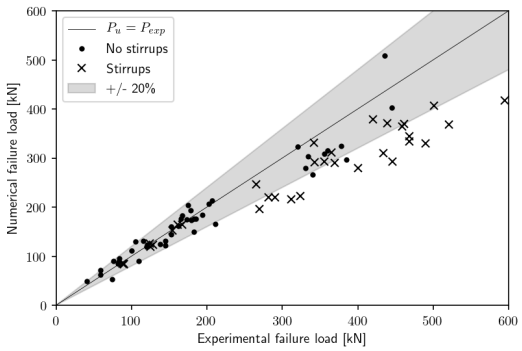

(b) Results R7 zoomed in

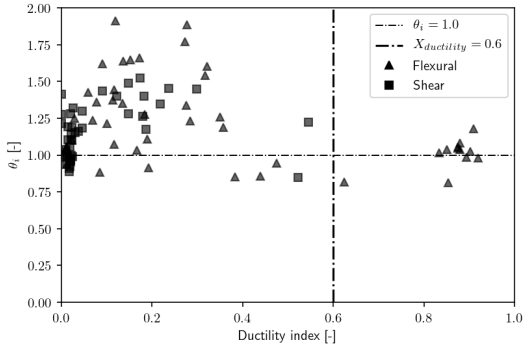

(c) Ductility index and model uncertainty for **experimental** failure mode

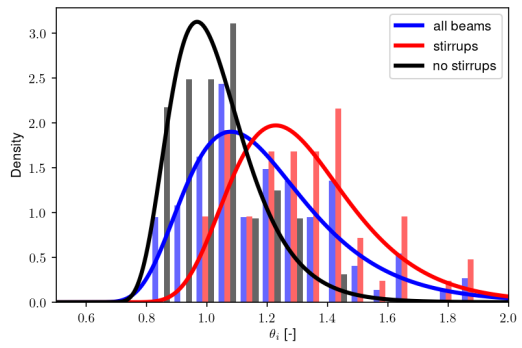

(d) Log-normal distributions fit to data

Figure A.10: NLFEA results for F1

A.3.2. F2

- Fixed crack, damage based retention
- 20 elements over height
- Shima beam bondslip reinforcement
- convergence E: 0.0001 OR F: 0.01
- max 40 regular Newton-Raphson iterations

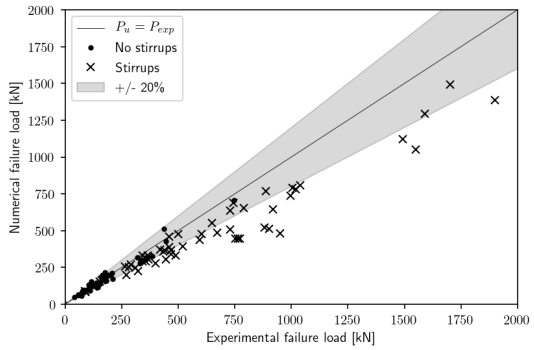

(a) All results for F2

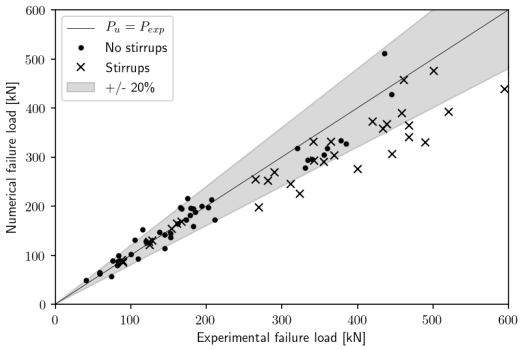

(b) Results F2 zoomed in

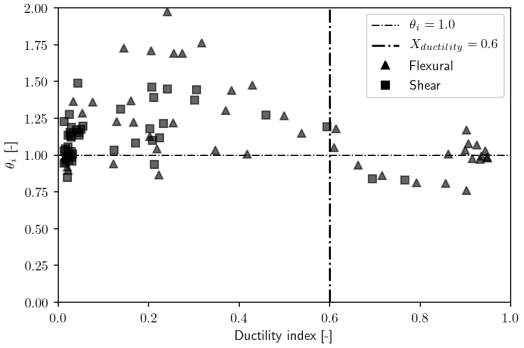

(c) Ductility index and model uncertainty for **experimental** failure mode

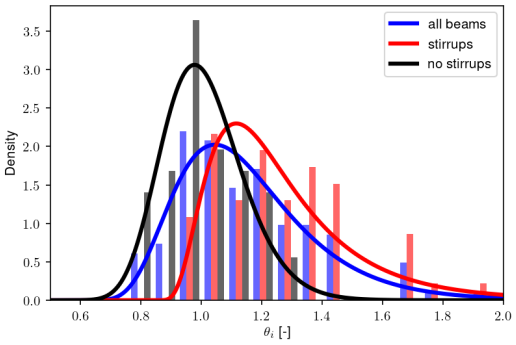

(d) Log-normal distributions fit to data

Figure A.11: NLFEA results for F2

A.3.3. F3

- Fixed crack, damage based retention
- 20 elements over height
- Shima beam bondslip reinforcement
- convergence E: 0.001 OR F: 0.01
- max 40 regular Newton-Raphson iterations

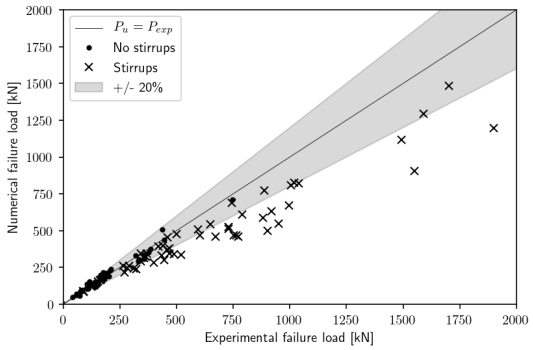

(a) All results for F3

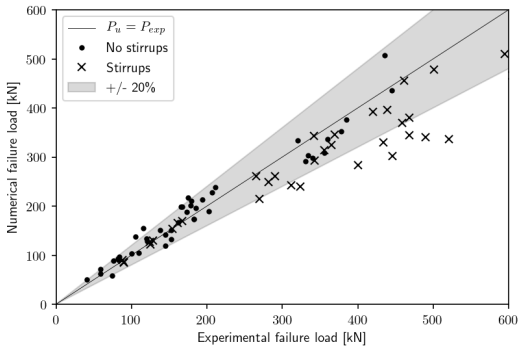

(b) Results F3 zoomed in

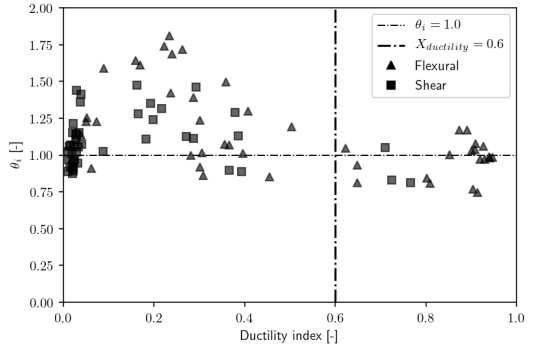

(c) Ductility index and model uncertainty for **experimental** failure mode

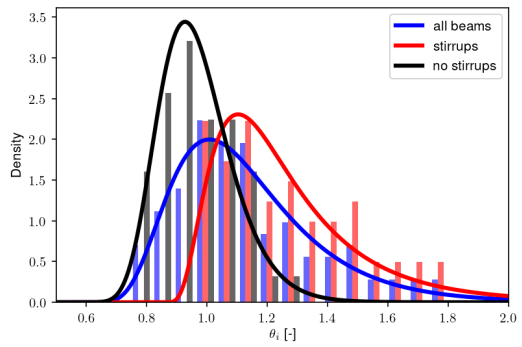

(d) Log-normal distributions fit to data

Figure A.12: NLFEA results for F3

A.3.4. F4

- Fixed crack, damage based retention
- 20 elements over height
- FIB MC2010 beam bondslip reinforcement
- convergence E: 0.0001 OR F: 0.01
- max 40 regular Newton-Raphson iterations

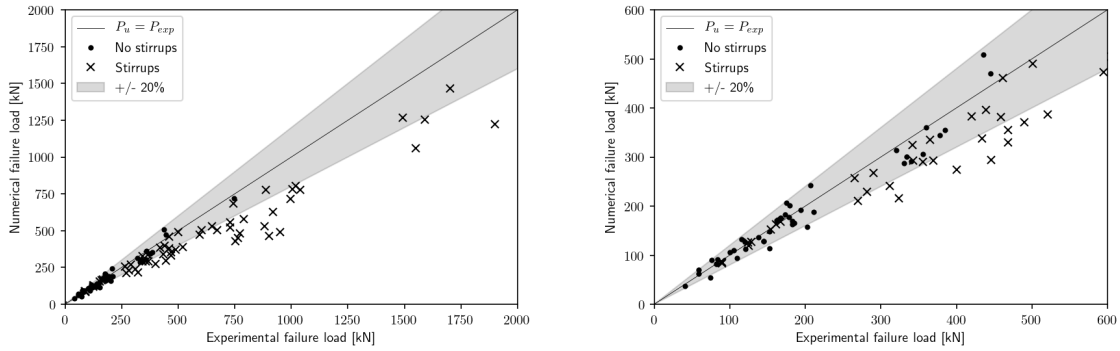

(a) All results for F4

(b) Results F4 zoomed in

Figure A.13: NLFEA results for F4

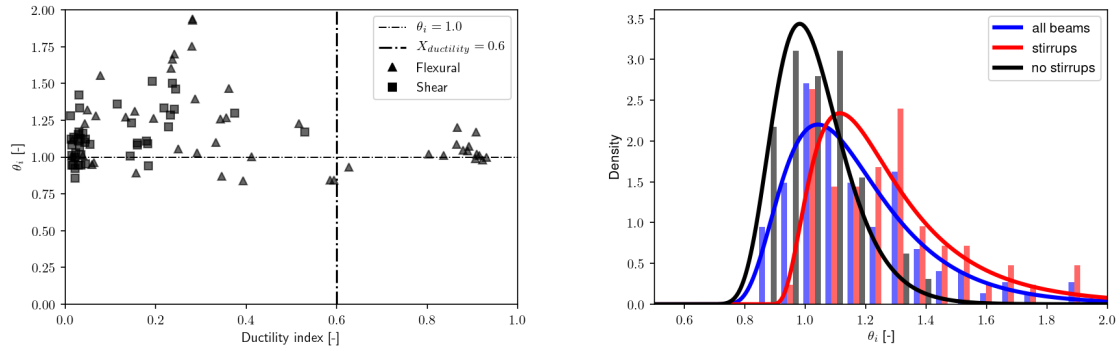

(a) Ductility index and model uncertainty for **experimental** failure mode

(b) Log-normal distributions fit to data

Figure A.14: NLFEA results for F4

A.3.5. F5

- Fixed crack, damage based retention
- 30 elements over height
- Shima beam bondslip reinforcement
- convergence E: 0.0001 OR F: 0.01
- max 40 regular Newton-Raphson iterations

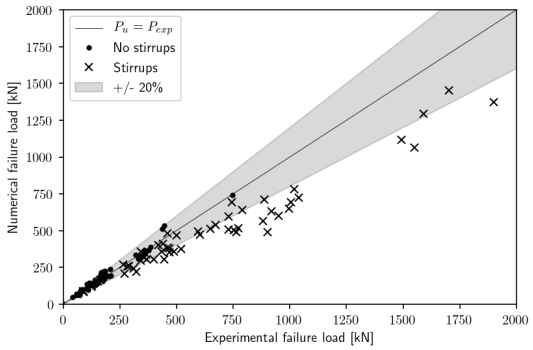

(a) All results for F5

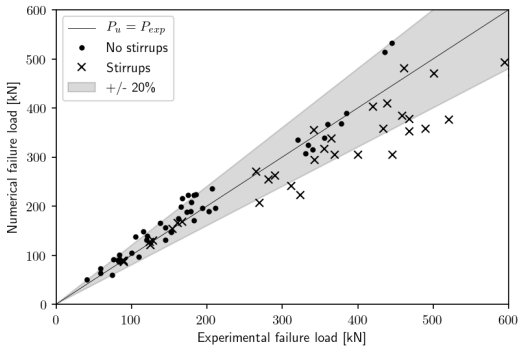

(b) Results F5 zoomed in

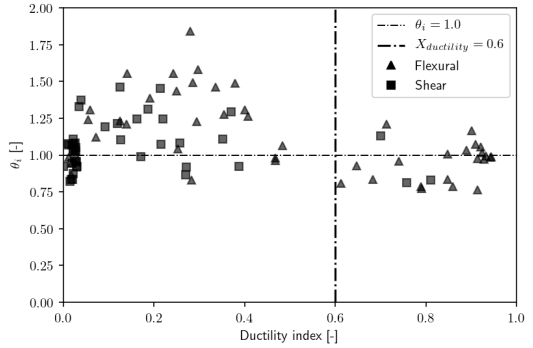

(c) Ductility index and model uncertainty for **experimental** failure mode

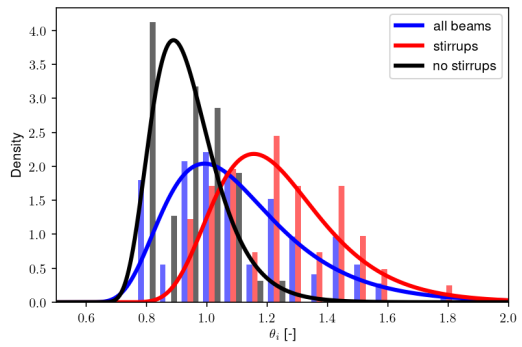

(d) Log-normal distributions fit to data

Figure A.15: NLFEA results for F5

A.3.6. F6

- Fixed crack, damage based retention
- 20 elements over height
- Shima beam bondslip reinforcement
- convergence E: 0.01 OR F: 0.1
- max 40 regular Newton-Raphson iterations

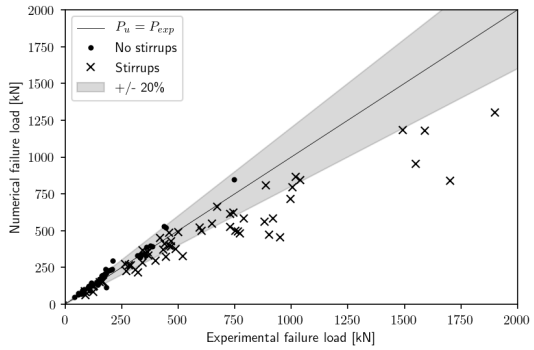

(a) All results for F6

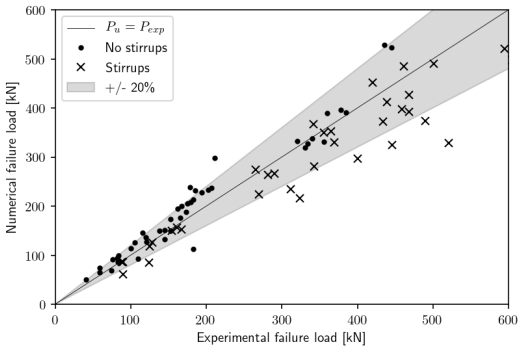

(b) Results F6 zoomed in

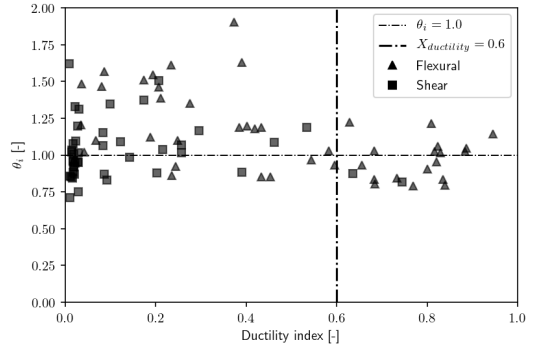

(c) Ductility index and model uncertainty for **experimental** failure mode

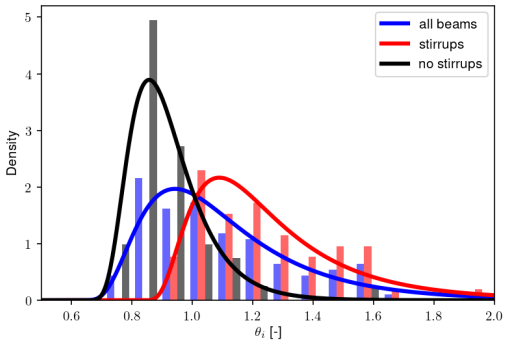

(d) Log-normal distributions fit to data

Figure A.16: NLFEA results for F6

A.3.7. F7

- Fixed crack, damage based retention
- 40 elements over height
- Shima beam bondslip reinforcement
- convergence E: 0.0001 OR F: 0.01
- max 40 regular Newton-Raphson iterations

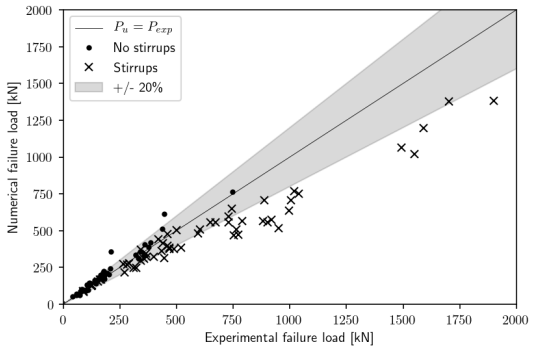

(a) All results for F7

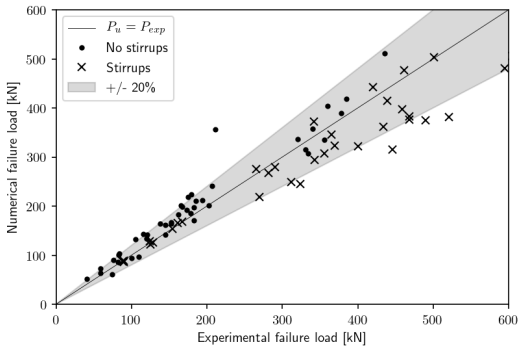

(b) Results F7 zoomed in

Figure A.17: NLFEA results for F7

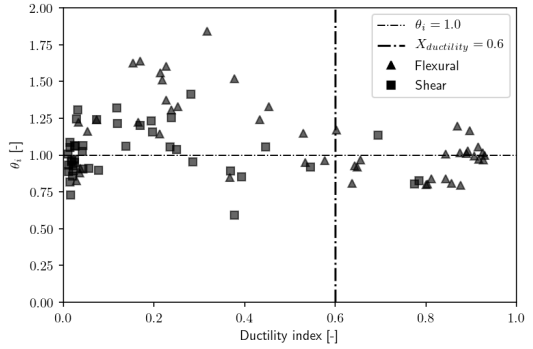

(a) Ductility index and model uncertainty for **experimental** failure mode

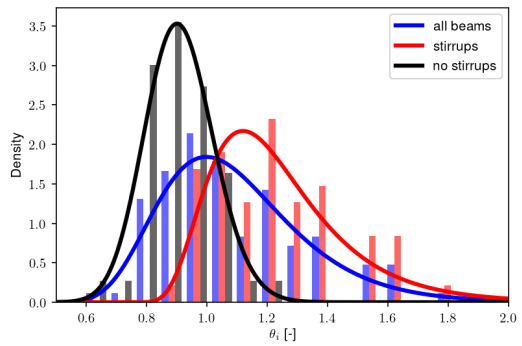

(b) Log-normal distributions fit to data

Figure A.18: NLFEA results for F7

A.3.8. F8

- Fixed crack, damage based retention
- 20 elements over height
- FIB MC2010 beam bondslip reinforcement
- convergence E: 0.0001 AND F: 0.01
- max 100 regular Newton-Raphson iterations

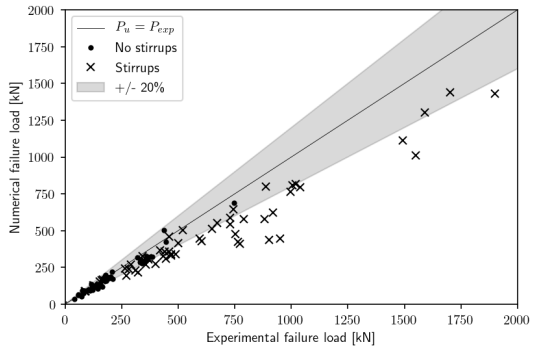

(a) All results for F8

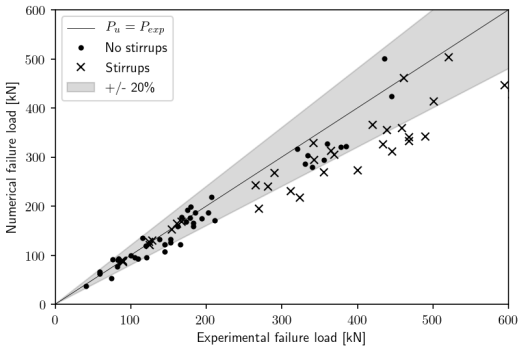

(b) Results F8 zoomed in

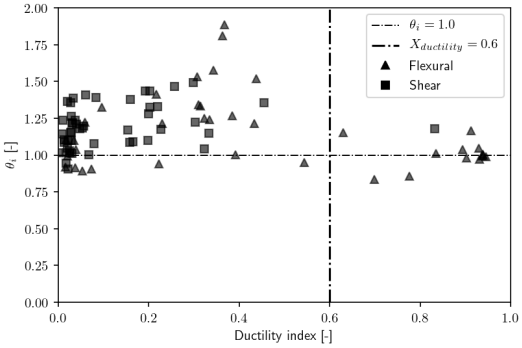

(c) Ductility index and model uncertainty for **experimental** failure mode

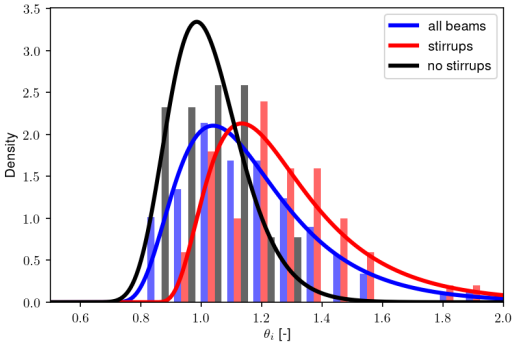

(d) Log-normal distributions fit to data

Figure A.19: NLFEA results for F8

A.3.9. F9

- Fixed crack, damage based retention
- 20 elements over height
- FIB MC2010 Beam bondslip reinforcement
- convergence E: 0.0001 OR F: 0.01
- max 100 regular Newton-Raphson iterations

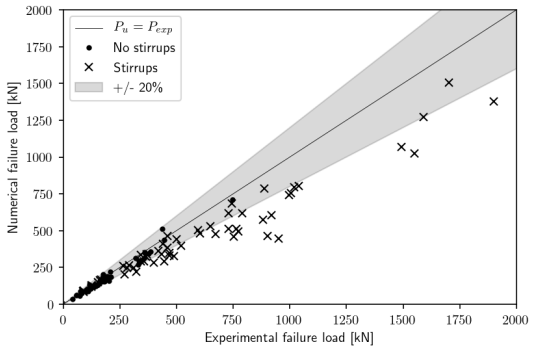

(a) All results for F9

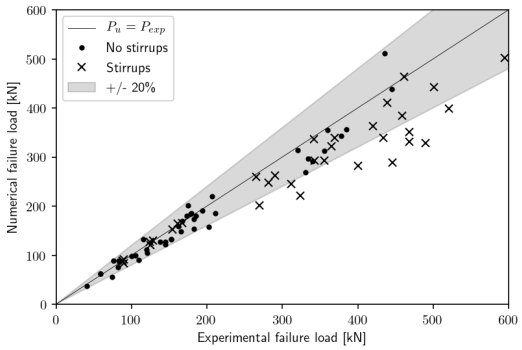

(b) Results F9 zoomed in

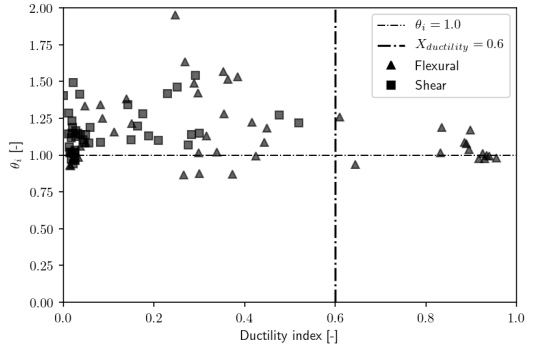

(c) Ductility index and model uncertainty for **experimental** failure mode

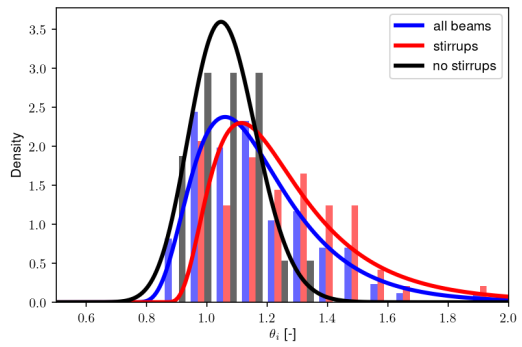

(d) Log-normal distributions fit to data

Figure A.20: NLFEA results for F9

A.3.10. F10

- Fixed crack, damage based retention
- 20 elements over height
- FIB MC2010 Truss bondslip reinforcement
- convergence E: 0.0001 OR F: 0.01
- max 100 regular Newton-Raphson iterations

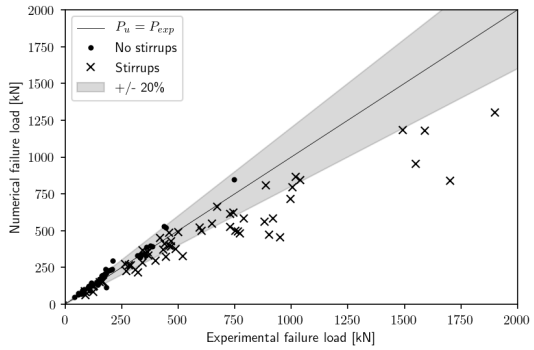

(a) All results for F10

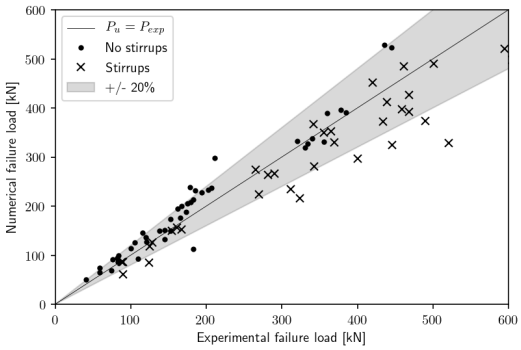

(b) Results F10 zoomed in

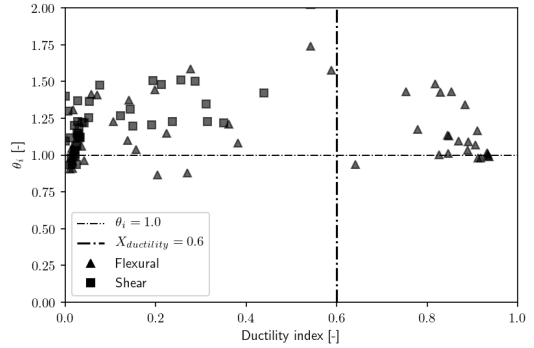

(c) All results for F10

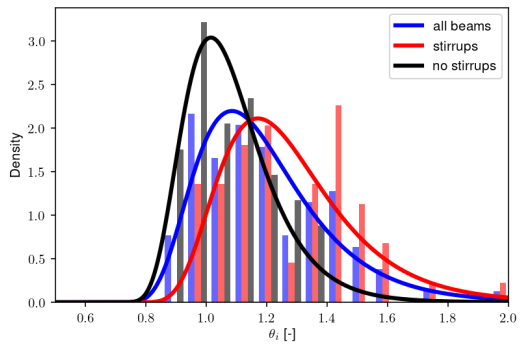

(d) Results F6 zoomed in

Figure A.21: NLFEA results for F10

Table A.1: Summary of found model uncertainty distributions

Solution strategy		No prior		MC2020 prior distribution		
	Group	μ_θ [-]	V_θ [-]	μ_θ [-]	V_θ [-]	γ_{Rd}
F1	All Beams:	1.196	0.198	1.171	0.193	1.08
F1	Stirrups:	1.322	0.17	1.296	0.167	0.946
F1	No stirrups:	1.034	0.14	1.024	0.134	1.151
F2	All Beams:	1.155	0.194	1.132	0.188	1.111
F2	Stirrups:	1.268	0.176	1.242	0.171	0.991
F2	No stirrups:	1.011	0.137	1.002	0.132	1.173
F3	All Beams:	1.136	0.205	1.111	0.198	1.146
F3	Stirrups:	1.265	0.177	1.24	0.172	0.995
F3	No stirrups:	0.969	0.13	0.962	0.126	1.212
F4	All Beams:	1.17	0.186	1.148	0.181	1.086
F4	Stirrups:	1.277	0.177	1.252	0.172	0.985
F4	No stirrups:	1.031	0.124	1.023	0.121	1.133
F5	All Beams:	1.112	0.202	1.089	0.195	1.165
F5	Stirrups:	1.245	0.163	1.224	0.159	0.992
F5	No stirrups:	0.94	0.123	0.935	0.12	1.238
F6	All Beams:	1.118	0.235	1.087	0.226	1.212
F6	Stirrups:	1.269	0.198	1.239	0.191	1.019
F6	No stirrups:	0.923	0.141	0.917	0.137	1.289
F7	All Beams:	1.096	0.218	1.07	0.211	1.208
F7	Stirrups:	1.239	0.173	1.216	0.168	1.01
F7	No stirrups:	0.911	0.131	0.907	0.129	1.291
F8	All Beams:	1.197	0.184	1.175	0.179	1.059
F8	Stirrups:	1.29	0.185	1.262	0.18	0.987
F8	No stirrups:	1.078	0.132	1.067	0.128	1.095
F9	All Beams:	1.177	0.173	1.158	0.169	1.061
F9	Stirrups:	1.268	0.177	1.243	0.172	0.993
F9	No stirrups:	1.061	0.11	1.053	0.108	1.084
F10	All Beams:	1.195	0.174	1.175	0.17	1.047
F10	Stirrups:	1.281	0.169	1.257	0.165	0.973
F10	No stirrups:	1.084	0.137	1.072	0.132	1.096
R1	All Beams:	1.105	0.215	1.079	0.207	1.193
R1	Stirrups:	1.078	0.091	1.072	0.092	1.044
R1	No stirrups:	1.143	0.319	1.087	0.292	1.315
R2	All Beams:	1.014	0.175	0.999	0.17	1.232
R2	Stirrups:	1.076	0.09	1.071	0.091	1.044
R2	No stirrups:	0.932	0.216	0.915	0.203	1.402
R3	All Beams:	0.998	0.174	0.983	0.17	1.251
R3	Stirrups:	1.07	0.109	1.062	0.108	1.074
R3	No stirrups:	0.903	0.192	0.891	0.182	1.402
R4	All Beams:	1.031	0.184	1.014	0.179	1.226
R4	Stirrups:	1.085	0.104	1.077	0.103	1.053
R4	No stirrups:	0.961	0.234	0.938	0.219	1.393
R5	All Beams:	1.025	0.182	1.008	0.177	1.231
R5	Stirrups:	1.083	0.092	1.077	0.093	1.04
R5	No stirrups:	0.949	0.233	0.927	0.218	1.407
R6	All Beams:	0.997	0.184	0.981	0.179	1.268
R6	Stirrups:	1.077	0.096	1.071	0.097	1.051
R6	No stirrups:	0.893	0.208	0.878	0.197	1.449
R7	All Beams:	1.023	0.184	1.006	0.179	1.236
R7	Stirrups:	1.082	0.109	1.074	0.108	1.062
R7	No stirrups:	0.946	0.227	0.926	0.212	1.401
R8	All Beams:	1.023	0.181	1.006	0.176	1.232
R8	Stirrups:	1.082	0.097	1.075	0.097	1.047
R8	No stirrups:	0.945	0.228	0.925	0.213	1.404
R9	All Beams:	1.052	0.152	1.04	0.149	1.153
R9	Stirrups:	1.096	0.105	1.088	0.104	1.044
R9	No stirrups:	0.996	0.185	0.98	0.174	1.262

B

Background and verification of ductility index

B.1. Introduction

In the analysis of failure of concrete beams, it is useful to be able to show the ductility of the failure. This can be done by so called 'visual interpretation' of crack patterns and load-displacement relations. Such way of describing important properties of beams or other structures could be seen as subjective and inexact.
Engen et al. [16] proposed a new way to deal with ductility. Here a so called 'ductility index', $X_{ductility}$, was introduced. This index is defined as the ratio of energy dissipation in the steel, $W_{pl,steel}$ versus total energy dissipation, $W_{pl,total}$, as in equation B.1. In order to calculate this index, information on the dissipated energy is needed.

$$X_{ductility} = \frac{W_{pl,Steel}}{W_{pl,total}} \tag{B.1}$$

B.1.1. Energy dissipated in the concrete

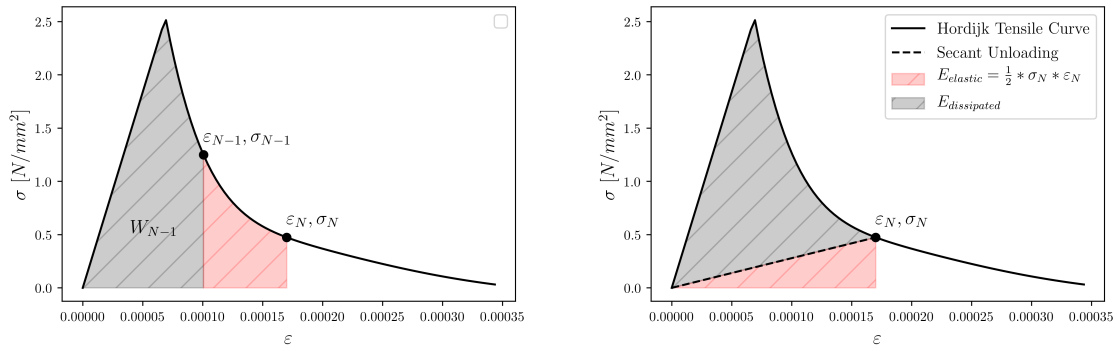

(a) Visualization of the integration

(b) Visualization of dissipated and elastic energy

Figure B.1: Visualization of dissipated energy calculation, the scaling by h is ignored as this is taken care of in the integration point volume.

The cumulative dissipated energy per integration point is determined by numerically integrating (equation 2) the stress-strain relation, subtracting the elastic part and multiplying that with the integration point volume as in equation 3. Please note that this formulation only holds in case of secant unloading, which is the default for the total strain crack model.This is however not the case in a material model considering reinforcements, where elastic unloading would be preferred.

The equations automatically work for both tension and compression softening as ε and σ both change sign.

$$W_n = W_{n-1} + \frac{1}{2} * (\sigma_{ij}^n + \sigma_{ij}^{n-1})(\varepsilon_{ij}^n - \varepsilon_{ij}^{n-1}) \quad \text{N/mm}^2 \tag{B.2}$$

$$W_{dissipated;n} = \left\{ W_n - \frac{1}{2}\sigma_{ij}^n \varepsilon_{ij}^n \right\} V_{IP} \quad \text{Nmm} \tag{B.3}$$

B.1.2. Steel contribution

The steel contribution in a similar manner, but here the elastic strain is required to determine the plastic strain. (this can also be defined the other way around, of course.)

$$W_n = W_{n-1} + \frac{1}{2}(\sigma_{ij}^n + \sigma_{ij}^{n-1})(\varepsilon_{ij}^n - \varepsilon_{ij}^{n-1}) \quad \text{N/mm}^2 \tag{B.4}$$

$$W_{dissipated;n} = \left\{ W_n - \frac{1}{2}\sigma_{ij}^n \varepsilon_{elastic;ij}^n \right\} V_{IP} \quad \text{Nmm} \tag{B.5}$$

B.1.3. On the contribution of bond-slip

When energy dissipation is assessed, it should be realised that also bond-slip or other nonlinear interfaces dissipate energy. Bond-slip behavior is, in DIANA, defined in a traction-slip [N/mm^2 - mm] relation. This indicates that the integration approach as shown in Figure B.1a and the equations that follow it, needs to be altered. To obtain the dissipated energy in a bond-slip interface, the following needs to be taken into account: The slip is absolute, so it has a unit of length, this can be seen as a strain multiplied by 'element length'. The traction is a stress. To obtain the total energy per element, not the integration point volume is needed (this is taken care of in the absolute slip values), but the perimeter of the reinforcement bar.

$$W_n = W_{n-1} + \frac{1}{2} * (t_f^n + t_f^{n-1})(ds_x^n - ds_x^{n-1}) * P * L \quad \text{Nmm} \tag{B.6}$$

Depending on what model is used, the unloading assumption is either linear elastic or secant.

$$W_{dissipated;n} = \left\{ W_n - \frac{1}{2}\sigma_{ij}^n \varepsilon_{ij}^n \right\} V_{IP} \quad \text{Nmm} \tag{B.7}$$

Two tests were done to investigate the actual impact of bond-slip dissipation on the results concerning the ductility index. One test concerned beam N2, as the experiment performed by Ashour [1] and one concerned beam OA2 as in the experiments by Vecchio and Shim [37]. To be conservative, the dissipated energy per integration point was assumed to be equal to equation B.6 and no elastic parts were subtracted.

Case OA2: (brittle)

Total strain energy in concrete: $4.28*10^5$ Nmm
Elastic strain energy in concrete: $3.17*10^5$ Nmm
Total strain energy in steel: $4.43*10^5$ Nmm
Elastic strain energy in steel: $4.39*10^5$ Nmm
Dissipated strain energy in bondslip: $2.00*10^3$ Nmm

Ductility index without accounting for bond-slip:

$$X_{ductil} = \frac{4.43*10^5 - 4.39*10^5}{4.28*10^5 + 4.43*10^5 - 3.17*10^5 - 4.39*10^5} = 0.0348 \quad [-]$$

With accounting for bond-slip behavior this turns into:

$$X_{ductil} = \frac{4.43*10^5 - 4.39*10^5}{4.28*10^5 + 4.43*10^5 - 3.17*10^5 - 4.39*10^5 + 2.00*10^3} = 0.0342 \quad [-]$$

It should be noted that the ductility index should be 0 in this case, as no yielding in the reinforcement occurs. The small value found can be attributed to the numerical integration of the stress-strain relations where a small error is made. The impact of the bond-slip dissipation on this is much smaller than that error.

Case N4: (ductile)

Total strain energy in concrete: $7.47*10^5$ Nmm
Elastic strain energy in concrete: $4.57*10^5$ Nmm
Total strain energy in steel: $2.09*10^6$ Nmm

Elastic strain energy in steel: $6.19*10^5$ Nmm
Dissipated strain energy in bondslip interfaces: 585.8 Nmm

$$X_{ductil} = \frac{2.09*10^6 - 6.19*10^5}{7.47*10^5 + 2.09*10^6 - 4.57*10^5 - 6.19*10^5} = 0.8353 \quad [-]$$

With accounting for bond-slip behavior this turns into:

$$X_{ductil} = \frac{2.09*10^6 - 6.19*10^5}{7.47*10^5 + 2.09*10^6 - 4.57*10^5 - 6.19*10^5 + 585.8} = 0.8350 \quad [-]$$

It is observed that the impact in a ductile case is in the same magnitude as the brittle case.

On the basis of these two case studies, the dissipation of energy in bond-slip interfaces is omitted from the formulation of the ductility index.

B.2. Verification of implementation

The implementation is verified by looking at a single element model as shown in Figure B.2: The model consists of one quadratic plane-stress element with a 2 × 2 Gaussian integration scheme, containing one embedded reinforcement bar. The dimensions are : 100×100×10 mm , the rightmost edge is displaced by 1mm, introducing an average strain of 1 % in both the concrete and steel. The displacement was applied in 2000 steps to assure an accurate representation of the tensile curve. To enforce cracking of just 1 column of integration points, the tensile strength and fracture energy were scaled by a factor 1000 for the other column, resulting in a linear elastic behavior in those integration points.

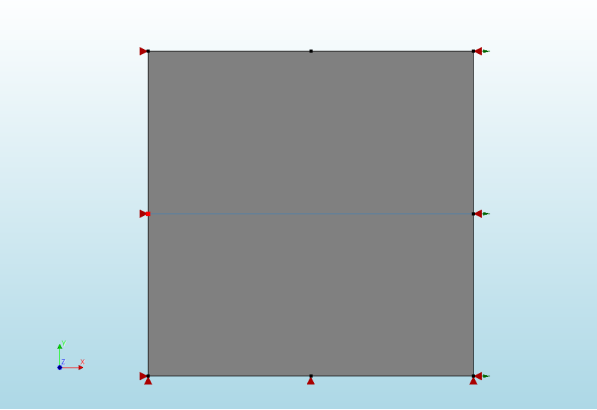

Figure B.2: Single element model

Concrete model	Total Strain Crack
Cracking model	Rotating
Tensile Curve	Hordijk
Tensile Strength	2.34 N/mm^2
E_c	34000 N/mm^2
Fracture energy G_F^I	0.148 N/mm
Crack Bandwidth h	fixed at 100 mm
Steel model	Von Mises Plasticity
E_s	200000 GPa
Yield Stress	556.5 N/mm^2
Hardening	No Hardening

Table B.1: Relevant material properties

Theoretically, the dissipated energy in each integration point should equal the fracture energy, divided by the crack bandwidth and multiplied by the integration point volume. The total dissipated energy would be that, but summed over the integration points, as in equation (B.8)

$$E_{diss} = \sum_{n=0}^{N_{IP}} \frac{G_F^I}{h} V_{IP}^n = \frac{0.148}{100} \times 50 \times 50 \times 10 \times 2 = 74 \quad \text{Nmm} \tag{B.8}$$

For the steel, only the cracked state of the concrete has to be addressed. This follows from: The strain at which the concrete cracks), the strain at which it does not have any tensile strength left) and the strain at which the steel yields. These are described in equations (B.9), (B.10) and (B.11) respectively.

$$\varepsilon_{cr} = \frac{f_t}{E} = \frac{2.34}{34000} = 6.882 * 10^{-5} \tag{B.9}$$

$$\varepsilon_{ult} = \frac{5.136 G_F^I}{1000 f_t} = \frac{5.136 * 0.148}{2340} = 3.248 * 10^{-4} \tag{B.10}$$

$$\varepsilon_{ys} = \frac{\sigma_y}{E_s} = \frac{556.5}{200000} = 2.7825 * 10^{-3} \tag{B.11}$$

From equations (B.10) and (B.11) follows that the steel does not dissipate any energy while the concrete has any capacity. Because of the high tensile strength at one side of the element, half of the concrete cracks while the other half is still behaving linear elastic. This means that the plastic strain in the steel localizes in one half of the element as well.

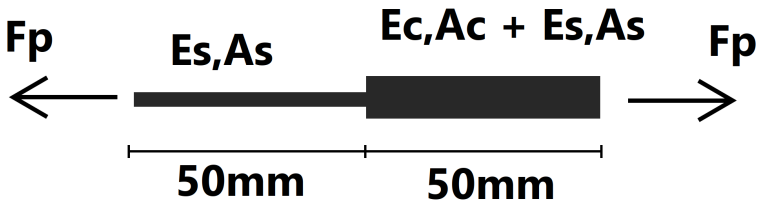

Figure B.3: Cracked state

The steel starts yielding at $F = F_p = \sigma_y * A_s$ The strain in the uncracked section equals $\varepsilon_2 = F_p/(E_c A_c + E_s A_s)$ From that, the elongation of the uncracked part is calculated as $\varepsilon_2 * 50$ mm$= \delta l_2$. The elongation from the cracked part follows as $\delta l_1 = 1 - \delta l_2$ and the strain of the cracked part equals $\varepsilon_1 = \delta l_1/50$ mm. The plastic strain is calculated by subtracting the elastic strain (equation (B.11)) from the total strain. From that the dissipated energy is calculated by multiplication with the yield stress.

ρ	A_s	ε_1	ε_2	ε_p	$W_{pl,c}$	$W_{pl,s}$	X_{ductil}
[%]	[mm^2]	[-]	[-]	[-]	[Nmm]	[Nmm]	Calculated
0.01	0.1	0.01999	1.636E-06	0.01721	74	47.903	0.3930
0.1	1	0.01998	1.627E-05	0.01720	74	478.624	0.8661
1	10	0.01984	1.545E-04	0.01706	74	4747.756	0.9847
2	20	0.01971	2.293E-04	0.01692	74	9418.542	0.9922
5	50	0.01937	6.324E-04	0.01659	74	23074.039	0.9968

Table B.2: Ductility indices for different reinforcement ratios

ρ	X_{ductil}	X_{ductil}	X_{ductil}
[%]	Calculated	Manual post-processing	FEA output
0.01	0.3930	0.3930	0.3930
0.1	0.8661	0.8660	0.8661
1	0.9847	0.9846	0.9846
2	0.9922	0.9922	0.9922
5	0.9968	0.9968	0.9968

Table B.3: Comparison of calculated ductility indices for different reinforcement ratios - manual post - processing means that the result was calculated manually from the DIANA output with estimated integration point volumes

B.2.1. Unloading

The case of unloading and ultimately pushing the specimen back in its original shape is investigated for the benchmark $\rho = 0.1$ %:

The expected ductility index is calculated in the following manner: Plastic strain $\varepsilon_p = 0.017201 + \varepsilon_1 - 2 * \varepsilon_{ys}$, as the specimen will be pushed back as far as it deformed . The dissipated energy in the concrete does not change.

$$X_{ductil} = \frac{\varepsilon_p * 556.5 * 50}{\varepsilon_p * 556.5 * 50 + 74} = 0.9224$$

The DIANA output in this case equals 0.92239

From tables B.2 and B.3; and from the fact that the expected ductility-index in case of unloading is found as well, it can be concluded that the algorithms have been implemented correctly and therefore the implementation of the ductility index is verified.

B.3. Examples

To illustrate this, two beams are selected: A 4-point bending test from Ashour [1], failing in a flexural manner. This beam is referred to as beam N2 in the paper and will be referred to as beam N2 (see Figure B.5a). Next to N2, a 3-point bending test from Vecchio & Shim [37] was selected, failing in brittle shear. Both beams were modelled using a Total Strain Crack (TSC) model with a fixed crack assumption.

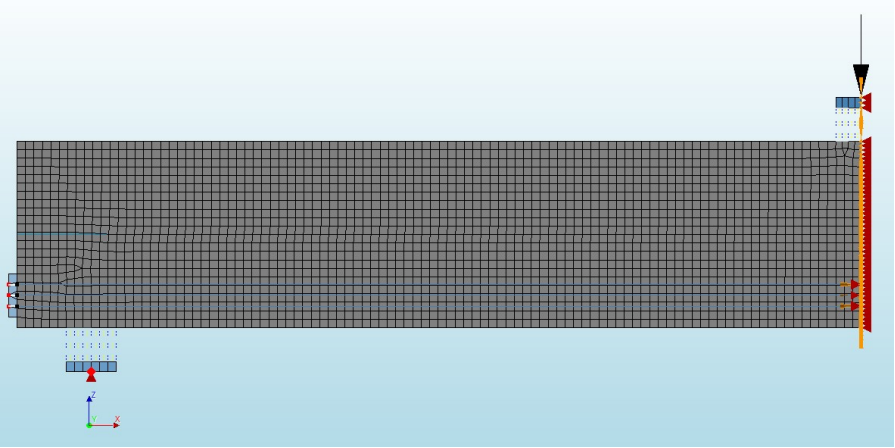

Figure B.4: Mesh and boundary conditions for beam OA2, mesh for N2 is comparable

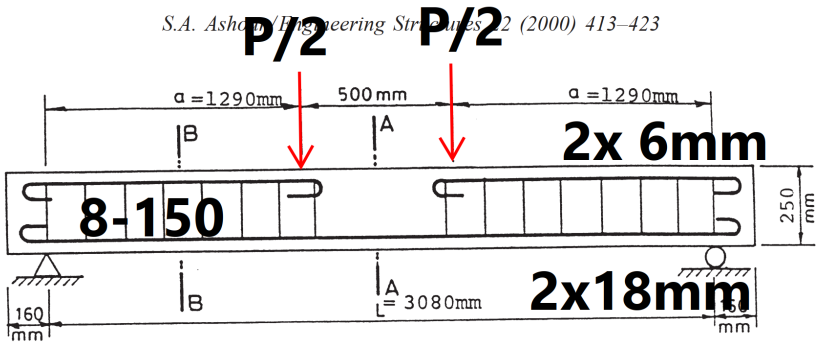

(a) beam N2 as described in [1]

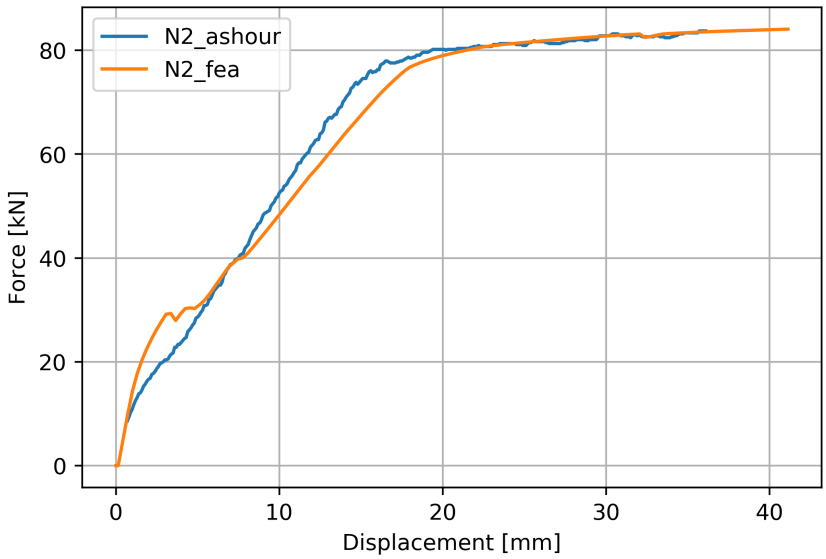

(b) Experimental (blue) and FEA (orange) results of beam N2

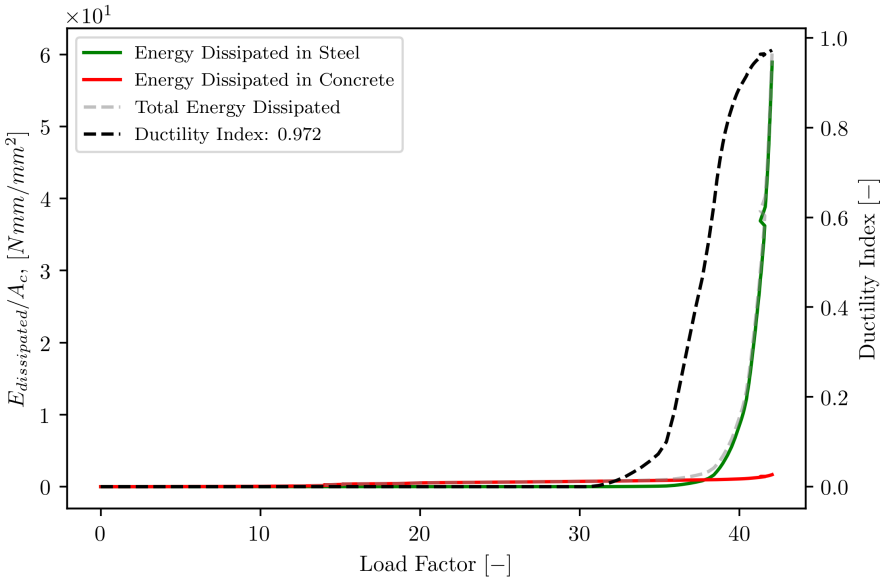

(c) Evolution of dissipated energy and ductility index in beam N2

Figure B.5: Overview of beam N2 from [1]

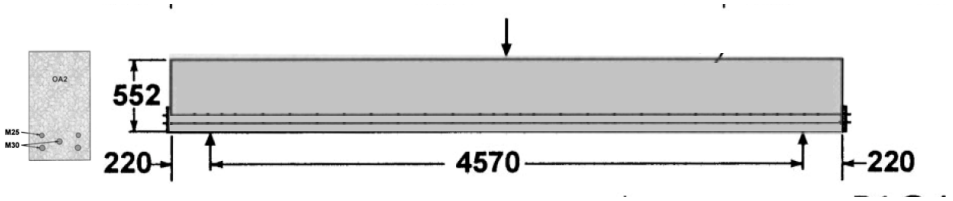

(a) beam OA2 as described in [37]

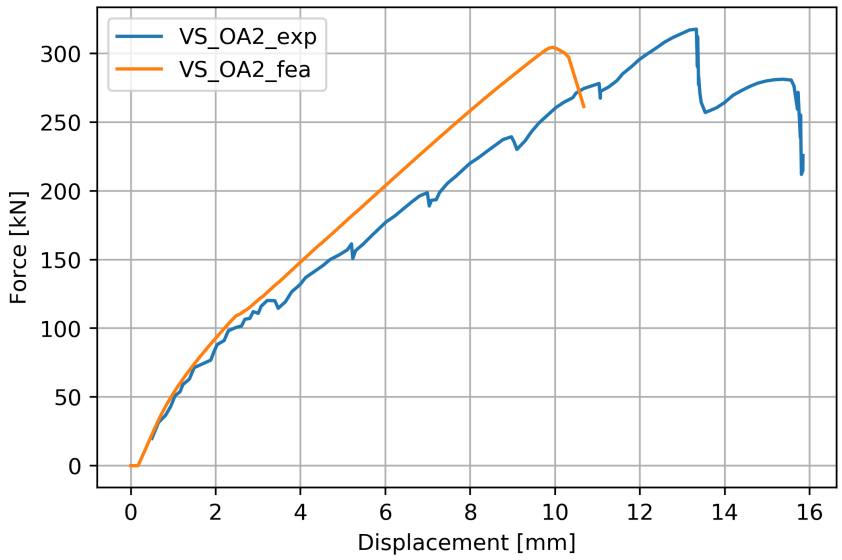

(b) Experimental (blue) and FEA (orange) results of beam OA2

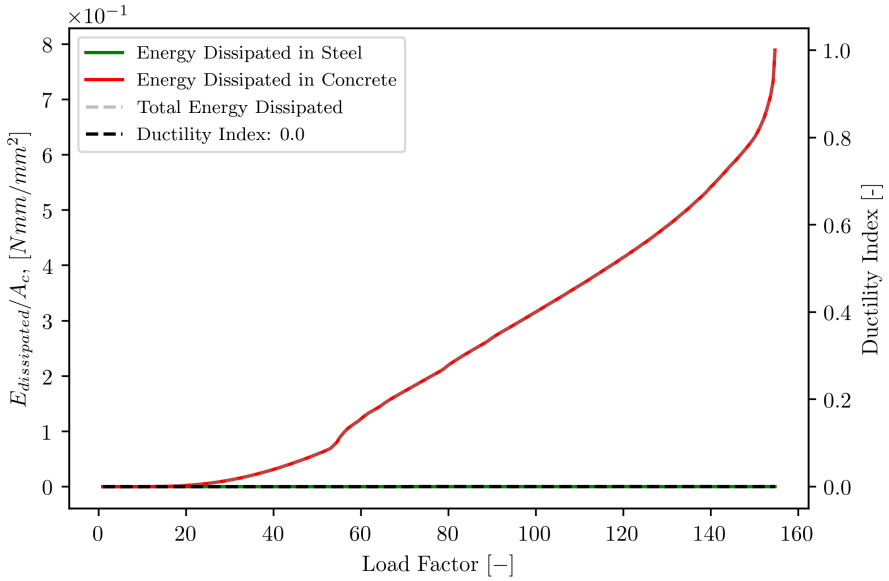

(c) Evolution of dissipated energy and ductility index in beam OA2

Figure B.6: Overview of beam OA2 from [37]

	OA2	N2
Concrete Crack	TSC Fixed	TSC Fixed
Shear Retention	Damage based	Damage based
Concrete Tensile	Hordijk	Hordijk
Concrete Compression	Parabolic	Parabolic
Tensile strength	f_{ctm}	f_{ctm}
Compressive Strength	25.9 MPa	48.61 MPa
Compressive Reduction	Vecchio & Collins 1993	Vecchio & Collins 1993
Confinement	Vecchio & Selby	Vecchio & Selby
Poisson Reduction	Damage based	Damage based
Reinforcement Bondslip	FIB MC2010	FIB MC2010
Reinforcement type	Beam	Beam
Von Mises type	Linear hardening	Linear hardening
Element type	Curved shell in-plane	Curved shell in-plane
Element name	CQ40S	CQ40S
Element size	25 mm	12.5 mm
Interpolation	3×3 Gaussian	3×3 Gaussian
Interpolation type	Quadratic	Quadratic
Thickness integration	2 point Gaussian	2 point Gaussian
Interface type	3D line	3D line
LoadSteps	$P_{ult}/50$	$P_{ult}/50$
Type	Force control	Force control
Help	Arclength + Linesearch	Arclength + Linesearch
Iteration scheme	Regular Newton-Raphson	Regular Newton-Raphson
Max iterations	40	20
Convergence criteria	F 0.01 + E 0.001	F 0.01 + E 0.001

Table B.4: Solution strategies for the beams

The properties of the finite element models are displayed in Table B.4. All concrete material properties are calculated from the mean compressive strength according to the Fib-MC2010 relations. The steel material properties are taken from the respective papers.

Figures B.5b and B.6b show that the finite element analysis results are close to the experimental results. The ductility index is calculated for both beams and displayed in Figures B.5c and B.6c for beams N2 and OA2 respectively. It shows that in beam OA2, all the energy is dissipated in the concrete. This indicates no reinforcement yielding, hence a brittle failure. The failure of beam N2, as shown in Figure B.5b, is very ductile. This is supported by Figure B.5c, where a ductility index close to one is obtained. The plot shows that most energy is dissipated during yielding of the reinforcement, that is where the ductility index goes from 0 to 0.97. Finally it is noted that in both plots B.5c and B.6c, the total energy is divided by the area of the cross-section. This was done to give a normalized quantity of energy dissipated per mm^2 concrete section and therefore being able to compare beams of different sizes more easily. With this it can be observed that the total energy dissipation per mm^2 in beam N2 is almost 100 times that of beam OA2.